SPRINGER BRIEFS IN ELECTRICAL AND COMPUTER ENGINEERING · CONTROL, AUTOMATION AND ROBOTICS

Chris T. Freeman
Eric Rogers
Jane H. Burridge
Ann-Marie Hughes
Katie L. Meadmore

Iterative Learning Control for Electrical Stimulation and Stroke Rehabilitation

Springer

SpringerBriefs in Electrical and Computer Engineering

Control, Automation and Robotics

More information about this series at http://www.springer.com/series/10198

Chris T. Freeman · Eric Rogers
Jane H. Burridge · Ann-Marie Hughes
Katie L. Meadmore

Iterative Learning Control for Electrical Stimulation and Stroke Rehabilitation

Springer

Chris T. Freeman
Department of Electronics and Computer Science
University of Southampton
Southampton
UK

Eric Rogers
Department of Electronics and Computer Science
University of Southampton
Southampton
UK

Jane H. Burridge
Faculty of Health Sciences
University of Southampton
Southampton
UK

Ann-Marie Hughes
Faculty of Health Sciences
University of Southampton
Southampton
UK

Katie L. Meadmore
School of Psychology
University of Southampton
Southampton
UK

ISSN 2191-8112 ISSN 2191-8120 (electronic)
SpringerBriefs in Electrical and Computer Engineering
ISSN 2192-6786 ISSN 2192-6794 (electronic)
SpringerBriefs in Control, Automation and Robotics
ISBN 978-1-4471-6725-9 ISBN 978-1-4471-6726-6 (eBook)
DOI 10.1007/978-1-4471-6726-6

Library of Congress Control Number: 2015941126

Springer London Heidelberg New York Dordrecht

Printed on acid-free paper

Springer-Verlag London Ltd. is part of Springer Science+Business Media (www.springer.com)

Contents

Chapter 1
Introduction

Stroke is the largest cause of disability in developed countries. One cause of a stroke is a blood clot that blocks a vessel in the brain and stops blood reaching the regions downstream. As a result some of the connecting nerve cells die and the person commonly suffers partial paralysis on one side of the body, termed hemiplegia. In the United Kingdom, as one example, approximately 50 % of people who survive a stroke require some form of rehabilitation to reduce impairment and assist with activities of daily living. Upper limb function is particularly important in regaining independence following stroke as impairments impact on daily living and well-being.

Research on rehabilitation following a stroke has consistently identified treatment intensity and goal oriented strategies as critical for successful therapeutic outcomes. The current prognosis for upper limb recovery following stroke is poor, with the literature reporting that complete recovery occurs in less than 15 % of patients with initial paralysis. Stroke is also an age-related disease, placing an increasing burden on long-term health and related resources unless improvements are made in achieving independence. Consequently there is a pressing need to improve the effectiveness of treatments.

To further maximize rehabilitation after stroke, novel therapeutic and cost-effective rehabilitation methods, or interventions, are required, which may combine different methodologies. For example, one possibility is to combine the application of assistive stimulation with robot-aided therapy and virtual reality. The premise is that this approach, supported by mobile technology, could be a major step towards enabling rehabilitation outside the hospital, where two of the major objectives are increased intensity of therapy and reduced cost.

To be accepted for use by health professionals any new method requires development of technology and clinical trials to establish feasibility. This monograph is based on a research programme that aims to combine the use of electrical stimulation, virtual reality and iterative learning control for upper-limb stroke rehabilitation. Iterative learning control was especially developed for systems, such as a gantry robot executing pick and place of objects, which repeat the same finite time task over and over again. Once each task is complete, the system resets and information generated

C.T. Freeman et al., *Iterative Learning Control for Electrical Stimulation and Stroke Rehabilitation*, SpringerBriefs in Control, Automation and Robotics, DOI 10.1007/978-1-4471-6726-6_1

during its completion is available for use in updating the control action to be applied during the next execution of the task.

The transfer of iterative learning control to rehabilitation is based on the patient making repeated attempts to complete a task, such as reaching out over a table top to an object, with electrical stimulation applied to the relevant muscle(s). As the patient attempts the task, performance is measured and the error between the supplied reference trajectory and that produced by the patient is calculated. The limb is then reset to the starting point and during this time an iterative learning control law, which makes explicit use of the error on the previous attempt, is used to adjust the level of electrical stimulation to be applied on the next attempt, where the use of previous trial error is unique to iterative learning control. If the patient is improving with each successive attempt, the level of stimulation should be reducing and the patient's voluntary effort increasing.

This monograph begins in the next chapter with a review of iterative learning control with emphasis on the particular laws used in stroke rehabilitation and pointers to the general literature. The following chapter then describes in general terms how iterative learning control can be transferred to the stroke rehabilitation domain and summarizes how health professionals assess the performance of a patient undergoing a rehabilitation programme based on repeated attempts at completion of a specified task. These assessment measures are used in the small-scale clinical trials that have supported the engineering developments.

The progress reported in this monograph is the outcome of three main research programs, which are described in successive chapters. To establish proof of concept, the first program considered movement in one plane and stimulated one muscle group (triceps) to control movement around the elbow joint. Patients tracked a moving trajectory with their hand whilst electrical stimulation was applied to assist with the movement. Following each trial, iterative learning control was used to update the electrical stimulation applied on the next trial. Results showed improvements in tracking accuracy during the sessions.

Following the successful proof of concept, the system was extended to movements in 3D space using a virtual reality tracking task. In this research, each patient's arm was supported by a robot that compensates for the effects of gravity, with electrical stimulation applied to the triceps and anterior deltoid muscle groups to control movement around elbow and shoulder joints. A clinical trial demonstrated the system's effectiveness, with improvements shown in tracking accuracy and in clinical assessment scores. The final program extended the research to include control of the hand and wrist during functional tasks. Iterative learning controlled electrical stimulation in this case is also applied to the extensors of the wrist and hand to assist with picking up and manipulating real world objects. Minimal robotic support is provided by a spring system and patient tracking is achieved using a Microsoft Kinect. The results of a clinical trial are also given.

The final chapter of this monograph gives critical overview of the results obtained and briefly discusses possible areas for future research. Other possible roles for iterative learning control in rehabilitation are also briefly discussed, e.g., the suppression of intention tremor in patients with Parkinsons disease.

Chapter 2
Iterative Learning Control—An Overview

This chapter gives the required background on iterative learning control. After introducing the defining characteristic of this form of control, attention is restricted to the laws used in the stroke rehabilitation research.

2.1 Introduction

The development of iterative learning control (ILC) emerged from industrial applications where the system involved executes the same operation many times over a fixed finite time interval. When each operation is complete, resetting to the starting location takes place and the next operation can commence immediately, or after a stoppage time. A common example is a gantry robot undertaking a pick and place operation in synchronization with a moving conveyor or assembly line. The sequence of operations is: (a) the robot collects a payload from a fixed location, (b) transfers it over a finite duration, (c) places it on the moving conveyor, (d) returns to the original location for the next payload and then (e) repeats the previous four steps for as many payloads as is required or can be transferred before it is required to stop.

To operate in pick and place mode it is necessary to supply the robot with a trajectory to follow and the task for a control law is to ensure that the robot follows the prescribed trajectory exactly or, more realistically, to within a specified tolerance. In addition to controlling its own movement and that of the payload, the control law must prevent other effects, such as disturbances and signal noise, from degrading tracking and thereby forcing it outside of the tolerance bound. If the robot begins to operate outside permissible limits, the control task is to bring it back within the specified limits as quickly as required or is physically possible. This task must be achieved without causing damage to, e.g., the sensing and actuating technologies used.

C.T. Freeman et al., *Iterative Learning Control for Electrical Stimulation and Stroke Rehabilitation*, SpringerBriefs in Control, Automation and Robotics, DOI 10.1007/978-1-4471-6726-6_2

In the ILC literature, each completion or execution of the task is described as a pass, iteration or trial, but in this monograph the latter term is exclusively used. Similarly, the finite time each trial takes to complete will be referred to as the trial length. Once a trial is finished, all data used and generated during its completion is available for use in computing the control action to be applied on the next trial. The use of such data is a form of learning and is the essence of ILC, embedding the mechanism through which performance may be improved by past experience.

The ILC mode of operation outlined above is the most common, i.e., complete a trial, reset and then repeat. This is different from repetitive control where the system continuously executes over the period of the reference signal, i.e., with no stoppage time between trials.

This chapter gives an overview of ILC, where the focus is on the algorithms that have been used to date in the technology transfer to next generation healthcare, with pointers to the literature for other design algorithms and applications. The particular area of next generation healthcare addressed is robotic-assisted upper limb stroke rehabilitation. In this context ILC is used to adjust the level of assistive stimulation applied during a treatment session where the patient attempts to re-learn a daily living task, such as reaching out to an object with the affected limb, by repeated attempts guided by a robot.

2.2 The Origins of ILC

The widely recognized starting point for ILC is Arimoto et al. (1984), which considered a simple first order linear servomechanism system for a voltage-controlled dc-servomotor. As in other areas, there is debate on the origins of ILC, for which the survey papers (Ahn et al. 2007; Bristow et al. 2006) and, in particular, Ahn et al. (2007) give coverage and relevant references. In the opening paragraphs of Arimoto et al. (1984) the analogy between ILC and human learning is drawn in the text: 'It is human to make mistakes, but it also human to learn from such experience. Is it possible to think of a way to implement such a learning ability in the automatic operation of dynamic systems?'.

The analysis in Arimoto et al. (1984) developed, using the servomotor example as a particular example, a control law applicable to systems required to track a desired reference trajectory **of a fixed trial length** T and **specified a priori**. On completion of each trial, **the system states reset** and during time taken to complete this task the **measured output** is used in the construction the next control output. The system dynamics were assumed to be **trial-invariant** and **invertible**. These distinguishing features led to the establishment of ILC as a major and ongoing area of control systems research and applications. Several of these assumptions, e.g., trial-invariant dynamics, have been relaxed in recent years but the concept of learning from experience gained over repeated trials of a task is retained.

Since it was first introduced ILC has broadened in breadth and depth, including links with established fields such as robust, adaptive and optimal control. Application areas have also expanded beyond industrial robotics and process control. In the

latter area, one starting point for the literature is the survey paper Wang et al. (2009), which also considers the connections with repetitive control and run-to-run control. This chapter now proceeds to consider the ILC theory and algorithms that have found novel application in stroke rehabilitation. For consistency, discrete descriptions of the dynamics are used.

2.3 ILC for Linear Systems

When ILC is applied to discrete dynamics the notation used for a scalar or vector valued variable in this monograph is $y_k(p),\ p = 0, 1, \ldots, T$. Here the nonnegative integer k is the trial number and $T \in \mathbb{N}$ denotes the number of samples on each trial, with the assumption of a constant sampling period. Suppose also that the dynamics of the system or process considered can be adequately modeled as linear and time-invariant. Then the state-space model of such a system in the ILC setting is

$$\begin{aligned} x_k(p+1) &= Ax_k(p) + Bu_k(p) \\ y_k(p) &= Cx_k(p),\ \ x_k(0) = x_0 \end{aligned} \tag{2.1}$$

where on trial k, $x_k(p) \in \mathbb{R}^n$ is the state vector, $y_k(p) \in \mathbb{R}^m$ is the output vector and $u_k(p) \in \mathbb{R}^l$ is the control input vector.

In this model it is assumed that the initial state vector does not change from trial-to-trial. The case when this assumption is not valid has also been considered in the literature. The dynamics are assumed to be disturbance-free but again this assumption can be relaxed. It also possible to write the dynamics in input-output form involving the convolution operator or take the one-sided z transform and hence analysis and design in the frequency domain is possible. To apply the z transform it is necessary to assume $T = \infty$ but in most cases the consequences of this requirement have no detrimental effects. For a more detailed analysis of cases where there are unwanted effects arising from this assumption, see the relevant references in Ahn et al. (2007), Bristow et al. (2006) and more recent work in Wallen et al. (2013).

Let $r(p) \in \mathbb{R}^m$ denote the supplied reference vector. Then the error on trial k is $e_k(p) = r(p) - y_k(p)$ and the core requirement in ILC is to construct a sequence of input functions $u_{k+1}(p),\ k \geq 0$, such that the performance achieved is gradually improved with each successive trial and after a 'sufficient' number of these the current trial error is zero or within an acceptable tolerance. Mathematically this can be stated as a convergence condition on the input and error of the form

$$\lim_{k\to\infty} ||e_k|| = 0,\ \lim_{k\to\infty} ||u_k - u_\infty|| = 0 \tag{2.2}$$

where u_∞ is termed the learned control and $||\cdot||$ denotes an appropriate norm on the underlying function space. As one possibility, let $||\cdot||_2$ denote the Euclidean norm of its argument and set $||e|| = \max_{p\in[0,T]} ||e(p)||_2$. The reason for including the requirement on the control vector is to ensure that strong emphasis on reducing

the trial-to-trial error does not come at the expense of unacceptable control signal demands. In application, only a finite number of trials will ever be completed but mathematically letting $k \to \infty$ is required in analysis of, e.g., trial-to-trial error convergence.

The standard form of ILC algorithm or law computes the current trial input as the sum of the input used on the previous trial and a corrective term, i.e.,

$$u_{k+1} = u_k + \Delta(u_k, e_k) \tag{2.3}$$

where $\Delta(u_k, e_k)$ is the correction term and is a function of the error and input recorded over the previous trial. A large number of variations exist for computing the correction term, including laws that make use of information generated on a finite number (greater than unity) of previous trials. For the stroke rehabilitation application it is the repeated performance of a finite duration task (with the input on the current trial computed by adding a corrective term that is directly influenced by the previous trial error) that makes ILC particulary suitable.

An extensively used analysis and design setting for discrete systems is based on lifting in the ILC setting. Suppose that (2.1) is asymptotically stable and hence all eigenvalues of the state matrix A have modulus strictly less than unity. If this is not the case then a stabilizing feedback control loop must be first applied. For simplicity, consider single-input single-output (SISO) systems with an assumed relative degree of one, and hence in (2.1) the first Markov parameter $CB \neq 0$. For the cases of multiple-input multiple-output (MIMO) systems and/or the assumption on the Markov parameter does not hold, refer to the relevant references in Ahn et al. (2007), Bristow et al. (2006).

Introduce

$$y_k = \begin{bmatrix} y_k(1) \\ y_k(2) \\ \vdots \\ y_k(T) \end{bmatrix}, \quad u_k = \begin{bmatrix} u_k(0) \\ u_k(1) \\ \vdots \\ u_k(T-1) \end{bmatrix}, \quad d = \begin{bmatrix} d(1) \\ d(2) \\ \vdots \\ d(T) \end{bmatrix}. \tag{2.4}$$

Then under the assumption that $r(0) = Cx_0$, (2.1) can be written in the form

$$y_k = Gu_k + d \tag{2.5}$$

with

$$G = \begin{bmatrix} p_1 & 0 & \dots & 0 \\ p_2 & p_1 & \dots & 0 \\ \vdots & \vdots & \ddots & \vdots \\ p_T & p_{T-1} & \dots & p_1 \end{bmatrix} \tag{2.6}$$

where $p_j = CA^{j-1}B$ and $d(j) = CA^j x_0$, $j = 1, \dots, T$.

2.3.1 Control Laws and Structural/Performance Issues

Consider the SISO version of the state-space model (2.1) and suppose that both the system dynamics and the measured output are deterministic, i.e., noise-free. Then a derivative, or D-type, ILC law constructs the current trial input as

$$u_{k+1}(p) = u_k(p) + K_d[e_k(p+1) - e_k(p)] \tag{2.7}$$

where K_d is a scalar to be designed such that $\lim_{k\to\infty} ||e_k|| = 0$. Also routine analysis shows that this condition holds if and only if $|1 - CBK_d| < 1$. Somewhat surprisingly, this condition is independent of the system dynamics embodied in state matrix A and can only be satisfied if $CB \neq 0$.

The reason why trial-to-trial error convergence (k) is independent of the system state matrix is the finite trial length, over which duration even an unstable linear system can only produce a bounded output. In design based on a lifted model, the solution is to first design a stabilizing feedback control law for the unstable system and then apply ILC to the lifted version of the resulting controlled system. This step may also be required for stable systems to ensure acceptable transient dynamics along the trials. This results in a two stage design whereas the repetitive process, a class of 2D linear systems, setting allows simultaneous design for trial-to-trial error convergence and along the trial dynamics, see, e.g., Hladowski et al. (2010, 2012) where experimental verification on a gantry robot that replicates many industrial processes to which ILC is applicable is also given.

If the system model has relative degree greater than one it follows immediately that trial-to-trial error convergence cannot be achieved. This problem arises for many ILC laws and has received considerable attention in the literature, where one starting point is again the relevant references in the survey papers (Ahn et al. 2007; Bristow et al. 2006). This feature is also present in the 2D systems/repetitive process designs. The most that can be done for a system of relative degree h is to lose control over the first $h-1$ samples along the trial and design a control law that gives convergence over the remaining samples.

In ILC, once trial k is complete the following information is available for the computation of the control u_{k+1}: (1) Information from the entire time duration of any previous trial and (2) Information up to the current sample on trial $k+1$. The following is one definition of causality in ILC.

Definition 2.1 An ILC law is causal if and only if the value of the input $u_{k+1}(p)$ at time p on trial $k+1$ is computed only using data in the time interval $[0, p]$ from the current and previous trials.

For standard linear systems at sample instant p the use of information at future samples $p+1, p+2, \ldots$ is non-causal and therefore any resulting control law cannot be implemented. The use of non-causal along the trial information in ILC laws is arguably the most important feature.

Consider the ILC control laws

$$u_{k+1}(p) = u_k(p) + K_p e_k(p+1) \tag{2.8}$$

and

$$u_{k+1}(p) = u_k(p) + K_p e_k(p) \tag{2.9}$$

where the first is ILC non-causal and the second is causal. Also let q denote the forward time shift operator acting on, e.g., $x(p)$ as $qx(p) = x(p+1)$. Then the dynamics of (2.1) can be written as

$$y_k(p) = G(q)u_k(p) + d(p) \tag{2.10}$$

where $d(p) = CA^p x_0$ and this term can be extended to represent exogenous system disturbances that enter on trial k. Moreover, this disturbance term influences the error on trial k as

$$e_k(p) = r(p) - G(q)u_k(p) - d(p) \tag{2.11}$$

Hence the non-causal ILC law (2.8) anticipates the disturbance d_{k+1} and uses the input $u_{k+1}(p)$ to preemptively compensate for its effects. This feature is not present in the causal ILC law (2.9).

Causal ILC laws can be shown to be equivalent to a feedback control, i.e., an equivalent control action can be obtained directly from the ILC law and it has been asserted that causal ILC algorithms have little merit. See the discussion, with supporting references, in Bristow et al. (2006) that counters this argument but in any case the vast majority of implemented ILC laws are non-causal.

The finite trial length in ILC allows non-causal signal processing to be used. For many implementations, this is exploited in the form of zero-phase filtering of the previous trial error prior to the computation of the next trial input. An experimental example where zero-phase filtering is used is the gantry robot based results reported in Hladowski et al. (2010, 2012). Essentially, zero-phase filtering between trials can be used to remove unwanted effects, e.g., noise from the measured signals.

A commonly used ILC law is given by

$$u_{k+1}(p) = Q(q)\left[u_k(p) + L(q)e_k(p+1)\right] \tag{2.12}$$

where $Q(q)$ is termed the Q-filter and $L(q)$ is the learning function, but these designations are not universally used in the literature. The Q-filter and learning function L can be non-causal, in the ILC sense, with impulse responses

$$\begin{aligned} Q(q) &= \ldots + q_{-2}q^2 + q_{-1}q + q_0 + q_1 q^{-1} + q_2 q^{-2} + \ldots \\ L(q) &= \ldots + l_{-2}q^2 + l_{-1}q + l_0 + l_1 q^{-1} + l_2 q^{-2} + \ldots . \end{aligned} \tag{2.13}$$

This algorithm has many variations, including phase-lead

$$u_{k+1}(p) = u_k(p) + le_k(p+h) \tag{2.14}$$

where the designation 'phase-lead' arises from the shifted term $le_k(p+h),\ h > 0$.

An ILC law of the form (2.12) can also be written in lifted form as

$$u_{k+1} = Q(u_k + Le_k) \tag{2.15}$$

The matrices G of (2.6), Q and L are Toeplitz and when the ILC law is causal Q and L are lower triangular. Other forms of Q and L, such as the fully populated case, correspond to non-causal ILC. Possibilities considered in the literature include time-varying functions, nonlinear functions and trial-to-trial (in k) functions. Imposing a band-diagonal structure results in Finite-Impulse Response (FIR) $Q(q)$ and $L(q)$ operators that can be causal or non-causal. The lifted model description is not applicable to differential dynamics and hence to applications where design by emulation is the only or preferred option. The repetitive process/2D system approach extends to this case.

2.3.2 Control Law Design

As in other control system design areas, the objectives must be specified, starting with stability. Consider applying the ILC law (2.12) to the system (2.10). Asymptotic stability in the SISO case then requires the existence of a real number $\hat{u} > 0$ such that $|u_k(p)| \leq \hat{u}$ for all $p \in [0, T]$ and $k \geq 0$, and for all $p \in [0, T]$, $\lim_{k\to\infty} u_k(p)$ exists and the learned control is $u_\infty(p) = \lim_{k\to\infty} u_k(p)$.

Using the lifted form, the controlled dynamics resulting from applying (2.12) to (2.10) can be written as

$$u_{k+1} = Q(I - LG)u_k + QL(r - d) \tag{2.16}$$

and stability holds if and only if all eigenvalues of the matrix $Q(I-LG)$ have modulus strictly less than unity, where I denotes the identity matrix of compatible dimensions. Matrix $Q(I - LG)$ is lower triangular and Toeplitz when the Q filter and learning function L are causal and all eigenvalues are equal and of value $q_0(1 - l_0 p_1)$. Hence stability requires $|q_0(1 - l_0 p_1)| < 1$ and this property cannot hold if the first Markov parameter $p_1 = 0$ as discussed previously in this chapter. Consult the references in Ahn et al. (2007), Bristow et al. (2006) for alternative settings to analyze the stability properties of this form of ILC.

Performance of an ILC system is different from the standard linear systems case as it is necessary to consider trial-to-trial and along the trial dynamics. In the former case, if the system considered above is asymptotically stable, the converged error in k is

$$e_\infty(p) = \lim_{k\to\infty} e_k(p) = r(p) - G(q)u_\infty(p) - d(p) \tag{2.17}$$

and again there is a z transform version of this result. Performance from trial-to-trial can, of course, be compared in many ways, where one measure is the difference between the final and initial trial errors, i.e., $e_\infty(p)$ and $e_0(p)$. Theorem 3 in Bristow et al. (2006) gives the conditions for convergence to zero error in the case when G and L are not identically zero. These conditions comprise asymptotic stability plus the requirement that $Q(q) = 1$. As discussed previously, in many cases it will also be necessary to design for acceptable transient dynamics along the trials.

Robustness is also an issue in ILC. Early research on the use of an $\mathcal{H}_\infty$ setting is given in Amann et al. (1996a), with other work referenced in the survey papers (Ahn et al. 2007; Bristow et al. 2006), and is largely based on assuming an uncertainty model to represent the unmodeled dynamics, such as norm-bounded. More recent work, such as Hladowski et al. (2010, 2012), uses Linear Matrix Inequalities (LMIs) to compute the robust control law with experimental verification on a gantry robot.

In applications terms, the core task in ILC design is to construct an open-loop signal that approximately inverts the plant's dynamics, tracks the reference and rejects repeating disturbances. In the ideal scenario ILC would only learn repeating disturbances and ignore noise and non-repeating disturbances. Four general control law design methods are now discussed in turn, starting with Proportional plus Derivative (PD)-type designs with tuning that can be applied to a system without extensive modeling and analysis.

2.3.3 Proportional Plus Derivative-Type ILC

Arimoto's original algorithm (2.7) can be expanded for SISO systems to form a PD-type ILC law, which can be written as

$$u_{k+1}(p) = u_k(p) + k_p e_k(p+1) + k_d[e_k(p+1) - e_k(p)]. \tag{2.18}$$

In the lifted setting, (2.18) corresponds to the choice $Q = I$ and

$$L = \begin{bmatrix} k_p + k_d & 0 & \dots & 0 \\ -k_d & k_p + k_d & \dots & 0 \\ 0 & -k_d & \dots & 0 \\ \vdots & \vdots & \ddots & \vdots \\ 0 & 0 & \dots & k_p + k_d \end{bmatrix} \tag{2.19}$$

An alternative is to use $e_k(p)$ instead of $e_k(p+1)$ in the second term on the right-hand side of (2.18). Also the generalization to MIMO systems is immediate.

Unlike Proportional plus Integral plus Derivative (PID) (or three term) control for standard systems, auto-tuning rules are not available for ILC design. Also monotonic trial-to-trial error convergence is not always possible with ILC PD-type laws and an

often used approach to approximately achieve this property is to include a low-pass Q filter in the control law, i.e., as in (2.12), pre-multiply the right-hand side of the control law by $Q(p)$. This filter can be used to block learning at high frequencies and also has other benefits, such as increased robustness and filtering of high-frequency noise.

In tuning-based design, one approach is to first select the Q filter type, such as Butterworth or Chebyshev, and order and then use the filter bandwidth as the tuning variable. This approach is extensively covered in the literature and, e.g., Bristow et al. (2006) gives intuitive guidelines for tuning to achieve good learning transients and low error. Again, the survey papers (Ahn et al. 2007; Bristow et al. 2006) are a starting point for the many methods available for ILC PD design.

2.3.4 Inverse ILC

Plant inversion, or inverse, ILC designs use models of the inverse plant dynamics as the learning function. For discrete systems the control law has the form

$$u_{k+1}(p) = u_k(p) + \hat{G}^{-1}(q)e_k(p) \tag{2.20}$$

or

$$u_{k+1}(p) = u_k(p) + q^{-1}\hat{G}^{-1}(q)e_k(p+1) \tag{2.21}$$

where, since the exact inverse will not often be computable, $\hat{G}^{-1}(q)$ denotes the approximate inverse of $G(q)$. The learning function is

$$L(q) = q^{-1}\hat{G}^{-1}(q) \tag{2.22}$$

which is causal and of zero relative degree, i.e., has the same number of zeros as poles.

2.3.5 Gradient Descent ILC

As in other areas, a natural approach to model based ILC is to minimize a suitable cost function. The gradient descent algorithm for ILC (Furuta and Yamakita 1987) considers the following cost-function for the discrete lifted model

$$J(u_{k+1}) = \|e_{k+1}\|^2,\ e_{k+1} = r - Gu_{k+1} \tag{2.23}$$

during each trial. Suppose also that the ILC law used is

$$u_{k+1} = u_k + \epsilon_{k+1}\delta_{k+1} \tag{2.24}$$

where ϵ_{k+1} is a scaling factor and δ_{k+1} is the vector that determines the direction of the update vector. Then the tracking error on trial $k+1$ is

$$\begin{aligned} J(u_{k+1}) &= J(u_k + \epsilon_{k+1}\delta_{k+1}) = \|e_{k+1}\|^2 \\ &= \|e_k\|^2 - 2\epsilon_{k+1}\delta_{k+1}^T G^T e_k + \epsilon_{k+1}^2 \delta_{k+1}^T G^T G \delta_{k+1} \end{aligned} \tag{2.25}$$

and hence

$$\|e_{k+1}\|^2 - \|e_k\|^2 = -2\epsilon_{k+1}\delta_{k+1}^T G^T e_k + \epsilon_{k+1}^2 \delta_{k+1}^T G^T G \delta_{k+1}. \tag{2.26}$$

Monotonic trial-to-trial error convergence occurs when the right-hand side in (2.26) is negative. One option is choosing $\delta_{k+1} = G^T e_k$, resulting in the control law

$$u_{k+1} = u_k + \epsilon_{k+1} G^T e_k \tag{2.27}$$

which corresponds to the choice $Q = I$ and $L = \epsilon_{k+1} G^T$ in the lifted setting.

2.3.6 Norm Optimal ILC

Norm Optimal ILC (NOILC) is a gradient-based update law that includes: (a) automatic choice of step size, and (b) potential for improved robustness through use of causal feedback (current trial error data) and feedforward of data from previous trials. The results below are from Amann et al. (1996b), see also papers cited in Ahn et al. (2007), Bristow et al. (2006) for other versions of this law.

The current trial input is chosen to minimize a cost function involving norms of the trial error and the difference between successive trial control inputs. A general treatment of the cost function and the problem solution in a Hilbert space setting can be found in Amann et al. (1996b). The cost function used for discrete dynamics in the ILC setting described by (2.1) is

$$\begin{aligned} J(u_{k+1}) = &\sum_{i=0}^{T-1} (e_{k+1}(i) - e_k(i))^T Q (e_{k+1}(i) - e_k(i)) \\ &+ \sum_{i=0}^{T-1} (u_{k+1}(i) - u_k(i)^T R (u_{k+1}(i) - u_k(i)) \end{aligned} \tag{2.28}$$

where Q and R are symmetric positive definite weighting matrices to be selected. Use of this cost function optimally reduces the trial-to-trial error and ensures that the control input on the next trial does not deviate too much from that used on the previous trial.

Following Amann et al. (1996b) the control input on trial $k+1$ is given by

$$u_{k+1}(p) = u_k(p) - \Big[\Big\{ B^T K(p) B + R \Big\}^{-1} B^T K(p) \times A \{ x_{k+1}(p) - x_k(p) \} \Big] + R^{-1} B^T \xi_{k+1}(p) \tag{2.29}$$

where $K(p)$ is the solution of the algebraic Riccati equation

$$K(p) = A^T K(p+1) A + C^T Q C - \Big[A^T K(p+1) B \times \Big\{ B^T K(p+1) B + R \Big\}^{-l} B^T K(p+1) A \Big] \tag{2.30}$$

with terminal boundary condition $K(T) = 0$. The feedforward predictive term $\xi_{k+1}(p)$ is generated after each trial as

$$\xi_{k+1}(p) = \Big\{ I + K(p) B R^{-1} B^T \Big\}^{-1} \Big\{ A^T \xi_{k+1}(p+1) + C^T Q e_k(p+1) \Big\} \tag{2.31}$$

with terminal boundary condition $\xi_{k+1}(T) = 0$. Moreover, NOILC can also be applied to the lifted model representation of the dynamics.

2.4 Nonlinear Model ILC

Nonlinear ILC has received substantial attention in the literature, especially trial-to-trial error convergence proofs. In this section the background on one method, Newton ILC, which has been used in the stroke rehabilitation research reported in this monograph, is given.

Nonlinear systems can, in general terms, be split into two groups; those that are affine in the control and those that are not. The former are assumed to be of the form

$$\begin{aligned} \dot{x}(t) &= f(x(t)) + B(x(t)) u(t) \\ y(t) &= h(x(t)) \end{aligned} \tag{2.32}$$

where x is the state vector, u is the input and y is the output. A special case is the following model generally used to express the dynamics of robotic systems

$$M_r(x(t)) \ddot{x}(t) - C_r(x(t), \dot{x}(t)) \dot{x}(t) - g_r(x(t)) - d_r(x(t), \dot{x}(t)) = \tau(u(t)) \tag{2.33}$$

where the vectors $x(t)$, $\ddot{x}(t)$, $\dot{x}(t)$ are the joint positions, velocities and accelerations, $\tau(u(t))$ is the actuator torque generated using a control input $u(t)$, $M_r(x)$ is the symmetric positive-definite inertial matrix, $C_r(x, \dot{x})$ is the Coriolis and centripetal acceleration matrix, $g_r(x)$ is the gravitational force vector and $d_r(x, \dot{x})$ is the friction torque vector.

The application of ILC to affine nonlinear systems uses a wide variety of laws but a critical common assumption is that the nonlinear system is smooth. This requirement

is often expressed as a global Lipschitz assumption on each of the functions in (2.32) of the form

$$\begin{aligned} |f(x_1) - f(x_2)| &\leq f_0|x_1 - x_2| \\ |B(x_1) - B(x_2)| &\leq b_0|x_1 - x_2| \\ |h(x_1) - h(x_2)| &\leq h_0|x_1 - x_2| \end{aligned} \tag{2.34}$$

The constants f_0, b_0 and h_0 are used in a contraction mapping setting to obtain (sufficient) conditions for trial-to-trial error convergence and ILC law design. Non-affine systems have the form

$$\begin{aligned} \dot{x}(t) &= f(x(t)) + B(x(t), u(t)) \\ y(t) &= h(x(t)) \end{aligned} \tag{2.35}$$

In the rehabilitation setting, control design is primarily undertaken using a discrete-time system representation. Obtaining discrete-time models for nonlinear systems is sometimes non-trivial but, e.g., trial-to-trial error convergence proofs are simpler and the final design is directly compatible with digital implementation. One other way to study and design ILC for nonlinear systems is to treat the nonlinearities as perturbations to a linearized system model.

2.4.1 Newton ILC

Newton ILC was proposed by Lin et al. (2006) and uses the full model in the computation of the next trial input. It is based on a general discrete-time state-space model of the form

$$\begin{aligned} x_k(p+1) &= f(x_k(p), u_k(p)) \\ y_k(p) &= h(x_k(p)) \end{aligned} \tag{2.36}$$

which can be obtained via discretization of its continuous-time counterpart. As in the linear case $p = 0, 1, \ldots, T$ is the sample number, $x_k(p)$ is the state vector, and in lifted form the output and input vectors are given by

$$\begin{aligned} y_k &= \left[y_k^T(0)\ y_k^T(1)\ \ldots\ y_k^T(T) \right]^T \\ u_k &= \left[u_k^T(0)\ u_k^T(1)\ \ldots\ u_k^T(T) \right]^T \end{aligned} \tag{2.37}$$

and the reference vector by

$$y_d = \left[y_d^T(0)\ y_d^T(1)\ \ldots\ y_d^T(T) \right]^T \tag{2.38}$$

The Newton ILC law takes the form

$$u_{k+1} = u_k + g'(u_k)^{-1} e_k \tag{2.39}$$

where $e_k = r - y_k$ is the tracking error. The term $g'(u_k)$ is equivalent to linearizing the system dynamics around u_k, with the system $\tilde{y} = g'(u_k)\tilde{u}$ corresponding to the following linear time-varying state-space model

$$\begin{aligned} \tilde{x}(p+1) &= A(p)\tilde{x}(p) + B(p)\tilde{u}(p) \\ \tilde{y}(p) &= C(p)\tilde{x}(p) \end{aligned} \tag{2.40}$$

over $p = 0, 1, \ldots, T$, with

$$\begin{aligned} A(p) &= \left(\frac{\partial f}{\partial x}\right)_{u_k(p), x_k(p)}, \quad B(p) = \left(\frac{\partial f}{\partial u_k}\right)_{u_k(p), x_k(p)} \\ C(p) &= \left(\frac{\partial h}{\partial x}\right)_{u_k(p), x_k(p)} \end{aligned} \tag{2.41}$$

The term $g'(u_k)^{-1}$ in (2.39) is computationally expensive and may be singular or contain excessive amplitudes and high frequencies. To overcome this difficulty, introduce

$$e_k = g'(u_k)\Delta u_{k+1} \tag{2.42}$$

and then $\Delta u_{k+1} = u_{k+1} - u_k$ equals the input that forces the system (2.40) to track the error e_k. This is also an ILC problem and can be solved in between experimental trials using any ILC law that converges globally. In this monograph NOILC is used.

References

Ahn H-S, Chen YQ, Moore KL (2007) Iterative learning control: brief survey and characterization. IEEE Trans Syst Man Cybern 37(6):1099–1121

Amann N, Owens DH, Rogers E, Wahl A (1996a) An $\mathcal{H}_\infty$ approach to iterative learning control design. Int J Adapt Control Signal Process 10(6):767–781

Amann N, Owens DH, Rogers E (1996b) Iterative learning control for discrete-time systems with exponential rate of convergence. Proc Inst Elect Eng, Part D, Control Theory Appl 143(2):217–224

Arimoto S, Kawamura S, Miyazaki F (1984) Bettering operation of robots by learning. J Robot Syst 2(1):123–140

Bristow DA, Tharayil M, Alleyne AG (2006) A survey of iterative learning control: a learning based method for high performance tracking control. IEEE Control Syst Mag 26(3):96–114

Furuta K, Yamakita M (1987) The design of a learning control system for multivariable systems. In: Proceedings of the IEEE international symposium on intelligent control, pp 371–376

Hladowski L, Galkowski K, Cai Z, Rogers E, Freeman CT, Lewin PL (2010) Experimentally supported 2D systems based iterative learning control law design for error convergence and performance. Control Eng Pract 18(4):339–348

Hladowski L, Galkowski K, Cai Z, Rogers E, Freeman CT, Lewin PL (2012) Output based iterative learning control design with experimental verification. J Dyn Syst Meas Control 134:021012-1–021012-10

Lin T, Owens DH, Hatonen J (2006) Newton method based iterative learning control for discrete non-linear systems. Int J Control 79(10):1263–1276

Wallen J, Gunnarsson S, Norrloff M (2013) Analysis of boundary effects in iterative learning control. Int J Control 86(3):410–415

Wang Y, Gao F, Doyle III FJ (2009) Survey on iterative learning control, repetitive control, and run-to-run control. J Process Control 19:1589–1600

Chapter 3
Technology Transfer to Stroke Rehabilitation

The link that extends ILC from industrial robotics to robotic-assisted stroke rehabilitation is described together with the methods a health professional uses to assess the ability and progress of a patient. This material underpins the remainder of the monograph.

3.1 Background on Stroke and Its Consequences

As discussed briefly in Chap. 1, stroke is a leading cause of disability world-wide (Hong and Saver 2009) and is usually caused when a blood clot blocks a vessel in the brain stopping the blood reaching the regions downstream. Alternatively, it may be caused by a haemorrhage, where a vessel ruptures and leaks blood into surrounding areas. As a result, some of the connecting nerve cells die and the person commonly suffers partial paralysis on one side of the body, termed hemiplegia.

Stroke is an age related disease (Denti et al. 2008) and, as the number of people aged 60 and above is predicted to increase from year to year, incidence is likely to rise (SA 2015). Prevalence is also likely to rise due to better survival rates and long-term care. Associated with these figures, the stroke burden is projected to increase from around 38 million disability-adjusted life years (DALYs) lost globally in 1990 to 61 million DALYs in 2020 (Murray et al. 2012).

The consequences of age related conditions, such as stroke, thus have a growing impact on the health and economic prosperity of countries. To give a country specific perspective, within England and Wales alone approximately 110,000 people have a stroke each year according to UK Department of Health figures from 2007 and stroke is now the third largest cause of death and the single largest cause of adult disability. The treatment of and productivity loss arising from stroke results in total societal costs of 8.9 billion UK pounds a year, with treatment costs accounting for approximately 5 % of the total UK state funded National Health Service costs (Saka et al. 2009).

C.T. Freeman et al., *Iterative Learning Control for Electrical Stimulation and Stroke Rehabilitation*, SpringerBriefs in Control, Automation and Robotics, DOI 10.1007/978-1-4471-6726-6_3

Neurorehabilitation, i.e., therapy to assist recovery of functions lost as a result of a neurological disorder, across the world is fragmented and the current prognosis for upper limb recovery following stroke remains poor; for 30–60 % of stroke patients the hemiplegic arm remains without function (Kwakkel et al. 2008b). It has been reported that 80 % of all post-stroke survivors show a reduced ability to use the paretic upper extremity in activities of daily living (Langhorne et al. 2011), which has been shown to be associated with poorer health-related quality of life and affects personal independence (Morris et al. 2013).

An obvious need exists to improve the efficiency and effectiveness of treatment, whilst remaining mindful that resources for healthcare workers and rehabilitation costs are limited. Technologies have the potential to provide intensive practice of a task, variety and feedback, which have been shown by conventional therapy and motor learning theory to be important. These ideas are being applied in new technologies which provide the opportunity for repeated practice, but a review found that the translation of rehabilitation technology research into clinical practice has been impeded by an absence of robust clinical effectiveness and usability evidence (Burridge and Hughes 2010).

3.1.1 Robotically-Assisted Stroke Rehabilitation

Brain cells killed after a stroke cannot re-grow, but the brain has some spare capacity and hence new connections can be made. The brain is continually and rapidly changing as new skills are learned, new connections are formed, and redundant ones disappear. A person who re-learns skills after a stroke goes through the same process as someone learning to play tennis or a baby learning to walk, requiring repeated practice of a task. Unfortunately, they can hardly move and therefore do not receive feedback on their performance.

The application of conventional therapy and motor learning theory provides evidence that intensity of practice of a task and feedback are important, see, for example, Pomeroy et al. (2006). In turn, this is motivating the development of novel treatments such as those that provide the opportunity for repetitive movement practice. Although the use of robotic therapy in upper limb rehabilitation is relatively recent, reviews of the literature suggest that robot-aided therapy improves motor control of the proximal upper limb and may improve functional outcomes (Prange et al. 2006). Moreover, electromechanical and robotic devices may have an advantage over conventional therapies in the frequency of movement repetitions because of an increased motivation to train and also the opportunity for independent exercise (Prange et al. 2006). Based on existing evidence, use of rehabilitation robots is recommended in the UK stroke guidelines (PS 2004).

Clinical evidence exists to support the therapeutic use of Functional Electrical Stimulation (FES), sometimes also referred to in the literature as electrical stimulation, to improve motor control (de Kroon et al. 2002). This form of stimulation makes muscles work by causing electrical impulses to travel along nerves in much

the same way as electrical impulses from the brain, and if carefully controlled, a useful movement can be made. Theoretical results from neurophysiology (Burridge and Ladouceur 2001) and motor learning research support clinical research with the conclusion that the therapeutic benefit of stimulation is maximized when applied co-incidently with a patient's own voluntary intention to move (de Kroon et al. 2005).

A hypothesis is proposed in Rushton (2003) to explain the added benefit of increased recovery when FES is used to mimic a weak or paralyzed movement, describing how the anterior horn (AH) cell synapses may be strengthened by receiving simultaneous impulses along the motor nerves due to FES and voluntary effort and thereby allowing the AH cells to compensate for damage to the subject's motor system. This hypothesis explains why the increased degree of functional recovery is closely related to the accuracy of the stimulation applied to assist the patient's own voluntary completion of a task.

A variety of FES model-based laws have been employed to control movement Zhang et al. (2007), however the majority are intended for Spinal Cord Injury (SCI) subjects, which is reflected in the number of approaches focused on the lower limb. Contributing factors to the far greater number of FES schemes available for the lower limb are the simplicity of the musculo-skeletal system compared with the upper limb and the relative ease of muscle selectivity and recruitment. Examples include optimal, $\mathcal{H}_\infty$, and fuzzy control of standing, sliding mode control of shank movement, data-driven control of the knee joint and multichannel PID control of the wrist. References to this work are given in Freeman et al. (2012).

Advanced techniques, such as those referenced above, have rarely transferred to clinical practice, especially in the case of stroke rehabilitation, where the strategies adopted are either open-loop, or the stimulation is triggered using limb position or Electromyographic (EMG) signals to provide a measure of the participant's intended movement. Closed-loop control has been achieved using EMG but this has not been incorporated in model-based controllers since EMG does not directly relate to the force or torque generated by the muscle. In the few cases where model-based control approaches have been used clinically, they have enabled a far higher level of tracking accuracy. The reasons for this are discussed in Freeman et al. (2012) with supporting references.

A principal reason for the lack of model-based methods finding application in a program of patient trials is the difficulty in obtaining reliable biomechanical models. In the clinical setting there is minimal set-up time, reduced control over environmental constraints and little possibility of repeating any one test in the program of treatment undertaken; control laws are required to perform to a minimum standard on a wide number of subjects and conditions. Moreover, the underlying musculo-skeletal system is highly sensitive to physiological conditions, including skin impedance, temperature, moisture and electrode placement, in addition to time-varying effects such as spasticity and fatigue (Baker et al. 1993). These problems are often exacerbated in the case of stroke because hemiplegic subjects exhibit both voluntary and involuntary responses to applied stimulation. The small number of model-based approaches that have been used in stroke rehabilitation therefore provide limited scope to adapt the applied stimulation to changes in the underlying system due to fatigue

or spasticity, leading to reduction in performance and an inability to fully exploit the therapeutic potential.

This monograph describes the application of ILC in stroke rehabilitation, including clinical trials that constitute the first major stage towards eventual transfer into practice. In contrast to the other approaches employed to control FES, ILC exploits the repeating nature of the patient's tasks in order to improve performance by learning from past experience. By updating the control input using data collected over previous attempts at the task, ILC is able to respond to physiological changes in the system, such as spasticity and the presence of the patient's voluntary effort, which would otherwise erode performance. Use of ILC can also closely regulate the amount of stimulation supplied, ensuring that minimum assistance is provided, thereby promoting the patient's maximum voluntary contribution to the task completion. As the treatment progresses this control action encourages patients to exert increasing voluntary effort with each trial, leading to a corresponding decrease in the level of FES applied.

The first research in this area concentrated on a planar problem that replicates the every day task of reaching out across a table top to, for example, a cup, where the aim was to establish the basic feasibility of using ILC in this setting. Figure 3.1 shows a stroke patient using the system designed for this purpose. More complicated tasks, such as reaching out and then lifting the arm are described in later chapters.

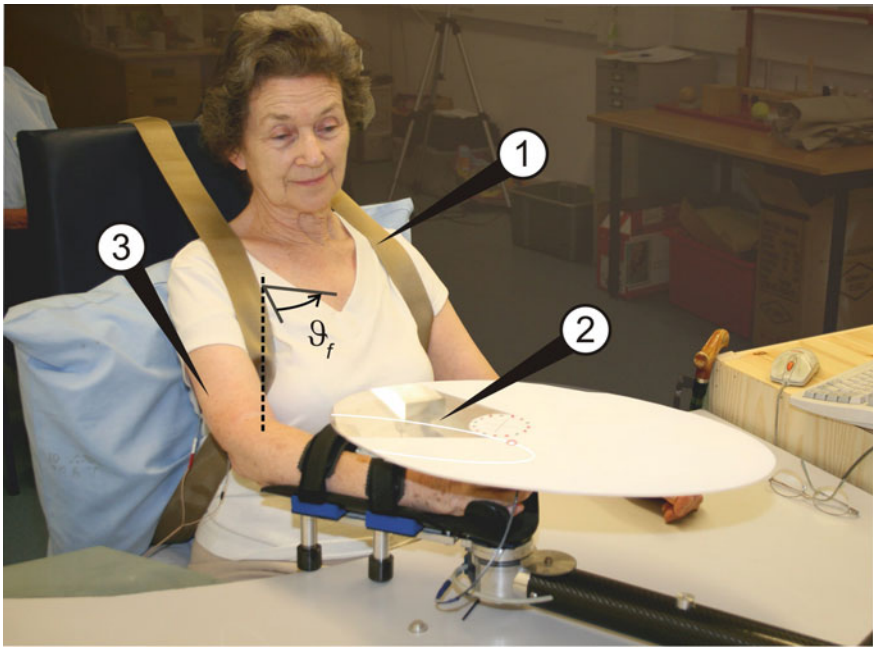

Fig. 3.1 A frontal view of a patient using the planar robotic workstation: showing (*1*) shoulder strapping, (*2*) tracking task, and (*3*) surface electrodes

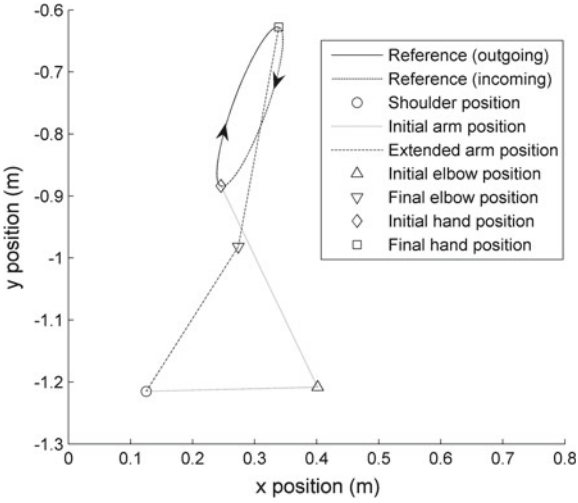

Fig. 3.2 Plan view of the patient's movement in the planar case

The patient in this figure is seated with her impaired arm supported by the robot and elliptical trajectories are projected onto a target above the hand. Also FES is applied to her triceps, using the surface electrodes, in order to assist tracking of a point that moves along the reference trajectory. At the end of the task, the arm is returned to the starting position in preparation for the next trial. During the reset time, plus a rest time to prevent muscle fatigue and allow transients to decay, an ILC law is used to calculate the stimulation to be applied on the next trial. The stimulation applied to the triceps muscle produces a torque about the elbow and the control problem is equivalent to controlling the angle ϑ_f in this figure. The shoulder strapping is to prevent forward movement by the patient's trunk during the trials, which would conflict with the desired objective of reaching out with the arm.

Figure 3.2 shows a plan view of the patient's movement in the planar case where the analogy with the pick and place operation for an industrial robot discussed in the previous chapter is clear. During the arm resetting time at the end of trial k, the ILC law uses a biomechanical model of the arm and muscle system, along with the previous tracking error, to produce the control signal, i.e., the FES, for application on the next trial.

The assessment of the results from clinical trials in this area must be based on the measures used by healthcare professionals. These are described below and the next chapter describes the ILC law design for this task and gives the results from a clinical trial.

3.2 Measurement in Neurorehabilitation

The purpose of measurement is two-fold. Firstly to design therapy (to make initial decisions and decide changes to therapy programmes) and secondly to measure progress. The World Health Organisation's International Classification of Function-

ing, Disability and Health (ICF) is a framework for measuring both health and disability (WHO 2001). It consists of domains that are 'health' and 'health related' described by two lists: body functions and structures, and activity and participant. Impairments are defined as problems in body function or structure, such as a significant deviation or loss, whereas activity is the execution of a task or action by an individual and participation is involvement in a life situation (society).

Active assisted or partially facilitated exercises are recommended for stroke patients who are unable to move by themselves (Jackson 2004). To measure the effectiveness of such techniques, healthcare professionals are more likely to use activity or participant based outcome measures that explain how effective an intervention has been. These may be more relevant to the patient than impairment based measures that normally require more equipment.

3.2.1 Validated Clinical Outcome Measures

Healthcare professionals conventionally use standardized validated clinical outcome measures to address changes in body functions and structures, or activities. There is little consensus within the literature regarding the best motor performance outcome measure for stroke patients, although it has been suggested that trials should use valid instruments that measure upper limb skills specifically, such as the Action Research Arm Test (ARAT) or Structural Myofascial Therapy (SMFT), to assess improvement in activities of daily living (Kwakkel et al. 2008a).

In the research described in this monograph, the primary measure for upper limb function is the ARAT (Carroll 1965). Movement, coordination and sensation of the upper limb have also been measured using the Fugl-Meyer Assessment (FMA) (Fugl-Meyer et al. 1975). Both of these measures are valid and reliable measures of post stroke function and impairments. Moreover, both of these ordinal measures have been extensively used in the clinical robotic and FES literature, but still have limitations including floor and ceiling effects, experimenter bias and inter-rater reliability across clinical trial sites. The ARAT was developed to monitor function related to every-day tasks and uses a hierarchical measure of grasp, grip, pinch and gross movement, where the reaching and grasping movements are rated on quality and speed in three dimensions. Also ARAT assesses primarily activity limitations, i.e., a patient's functional loss when interacting with the environment by means of the upper limb.

The FMA (Fugl-Meyer et al. 1975) primarily assesses changes in upper limb impairment in terms of loss or abnormality of movement, i.e., the ability to perform movements in accordance with specified joint motion pattern. It is an ordinal scale testing gross movement, coordination and sensation of the upper limb. The motor part of the scale scores a maximum of 66 points: section A (shoulder, elbow and forearm 36 points,), B (wrist 10 points), C (hand 14 points) and D (co-ordination/speed 6 points). The test is appropriate for severe to mildly affected patients and provides an adequate, reproducible and fairly standardized picture of a patient's sensorimotor

and joint characteristics. In terms of resolution, the FMA could, in contrast to the ARAT, detect differences throughout the spectrum of motor dysfunction of the study population and is less affected by floor or ceiling effects.

3.2.2 Robotic Measurements and Their Limitations

Robot-generated and other technology-based measures can measure new and potentially useful variables in upper limb neurorehabilitation including quality of movement, kinematic, kinetic, muscle activity, psychomotric and effort measures. Additionally, it has been suggested that the coarse nature of clinical outcome measures fails to show detail important for optimizing therapy (Krebs et al. 2000). The use of robots could address some of the limitations of the clinical scales through: increased sensitivity to change to detect changes not sufficiently large to be picked up by the clinical scales; reducing the subjective nature of the scoring; providing a direct measure of the support being provided and offering more frequent monitoring to detect changes in function during the intervention than the conventional clinical assessments.

References

Baker LL, McNeal DR, Benton LA, Bowman BR, Waters RL (1993) NeuroMuscular electrical stimulation: a practical guide, 3rd edn. Rancho Rehabilitation Engineering Program, Rancho Los Amigos Medical Centre

Burridge JH, Hughes A-M (2010) Potential for new technologies in clinical practice. Curr Opin Neurol 23:671–677

Burridge JH, Ladouceur M (2001) Clinical and therapeutic applications of neuromuscular stimulation: A review of current use and speculation into future developments. Neuromodulation 4(4):147–154

Carroll D (1965) A quantitative test for upper extremity function. J Chronic Disabil 18:479–491

de Kroon JR, van der Lee JH, Izerman MJ, Lankhorst GJ (2002) Therapeutic electrical stimulation to improve motor control and functional abilities of the upper extremity after stroke: a systematic review. Clin Rehabil 16:350–360

de Kroon JR, Ijzerman MJ, Lankhorst GJ, Zilvold G (2005) Relation between stimulation characteristics and clinical outcome in studies using electrical stimulation to improve motor control of upper extremity in stroke. J Rehabil Med 35:65–74

Denti L, Agosti M, Franceshini M (2008) Outcome predictors of rehabilitation for first stroke in the elderly. Eur J Phys Rehabil Med 44:3–11

Freeman CT, Rogers E, Hughes A-M, Burridge JH, Meadmore KL (2012) Iterative learning control in health care: electrical stimulation and robotic-assisted upper-limb stroke rehabilitation. IEEE Control Syst Mag 32(1):18–43

Fugl-Meyer AR, Jaasko L, Leyman I, Olsson S, Steglind S (1975) The post-stroke hemiplegic patient. 1. a method for evaluation of physical performance. Scand J Rehabil Med 7:13–31

Hong KS, Saver J (2009) Quantifying the value of stroke disability outcomes: WHO global burden of disease project disability weights for each level of the modified Rankin scale. Stroke 4:3828–3833

Intercollegiate working Party for Stroke. National clinicial guidelines for stroke (2004) Royal College of Physicians
International Classification of Functioning, Disability and Health (ICF) (2001) World Health Organisation
Jackson J (2004) Specific treatment techniques. In: Stokes M (ed) Physical management in neurological rehabilitation. Elsevier, Edinburgh
Krebs HI, Volpe BT, Aisen ML, Hogan N (2000) Increasing productivity and quality of care: robotic-aided neuro-rehabilitation. J Rehabil Res Dev 37(6):639–652
Kwakkel G, Kollen B, Krebs HI (2008a) Effects of robot-assisted therapy on upper limb recovery after stroke: a systematic review. Stroke 34:2181–2186
Kwakkel G, Kollen BJ, Krebs HI (2008b) Effects of robot-assisted therapy on upper limb recovery after stroke: a systematic review. Neurorehabil Neural Repair 22:111–121
Langhorne P, Bernhardt J, Kwakkel G (2011) Stroke rehabilitation. Lancet 377:1693–702
Morris JH, Van Wijc F, Joice S, Donaghy M (2013) Predicting health related quality of life 6 months after stroke: the role of anxiety and upper limb dysfunction. Disabil Rehabil 35(4):291–299
Murray CJL et al (2012) Disability-adjusted life years (DALYs) for 291 diseases and injuries in 21 regions, 1990–2010: a systematic analysis for the Global Burden of Disease Study 2010. Lancet 380:2197–2223
Pomeroy VM, King L, Pollack A, Baily-Hallon A, Longhorne P (2006) Electrostimulation for promoting recovery of movement or functional ability after stroke. Cochrane Database Syst Rev Issue 2, Art. No.: CD003241. doi:10.1002/14651858.CD003241.pub2
Prange GB, Jannick MA, Groothuis-Oudshoorn CGM, Hermens M, Ijzerman MJ (2006) Systematic review of the effect of robot-aided therapy on recovery of the hemiparetic arm after stroke. J Rehabil Res Dev 43:171–184
Rushton DN (2003) Functional electrical stimulation and rehabilitation—an hypothesis. Med Eng Phys 1:75–78
Saka O, McGuire A, Wolfe C (2009) Cost of stroke in the United Kingdom. Age Ageing 38:27–32
Stroke Association (2015). Available from https://www.stroke.org.uk/resources/state-nation-stroke-statistics
Zhang D, Guan TH, Widjaja F, Ang WT (2007) Functional electrical stimulation in rehabilitation engineering: a survey. In: Proceedings of the international conference on rehabilitation engineering and assistive technology, pp 221–226

Chapter 4
ILC Based Upper-Limb Rehabilitation—Planar Tasks

This chapter details how an ILC based system for planar tasks has been developed to the stage of a small scale clinical trial. The results of tests conducted on 18 unimpaired volunteers who do not provide voluntary effort are given. These results contributed to the granting of ethical approval for the clinical trial with 5 stroke patients.

4.1 Robot Design

Several robotic devices for the application of robotic therapy to stroke patients through purely mechanical manipulation of their arms, such as the MIT Manus (Krebs et al. 1998) and GENTLE/s systems (Loureiro et al. 2004), have been developed but this form of treatment has hitherto not been combined with the application of FES (or ILC). To provide a controlled environment in which to apply stimulation an experimental test facility incorporating a five-link planar robotic arm and an overhead trajectory projection system has been developed. The patient is seated with their arm strapped to the robot, and the trajectory is projected onto a target mounted above their hand. In operation, a light spot moves along this trajectory and on each trial the task for the patient is to track the progression of this spot using a combination of voluntary control and surface FES applied to muscles in the impaired shoulder and arm. During the trials, the robotic arm provides control over the dynamics experienced by the patient and produces an assistive torque when necessary.

The robotic workstation developed is shown in Fig. 4.1 (Freeman et al. 2009a). In this setting, the links of the robot are labeled 1–5, and the upper arm and forearm are labeled u and f respectively. The vectors $\boldsymbol{x}_0$, $\boldsymbol{y}_0$ and $\boldsymbol{z}_0$ are components of the robotic base coordinate frame and $\boldsymbol{x}_1$, $\boldsymbol{y}_1$ and $\boldsymbol{z}_1$ are those of the human arm base coordinate frame, the two systems being related by a translation. Two coaxially mounted DC brushless motors actuate links 1 and 2 and a 4000-line encoder is mounted on each motor shaft to record the angle of these links. The patient is strapped to the extreme fifth link and grips a cushioned handle which is rigidly connected to

C.T. Freeman et al., *Iterative Learning Control for Electrical Stimulation and Stroke Rehabilitation*, SpringerBriefs in Control, Automation and Robotics, DOI 10.1007/978-1-4471-6726-6_4

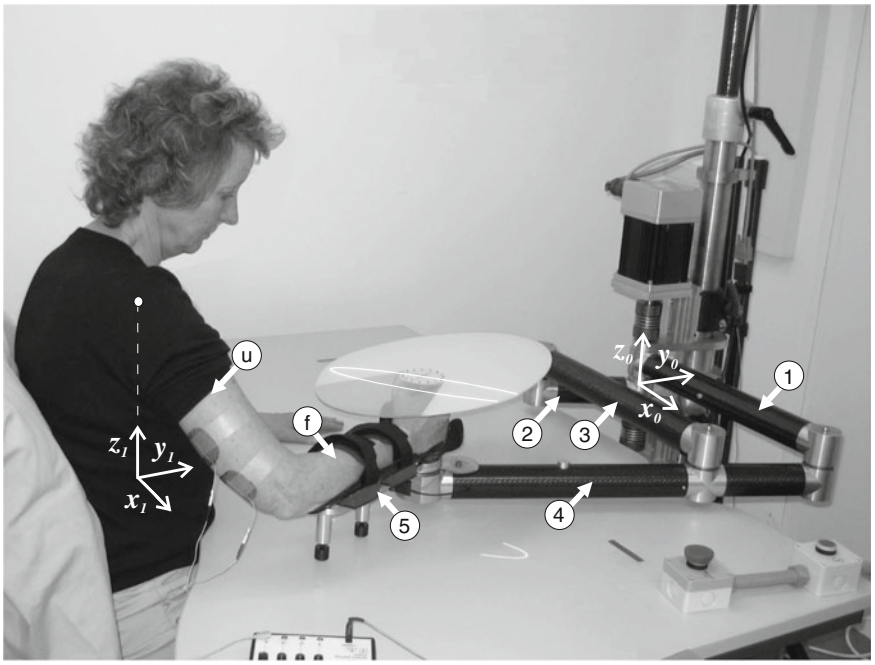

Fig. 4.1 Unimpaired subject using the robotic workstation

a 6 axis force/torque sensor, which records the force they apply to the robotic end effector.

Forces of up to 200 N applied in the horizontal plane can be measured with a resolution of 0.0122 N. The fifth link also contains a 4000-line encoder to measures its angle and Light Emitting Diodes (LEDs) to provide visual feedback of the tracking performance. The robotic arm is used to constrain the patient's arm, to impose forces on the end-effector that make the task feel 'natural' to the patient, to apply assistance during the performance of tracking tasks and to move the patient's arm when necessary. During a treatment session, the patient's task is to track a range of trajectories that are projected onto a target positioned above their hand. All tests are controlled using a graphical user interface running on the host PC.

Figure 4.2 shows the geometry of the dual human and robotic system. The robot joint angle vector is $\boldsymbol{q}_r = [\vartheta_1 \ \vartheta_2]^T$, where ϑ_1 and ϑ_2 are the joint angles corresponding to links 1 and 2 respectively. Moreover, the axes of all the robot joints are parallel to z_0, and the links are labeled to correspond with Fig. 4.1. Also the torque supplied by the motors is given by $\boldsymbol{\tau}_r = [\tau_1 \ \tau_2]^T$, where τ_1 and τ_2 are applied to actuate joints 1 and 2 respectively.

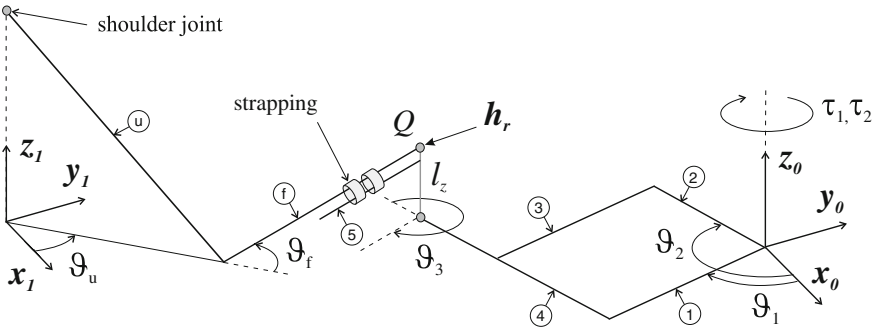

Fig. 4.2 Geometry of combined human arm and robotic arm system

It is assumed that the patient interacts with the robot by applying a vector of forces and torques at the point Q, which has a z_0 component of l_z. This corresponds to the vertical distance of the patient's hand above the force/torque sensor. The vector of the components of these forces applied in the $\boldsymbol{x}_0$ and $\boldsymbol{y}_0$ directions is given by $\boldsymbol{h}_r$. The patient's arm is strapped to the fifth link of the robot and the human arm model therefore includes the properties of this link, which will not be included in the model of the robot. To ensure the robot's safe interaction with an unknown environment, a form of impedance control, detailed in Colgate and Hogan (1988), is used to govern the torque demand supplied to the motors. This strategy has previously been used to control robotic therapy devices (Krebs et al. 1998), although alternative approaches could be used, such as force or compliant control, e.g., Siciliano and Villani (1999).

The controller compensates for the inertial and damping properties of the robotic arm and at point Q, yields dynamics

$$\boldsymbol{h}_r = \boldsymbol{K}_{K_x}\tilde{\boldsymbol{x}}_r + \boldsymbol{K}_{B_x}\dot{\tilde{\boldsymbol{x}}}_r + \boldsymbol{K}_{M_x}\ddot{\tilde{\boldsymbol{x}}}_r \tag{4.1}$$

where $\hat{\boldsymbol{x}}_r$ is the reference position, $\tilde{\boldsymbol{x}}_r = \hat{\boldsymbol{x}}_r - \boldsymbol{x}_r$, $\boldsymbol{x}_r = \boldsymbol{k}_r(\boldsymbol{q}_r)$, $\dot{\boldsymbol{x}}_r = \boldsymbol{J}_r(\boldsymbol{q}_r)\dot{\boldsymbol{q}}_r$ and $\ddot{\boldsymbol{x}}_r = \boldsymbol{J}_r(\boldsymbol{q}_r)\ddot{\boldsymbol{q}}_r + \dot{\boldsymbol{J}}_r(\boldsymbol{q}_r, \dot{\boldsymbol{q}}_r)\dot{\boldsymbol{q}}_r$. Also the direct kinematics equation for the robotic system is $\boldsymbol{x}_r = \boldsymbol{k}_r(\boldsymbol{q}_r)$ and $\boldsymbol{J}_r^T(\boldsymbol{q}_r)$ is the Jacobian of this system. When the robot is moved freely by the patient in the absence of assistance, the gain matrices are set as $\boldsymbol{K}_{K_x} = \boldsymbol{0}$, $\boldsymbol{K}_{B_x} = K_{B_x}\boldsymbol{I}$ and $\boldsymbol{K}_{M_x} = K_{M_x}\boldsymbol{I}$, where $\boldsymbol{I}$ is the identity matrix of compatible dimensions. The values of $K_{B_x} > 0$ and $K_{M_x} > 0$ are tuned to create a 'natural' feel, and an additional requirement is that $\hat{\boldsymbol{x}}_r$ has constant value. Moreover, the robot is required to move the patient's arm along predefined trajectories. Hence it is necessary to set $\boldsymbol{K}_{K_x} = K_{K_x}\boldsymbol{I}$ with $K_{K_x} > 0$ and the three gains tuned to produce the required tracking performance. Gain matrix selection for the case where the robot applies assistance during tracking tasks is described below.

4.2 Human Arm Model

In this section a mathematical description of the patient's arm is derived, consisting of a model of the passive dynamical system to which the torque generating properties of the stimulated muscle is then added. This section is based on research reported in Freeman et al. (2007, 2009b).

4.2.1 Passive System

Figure 4.3 gives a more detailed description of the geometry of the constrained human arm model of Fig. 4.2, where the first link represents the upper arm, from the shoulder joint to the elbow, with length $(l_{u1}+l_{u2})$ and the second represents the forearm, from the elbow to the thumb web, with length $(l_{f1}+l_{f2})$. The constraint means that the forearm must lie in the horizontal plane and rotation is possible about the axis along the upper arm. Point Q denotes where the patient's hand grasps the robot and only forces and torques along unconstrained directions are shown (only rotation about the axis parallel to $\boldsymbol{z}_1$ is unconstrained at this point, rotation is not possible about the two orthogonal axes). The triceps muscle has been selected for stimulation since stroke patients typically experience problems with shoulder and elbow extension during reaching tasks (Lum et al. 2004).

Actuation of the triceps muscle is modeled as a torque, $T_\beta \geq 0$, acting about an axis orthogonal to both the upper arm and forearm. Components of the forces in the $\boldsymbol{x}_1$ and $\boldsymbol{y}_1$ directions applied by the patient's hand at the point of interaction with the robot are denoted by F_{x_1} and F_{y_1} respectively. A point, $\boldsymbol{x}_r$, in the robot coordinate system is expressed in the human arm system by a point, $\boldsymbol{x}_a$, such that

$$\boldsymbol{x}_r = \boldsymbol{x}_a + \begin{bmatrix} l_x & l_y & l_z \end{bmatrix}^T \tag{4.2}$$

where l_x and l_y represent the $\boldsymbol{x}_0$ and $\boldsymbol{y}_0$ components, respectively, of the shoulder joint position in the robot coordinate system.

If $\boldsymbol{V}_u$ and $\boldsymbol{V}_f$ are vectors aligned along the upper arm and forearm, respectively, the horizontal constraint requires that $\boldsymbol{V}_f$ has a $\boldsymbol{z}_1$ component of zero. In this case the unitary axis about which T_β is applied is given by

$$\boldsymbol{V}_e = \frac{\boldsymbol{V}_u \times \boldsymbol{V}_f}{|\boldsymbol{V}_u \times \boldsymbol{V}_f|} = \frac{1}{\sqrt{1-c_f^2 c_\gamma^2}} \begin{bmatrix} -s_{uf}s_\gamma & c_{uf}s_\gamma & -s_f c_\gamma \end{bmatrix}^T \tag{4.3}$$

where c_f and c_γ denote $\cos(\vartheta_f)$ and $\cos(\gamma)$, respectively. Similarly, s_f and s_γ denote $\sin(\vartheta_f)$ and $\sin(\gamma)$. In addition, c_u and s_u are used to denote $\cos(\vartheta_u)$ and $\sin(\vartheta_u)$, respectively, and s_{uf} and c_{uf} denote $\sin(\vartheta_u+\vartheta_f)$ and $\cos(\vartheta_u+\vartheta_f)$, respectively. For arbitrary γ, $\boldsymbol{V}_e$ has a $\boldsymbol{z}_1$ component of zero when $\vartheta_f = 0$ and is given by

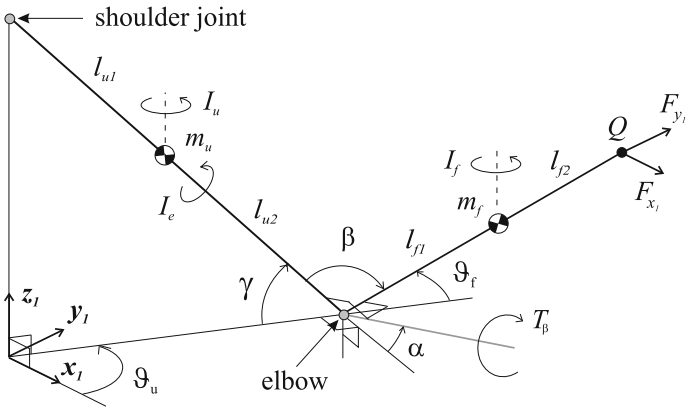

Fig. 4.3 Geometry of constrained human arm

$$\hat{\boldsymbol{V}}_e = \begin{bmatrix} -s_u & c_u & 0 \end{bmatrix}^T \tag{4.4}$$

As ϑ_f increases, the angle that $\boldsymbol{V}_e$ rotates about the upper arm, starting from $\hat{\boldsymbol{V}}_e$, is given by

$$\alpha(\vartheta_f) = \arccos\left(\frac{\boldsymbol{V}_e \cdot \hat{\boldsymbol{V}}_e}{|\boldsymbol{V}_e||\hat{\boldsymbol{V}}_e|}\right) = \arccos\left(\frac{c_f s_\gamma}{\sqrt{1 - c_f^2 c_\gamma^2}}\right) \tag{4.5}$$

The elbow angle is equal to

$$\beta(\vartheta_f) = \arccos\left(\frac{\boldsymbol{V}_u \cdot \boldsymbol{V}_f}{|\boldsymbol{V}_u||\boldsymbol{V}_f|}\right) = \arccos\left(-c_f c_\gamma\right) \tag{4.6}$$

and the dynamic model of the constrained arm can be written in the form

$$\boldsymbol{B}_a(\boldsymbol{q}_a)\ddot{\boldsymbol{q}}_a + \boldsymbol{C}_a(\boldsymbol{q}_a, \dot{\boldsymbol{q}}_a)\dot{\boldsymbol{q}}_a + \boldsymbol{F}_a(\boldsymbol{q}_a, \dot{\boldsymbol{q}}_a) = \boldsymbol{\tau_a} - \boldsymbol{J}_a^T(\boldsymbol{q}_a)\boldsymbol{h}_a \tag{4.7}$$

where $\boldsymbol{q}_a = [\vartheta_u \ \vartheta_f]^T$, $\boldsymbol{\tau}_a = \begin{bmatrix} 0 & T_\beta \frac{-s_f c_\gamma}{\sqrt{1-c_f^2 c_\gamma^2}} \end{bmatrix}^T$, $\boldsymbol{h}_a = [F_{x_1} \ F_{y1}]^T$ and the remaining terms are

$$\boldsymbol{B}_a(\boldsymbol{q}_a) = \begin{bmatrix} b_{a1} & b_{a2} \\ b_{a2} & b_{a3} \end{bmatrix}, \quad \boldsymbol{C_a}(\boldsymbol{q}_a, \dot{\boldsymbol{q}}_a) = \begin{bmatrix} -2c_{a1}\dot{\vartheta}_f & -c_{a1}\dot{\vartheta}_f \\ c_{a1}\dot{\vartheta}_u & c_{a2}\dot{\vartheta}_f \end{bmatrix} \tag{4.8}$$

$$\boldsymbol{J}_a^T(\boldsymbol{q}_a) = \begin{bmatrix} -(l_{u1}+l_{u2})c_\gamma s_u - (l_{f1}+l_{f2})s_{uf} & (l_{u1}+l_{u2})c_\gamma c_u + (l_{f1}+l_{f2})c_{uf} \\ -(l_{f1}+l_{f2})s_{uf} & (l_{f1}+l_{f2})c_{uf} \end{bmatrix} \tag{4.9}$$

with

$$\begin{aligned} b_{a1} &= m_u(l_{u1}c_\gamma)^2 + I_u + m_f(l_{f1}^2 + ((l_{u1}+l_{u2})c_\gamma)^2 \\ &\quad + 2(l_{u1}+l_{u2})c_\gamma l_{f1}c_f) + I_f \\ b_{a2} &= m_f(l_{f1}^2 + (l_{u1}+l_{u2})c_\gamma l_{f1}c_f) + I_f \\ b_{a3} &= m_f l_{f1}^2 + I_f + I_e\left(\frac{s_\gamma}{1-c_f^2c_\gamma^2}\right)^2 \\ c_{a1} &= m_f(l_{u1}+l_{u2})c_\gamma l_{f1}s_f, \quad c_{a2} = -2I_e\left(\frac{s_\gamma^2 c_\gamma^2 c_f s_f}{(1-c_f^2c_\gamma^2)^3}\right) \end{aligned} \tag{4.10}$$

The relationship $\boldsymbol{h}_a = -\boldsymbol{h}_r$ is a consequence of the connection between the robotic and human arm systems. Various forms of the friction term $\boldsymbol{F}_a(\boldsymbol{q}_a, \dot{\boldsymbol{q}}_a)$ have been considered to achieve a compromise between repeatability and the accuracy of the overall model. The most general form considered is

$$\boldsymbol{F}_a(\boldsymbol{q}_a, \dot{\boldsymbol{q}}_a) = \begin{bmatrix} F_{a1}(\vartheta_u, \dot{\vartheta}_u) & F_{a2}(\vartheta_f, \dot{\vartheta}_f) \end{bmatrix}^T \tag{4.11}$$

where $F_{a1}(\cdot)$ and $F_{a2}(\cdot)$ are piecewise linear functions.

4.2.2 Muscle Model

To account for the action of the triceps, an established model of the torque, T_β, generated by electrically stimulated muscle acting about a single joint is given by

$$T_\beta(\beta, \dot{\beta}, u, t) = g(u, t) \times F_{ma}(\beta, \dot{\beta}) + F_{mp}(\beta, \dot{\beta}) \tag{4.12}$$

where u denotes the stimulation pulsewidth applied and β is the joint angle (Shue et al. 1995). In this model a Hammerstein structure incorporating a static non-linearity, $h_{IRC}(u)$, representing the isometric recruitment curve, cascaded with linear activation dynamics, $h_{LAD}(t)$, produces the first term, $g(u, t)$. The activation dynamics can be adequately captured using a critically damped second order system as described in, e.g., Baratta and Solomonow (1990), the term $F_{ma}(\beta, \dot{\beta})$ models the multiplicative effect of the joint angle and joint angular velocity on the active torque developed by the muscle and the term $F_{mp}(\beta, \dot{\beta})$ accounts for the passive properties of the joint.

Given that γ is invariant, (4.6) means that $F_{mp}(\beta, \dot{\beta})$ is accounted for by the most general form of $\boldsymbol{F}_a(\boldsymbol{q}_a, \dot{\boldsymbol{q}}_a)$ considered. Hence additional forms of friction are not added to the existing model. Details of the procedures used to establish the parameters of the muscle model given above are detailed in Freeman et al. (2007) and further results on the use of system identification to determine a model for the muscle response can be found in Le et al. (2010, 2012).

4.2.3 Robotic Assistance and Trajectory Choice

The action of the robotic arm necessary to make the task a feasible yet productive one is the subject of this section, where the following points concern the choice of trajectory and role of the robot during task completion:

1. The trajectories will be elliptical reaching tasks for each patient's dominant arm and should be achievable given their identified arm model.
2. The triceps muscle will provide the only actuating torque about the elbow and the robotic arm will use the control action given by (4.1) to make the dynamics about the elbow feel 'natural' to the patient.
3. The robotic arm will provide a torque acting about the patient's shoulder to track the reference in a manner entirely governed by the angle of the forearm, which makes the task feasible without lessening the role played by the triceps.

The development of the robotic control scheme to achieve these goals is described next.

4.2.4 Robotic Control Scheme

Combining the human arm model described by (4.7) and the end effector dynamics (4.1) gives

$$\boldsymbol{B}_a(\boldsymbol{q}_a)\ddot{\boldsymbol{q}}_a + \boldsymbol{C}_a(\boldsymbol{q}_a, \dot{\boldsymbol{q}}_a)\dot{\boldsymbol{q}}_a + \boldsymbol{F}_a(\boldsymbol{q}_a, \dot{\boldsymbol{q}}_a) = \boldsymbol{\tau}_a + \boldsymbol{J}_a^T(\boldsymbol{q}_a)\left(\boldsymbol{K}_{K_x}\tilde{\boldsymbol{x}}_a + \boldsymbol{K}_{B_x}\dot{\tilde{\boldsymbol{x}}}_a + \boldsymbol{K}_{M_x}\ddot{\tilde{\boldsymbol{x}}}_a\right) \quad (4.13)$$

where $\hat{\boldsymbol{x}}_a = \hat{\boldsymbol{x}}_r - [l_x \; l_y \; l_z]^T$ has been enforced to give $\tilde{\boldsymbol{x}}_a = \tilde{\boldsymbol{x}}_r$. To separate the dynamics of the end-effector in the directions corresponding to the human arm joint angles, requires

$$\boldsymbol{K}_{K_x}\tilde{\boldsymbol{x}}_a + \boldsymbol{K}_{B_x}\dot{\tilde{\boldsymbol{x}}}_a + \boldsymbol{K}_{M_x}\ddot{\tilde{\boldsymbol{x}}}_a = \boldsymbol{J}_a^{-T}(\boldsymbol{q}_a)\left(\boldsymbol{K}_{K_q}\tilde{\boldsymbol{q}}_a + \boldsymbol{K}_{B_q}\dot{\tilde{\boldsymbol{q}}}_a + \boldsymbol{K}_{M_q}\ddot{\tilde{\boldsymbol{q}}}_a\right) \quad (4.14)$$

where $\tilde{\boldsymbol{q}}_a = \hat{\boldsymbol{q}}_a - \boldsymbol{q}_a$ and $\hat{\boldsymbol{q}}_a = \boldsymbol{k}_a^{-1}(\hat{\boldsymbol{x}}_a)$. Hence

$$\boldsymbol{B}_a(\boldsymbol{q}_a)\ddot{\boldsymbol{q}}_a + \boldsymbol{C}_a(\boldsymbol{q}_a, \dot{\boldsymbol{q}}_a)\dot{\boldsymbol{q}}_a + \boldsymbol{F}_a(\boldsymbol{q}_a, \dot{\boldsymbol{q}}_a) = \boldsymbol{\tau}_a + \boldsymbol{K}_{K_q}\tilde{\boldsymbol{q}}_a + \boldsymbol{K}_{B_q}\dot{\tilde{\boldsymbol{q}}}_a + \boldsymbol{K}_{M_q}\ddot{\tilde{\boldsymbol{q}}}_a \quad (4.15)$$

and to satisfy the requirements of points 2 and 3 above requires

$$\boldsymbol{K}_{K_q} = \begin{bmatrix} K_{K_1} & 0 \\ 0 & 0 \end{bmatrix}, \quad \boldsymbol{K}_{B_q} = \begin{bmatrix} K_{B_1} & K_{B_2} \end{bmatrix}$$
$$\boldsymbol{K}_{M_q} = \begin{bmatrix} K_{M_1} & 0 \\ 0 & K_{M_2} \end{bmatrix} \quad (4.16)$$

with $\hat{\boldsymbol{q}}_a = \begin{bmatrix} \hat{\vartheta}_u & c \end{bmatrix}^T$, where c is a constant and $K_{K_1}, K_{B_1}, K_{B_2}, K_{M_1}, K_{M_2} \geq 0$. This allows a choice of arbitrary second order dynamics to be imposed about the shoulder and the damping and inertia about the elbow to be prescribed.

The right-hand side of (4.15) now is

$$\boldsymbol{\tau}_a + \begin{bmatrix} K_{K_1}\tilde{\vartheta}_u + K_{B_1}\dot{\tilde{\vartheta}}_u + K_{M_1}\ddot{\tilde{\vartheta}}_u \\ -K_{B_2}\dot{\vartheta}_f - K_{M_2}\ddot{\vartheta}_f \end{bmatrix}$$

and gives the required dynamic relationship for both components of the torque on the assumption that $\hat{\vartheta}_f = c$ and therefore $\dot{\hat{\vartheta}}_f = \ddot{\hat{\vartheta}}_f = 0$. This last assumption is unsuitable for the desired references and hence this control scheme is not appropriate for the intended tracking task. Alternatively, assuming that $\dot{\hat{\vartheta}}_u$ and $\ddot{\hat{\vartheta}}_u$ are sufficiently small, the controller can still provide asymptotic stability to externally applied forces if the right-hand side of (4.15) is

$$\boldsymbol{\tau}_a + \begin{bmatrix} K_{K_1}\tilde{\vartheta}_u - K_{B_1}\dot{\vartheta}_u - K_{M_1}\ddot{\vartheta}_u \\ -K_{B_2}\dot{\vartheta}_f - K_{M_2}\ddot{\vartheta}_f \end{bmatrix}$$

This last requirement is satisfied if $\hat{\boldsymbol{q}}_a = \begin{bmatrix} \hat{\vartheta}_u & \hat{\vartheta}_f \end{bmatrix}^T$ and (4.1) is replaced by

$$\boldsymbol{h}_r = \boldsymbol{K}_{K_x}\tilde{\boldsymbol{x}}_r - \boldsymbol{K}_{B_x}\dot{\boldsymbol{x}}_r - \boldsymbol{K}_{M_x}\ddot{\boldsymbol{x}}_r \tag{4.17}$$

In this case (4.14) is replaced by

$$\boldsymbol{K}_{K_x}\tilde{\boldsymbol{x}}_a - \boldsymbol{K}_{B_x}\dot{\boldsymbol{x}}_a - \boldsymbol{K}_{M_x}\ddot{\boldsymbol{x}}_a = \boldsymbol{J}_a^{-T}(\boldsymbol{q}_a)\left(\boldsymbol{K}_{K_q}\tilde{\boldsymbol{q}}_a - \boldsymbol{K}_{B_q}\dot{\boldsymbol{q}}_a - \boldsymbol{K}_{M_q}\ddot{\boldsymbol{q}}_a\right) \tag{4.18}$$

and the required values of $\hat{\vartheta}_u$ and $\hat{\vartheta}_f$ are obtained by comparing the components of (4.18) as

$$\boldsymbol{K}_{K_x}\left(\hat{\boldsymbol{x}}_a - \boldsymbol{x}_a\right) = \boldsymbol{J}_a^{-T}(\boldsymbol{q}_a)\begin{bmatrix} K_{K_1}\left(\hat{\vartheta}_u - \vartheta_u\right) \\ 0 \end{bmatrix} = \frac{K_{K_1}\left(\hat{\vartheta}_u - \vartheta_u\right)}{(l_{u1} + l_{u2})c_\gamma s_f}\begin{bmatrix} c_{uf} \\ s_{uf} \end{bmatrix}. \tag{4.19}$$

Hence

$$\boldsymbol{K}_{K_x} = \frac{K_{K_1}\left(\hat{\vartheta}_u - \vartheta_u\right)}{\left|\hat{\boldsymbol{x}}_a - \boldsymbol{x}_a\right|(l_{u1} + l_{u2})c_\gamma s_f}\boldsymbol{I} \tag{4.20}$$

and

$$\hat{\boldsymbol{x}}_a = \boldsymbol{x}_a + \left|\hat{\boldsymbol{x}}_a - \boldsymbol{x}_a\right|\begin{bmatrix} c_{uf} \\ s_{uf} \end{bmatrix} \tag{4.21}$$

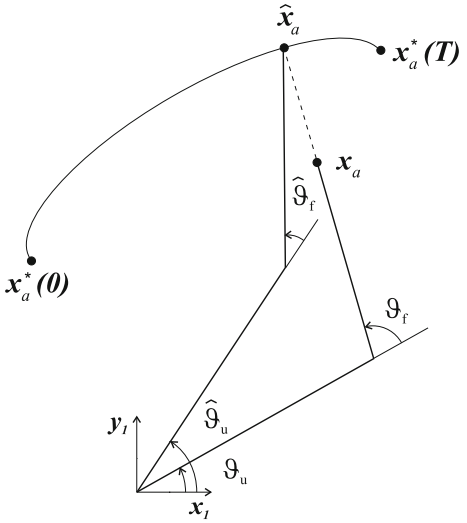

Fig. 4.4 Trajectory geometry

The above analysis shows that $\hat{\boldsymbol{x}}_a$ is not uniquely defined but can be any point lying on a line extending along the forearm and passing through $\boldsymbol{x}_a$ and to meet the tracking task it must be equal to the point of intersection with the trajectory. This requirement is illustrated in Fig. 4.4, where $\boldsymbol{x}_a^*(t) = \boldsymbol{k}_a(\boldsymbol{q}_a^*(t))$ and the trajectory is defined by

$$\boldsymbol{q}_a^*(t) = \left[\vartheta_u^*(t)\ \vartheta_f^*(t)\right]^T,\ \ 0 \le t \le T \tag{4.22}$$

Eliminating t from the components gives $\vartheta_u = \Psi(\vartheta_f)$ and the reference is defined formally as

$$\begin{gathered}\hat{\boldsymbol{x}}_a = \boldsymbol{\Omega}\left(\boldsymbol{x}_a, \Psi(\cdot)\right) := \boldsymbol{k}_a\left(\begin{bmatrix}\Psi(\hat{\vartheta}_f)\\ \hat{\vartheta}_f\end{bmatrix}\right)\\ \left|\boldsymbol{k}_a\left(\begin{bmatrix}\Psi(\hat{\vartheta}_f)\\ \hat{\vartheta}_f\end{bmatrix}\right) = \boldsymbol{x}_a + \lambda\begin{bmatrix}c_{uf}\\ s_{uf}\end{bmatrix}\right.\end{gathered} \tag{4.23}$$

where λ is a scalar.

The final control system is shown in Fig. 4.5 where, given (4.16),

$$\boldsymbol{K}_{B_x} = \boldsymbol{J}_a^{-T}(\boldsymbol{q}_a)\boldsymbol{K}_{B_q}\boldsymbol{J}_a^{-1}(\boldsymbol{q}_a) \tag{4.24}$$

and

$$\boldsymbol{K}_{M_x}\left(\boldsymbol{J}_a(\boldsymbol{q}_a)\ddot{\boldsymbol{q}}_a + \dot{\boldsymbol{J}}_a(\boldsymbol{q}_a, \dot{\boldsymbol{q}}_a)\dot{\boldsymbol{q}}_a\right) = \boldsymbol{J}_a^{-T}(\boldsymbol{q}_a)\boldsymbol{K}_{M_q} \tag{4.25}$$

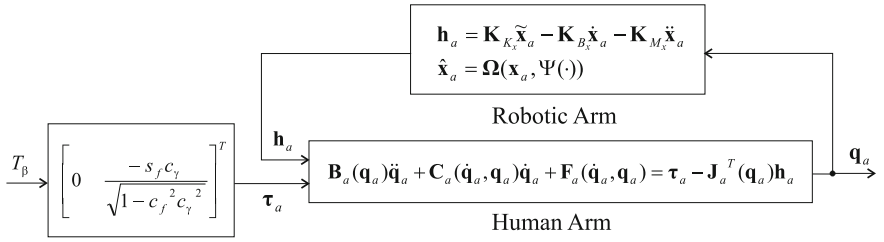

Fig. 4.5 Human arm system with robotic assistance

Also, using (4.23), (4.20) can be written explicitly as

$$\boldsymbol{K}_{K_x}(\boldsymbol{x}_a, \Psi(\cdot)) = \frac{K_{K_1}\left(\Psi(\hat{\vartheta}_f) - \vartheta_u\right)}{\lambda(l_{u1} + l_{u2})c_\gamma s_f}\boldsymbol{I} \tag{4.26}$$

4.2.5 Trajectory Selection for ILC Design

How the trajectories feel to the patient is critical and impacts on the selection of K_{B_2} and K_{M_2} as follows:

1. For $\Psi(\vartheta_f)$ to be a one-one continuous function, both $\vartheta_u^*(t)$ and $\vartheta_f^*(t)$ must be monotone.
2. With the use of robotic assistance, it is shown in Freeman et al. (2009c) that the behavior of the electrically stimulated tricep can be approximated by the system represented schematically in Fig. 4.6. The approximations invoked are based on experimentally confirmed properties of the human arm model and the ability of the robotic control system to provide accurate tracking of $\hat{\vartheta}_u$ by ϑ_u.
   Given $T_\beta \geq 0$, 1) above requires that $\vartheta_f^*(t)$ is monotonically decreasing. Moreover, given the geometry of the task shown in Fig. 4.4, this last requirement requires that the line joining $\boldsymbol{x}_a^*(T)$ and $\boldsymbol{x}_a^*(0)$ passes through the origin of the arm system, since at both these points the direction of the elliptical trajectory is orthogonal to the major axis.
3. Under the assumption that $\vartheta_f^*(t)$ is tracked perfectly, the torque that must be applied to the arm system shown in Fig. 4.6 is given by

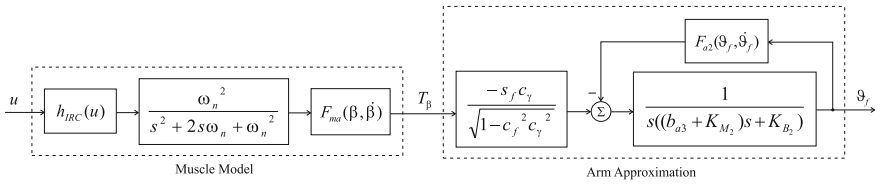

Fig. 4.6 Approximate model of the stimulated human arm

$$T^*_\beta(t) \approx \left(\frac{-\sqrt{1-c^2_{f^*(t)}c^2_\gamma}}{s_{f^*(t)}c_\gamma}\right)\Big\{K_{B_2}\dot{\vartheta}^*_f(t) + \left(K_{M_2}+b_{a3}\right)\ddot{\vartheta}^*_f(t) + F_{a2}\left(\vartheta^*_f(t), \dot{\vartheta}^*_f(t)\right)\Big\} \tag{4.27}$$

and the required stimulation, $u^*(t)$, must satisfy

$$\int_0^t h_{IRC}\left(u^*(\tau)\right) h_{LAD}\left(t-\tau\right) d\tau = \frac{T^*_\beta(t)}{F_{ma}(\beta^*(t), \dot{\beta}^*(t))} \tag{4.28}$$

where $\beta^*(t)$ corresponds to the reference trajectory such that $\beta^*(t) = \beta(\vartheta^*_f(t), t)$. This expression limits the magnitude and rate of change of any achievable torque trajectory.

In application the existence of a solution to (4.28) will be ensured by selecting slow trajectories that comprise half ellipse segments that are comfortably within both the robot's and the patient's workspace. The start and end points will be chosen such that they can be reached by a smooth extension of the elbow and individually calculated for each patient depending on their maximum reach capability. Moreover, the gains K_{B_2} and K_{M_2} are selected to: (i) mimic a realistic activity, (ii) provide a high level of stability in response to sudden stimulation inputs and (iii) to require that a moderate level of work is generated by the patient's muscles in order to track the trajectory.

The effects of these requirements on the overall control scheme will discussed later in the chapter.

4.3 Control Laws

In this section, two strategies to control the stimulation applied to the patient are developed. The first consists of a linearizing controller in a simple structure feedback arrangement and the second augments this arrangement by adding an ILC feedforward action generated by one of two laws.

4.3.1 Linearizing Control Law

The first component of this control law is $h^{-1}_{IRC}(\cdot)$, which is the inverse of the isometric recruitment curve that has been identified for each patient and the remaining action of the control law is motivated by the form of the remaining non-linear terms $-s_f c_\gamma / \sqrt{1-c^2_f c^2_\gamma}$, $F_{ma}(\beta, \dot{\beta})$ and $F_{a2}(\vartheta_f, \dot{\vartheta}_f)$ of the arm model of Fig. 4.6. The value of all three functions vary only slowly when the trajectories considered in

this chapter are followed perfectly (Freeman et al. 2007), where this conclusion is based on examining the graphs of each function using the substitutions $\vartheta_f = \vartheta_f^*(t)$, $\dot{\vartheta}_f = \dot{\vartheta}_f^*(t)$, $\beta = \beta^*(t)$ and $\dot{\beta} = \dot{\beta}^*(t)$ for the trajectories used.

The control action taken attempts to remove the effect of these functions and hence produce a system that approximates the linear activation dynamics in series with the linear arm dynamics (the transfer-functions appearing in the left and right sub-systems, respectively, of Fig. 4.6). To achieve this, the control law next applies the gain term

$$\frac{-\sqrt{1-c_f^2c_\gamma^2}}{s_f c_\gamma F_{ma}(\beta,\dot{\beta})} = \left(-s_f c_\gamma / \sqrt{1-c_f^2c_\gamma^2}\right)^{-1} \left(F_{ma}(\beta,\dot{\beta})\right)^{-1} \tag{4.29}$$

to address the multiplicative effect of the first two non-linear terms and then $F_{a2}(\vartheta_f, \dot{\vartheta}_f)$ is added to the input in order to cancel the additive effect of the third non-linear term. The linearizing control law therefore is

$$u = h_{IRC}^{-1}\left(\left(F_{a2}(\vartheta_f,\dot{\vartheta}_f)+w\right)\frac{-\sqrt{1-c_f^2c_\gamma^2}}{s_f c_\gamma F_{ma}(\beta,\dot{\beta})}\right) \tag{4.30}$$

The validity of this approach will now be investigated where, for conciseness, attention is restricted to the case where $F_{a2}(\cdot)$ and $F_{ma}(\cdot)$ are functions of their first argument only. This results in the system of Fig. 4.7 where

$$g(\vartheta_f) = \frac{-s_f c_\gamma F_{ma}(\beta(\vartheta_f))}{\sqrt{1-c_f^2c_\gamma^2}} \tag{4.31}$$

and Π denotes multiplication of inputs. In Freeman et al. (2009c) an equivalent state-space model for this system is derived, and then linearized at time $\bar{t}$. When

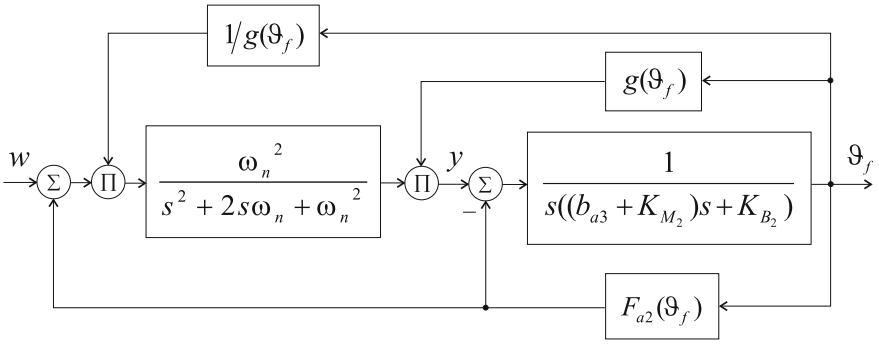

Fig. 4.7 Stimulated arm system and linearizing controller

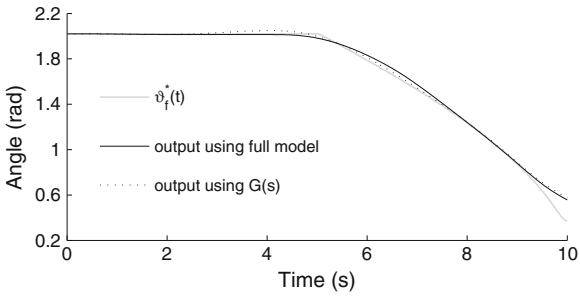

Fig. 4.8 Comparison of $G(s)$ with full arm model

the first derivatives of $F_{a2}(\vartheta_f)$ and $g(\vartheta_f)$ are zero for all t, this linearized system corresponds with the desired relationship

$$G(s) = \frac{\vartheta_f(s)}{w(s)} = \frac{\omega_n^2}{s^2 + 2s\omega_n + \omega_n^2} \cdot \frac{1}{s\left((b_{a3} + K_{M_2})s + K_{B_2}\right)} \tag{4.32}$$

To ensure that (4.32) adequately approximates the system behavior when the derivatives are non-zero, trajectories must be chosen over which $g_1(t)$, $g_2(t)$ and $F'_{a2}(\cdot)$ are small. Further analysis of the terms involving $g_1(\bar{t})$, $g_2(\bar{t})$ concludes that their effect can also be reduced by ensuring that the dynamics of the arm system are slower than the activation dynamics (Freeman et al. 2009c). This also reduces the effect of the terms involving $F'_{a2}(\vartheta_f(\bar{t}))$ and one way of confirming that this is the case is to construct Bode plots with $g_1(\bar{t}), g_2(\bar{t}) = 0$ using various values of $F'_{a2}(\vartheta_f(\bar{t}))$. The same goal could, of course, be achieved if it were possible to obtain more rapid activation dynamics from the patients using the system.

The choice of trajectories and arm dynamics must correspond to a model that is well approximated by (4.32). To verify this, simulations were conducted where the output of this system was compared with that of the linearizing control law applied to the full model shown in Fig. 4.6. The applied input, w, was chosen to result in approximate tracking of the more rapid of the demands used. Figure 4.8 shows results using the identified model parameters of one of the patients tested in the clinical trial described later in this chapter. The model outputs are in close agreement, which supports the use of $G(s)$ to approximate the combined linearizing control law and arm system in the remainder of this chapter. Care must be taken, however, to ensure that the control laws subsequently considered are robust to the modeling error present in the system.

Linearization along a trajectory is a standard approach that allows the linearized dynamics to be used to infer properties of the nonlinear system when the state variables and input are close to those of the linearized system. In particular, if the resulting time-varying system is stable then the nonlinear system also has that property in some neighborhood of the trajectory. This technique can be applied to assess the local stability and robustness of the proposed control law by using trajectories comprising experimental test data or those resulting from simulations using the system model.

Stability of the linearized system can then be assessed using well known methods for linear time-varying systems. This can then be repeated whilst varying the model parameters to gain a broader picture of the system robustness and performance properties.

The linearized system variation with respect to F_{a2} and F_{ma} depends only on F'_{a2}, and the values of F_{ma}, F'_{ma} and F''_{ma} respectively. Hence the stability of the system can be examined through variation of these quantities, together with variation of the remaining model parameters, in order to provide a measure of robustness.

4.3.2 Feedback Controller

The next stage is to choose a feedback controller to supply the torque demand, w, necessary for the system to track the specified references. A PD controller is used whose transfer-function is approximated as

$$C(s) = \frac{K_d s + 1}{\epsilon K_d s + 1} \tag{4.33}$$

with $\epsilon \in [\frac{1}{6}, \frac{1}{20}]$. Figure 4.9 shows the resulting control system.

The level of stimulation that first produces a response from the triceps, u_m, is used to supply an offset such that the feedback system operates within the torque generating capabilities of the muscle. Moreover, the feedback controller is tuned for each patient with an emphasis on robustness, since stability is of greater concern than accurate tracking and therefore a conservative bandwidth and high gain and phase margins are desired.

To illustrate the role of the end-effector dynamics on the system bandwidth, Bode plots of the closed-loop system are shown in Fig. 4.10 for the ratios $\frac{b_{a3}+K_{M_2}}{K_{B_2}} = 0.03$, 0.07, 0.4, 0.8 and 1.5 respectively. These have been created using an experimentally identified value of $\omega_n = 0.85\pi$, and, for ease of comparison, they have all been tuned using the standard Zeigler-Nichols rules. The corresponding closed-loop systems are denoted by P_a, P_b, ... P_e, and their respective bandwidths are $\omega_b = 0.53, 0.45, 0.42$, 0.23 and 0.16 Hz. Altering $\frac{b_{a3}+K_{M_2}}{K_{B_2}}$ cannot produce bandwidths much in excess of these for the given control law and tuning method due to the limiting factor of the muscle dynamics. It is desirable to select a ratio that makes the task feel natural to the patient, but does not lead to too narrow a system bandwidth which would necessitate

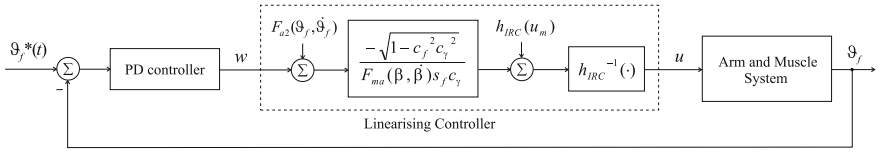

Fig. 4.9 Block diagram of feedback control system

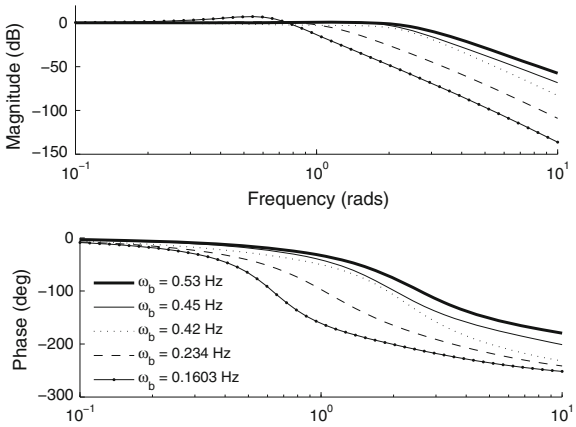

Fig. 4.10 Bode plots of linearized feedback systems for different end-effector dynamics

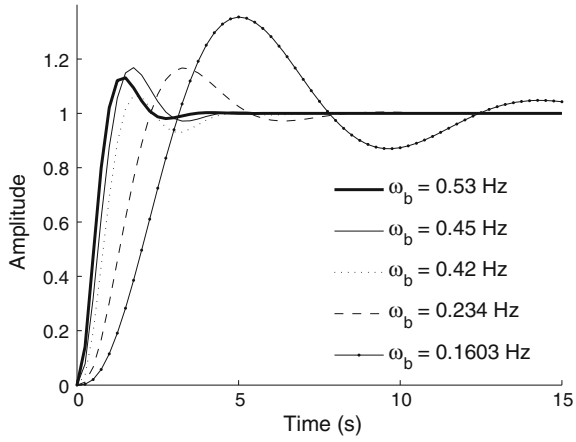

Fig. 4.11 Step responses of linearized feedback systems for different end-effector dynamics

an excessive controller effort and correspondingly large levels of muscle torque in order to accomplish the task. Step responses corresponding to the systems examined are shown in Fig. 4.11.

The next subsections examine the effect of the end-effector dynamics on the ILC law performance.

4.3.3 Phase-Lead ILC

The phase-lead ILC law has been shown to provide excellent results despite its simplicity and limited parameter set, see the references in Chap. 2. In the case of discrete dynamics this law in the z-transform domain is of the form

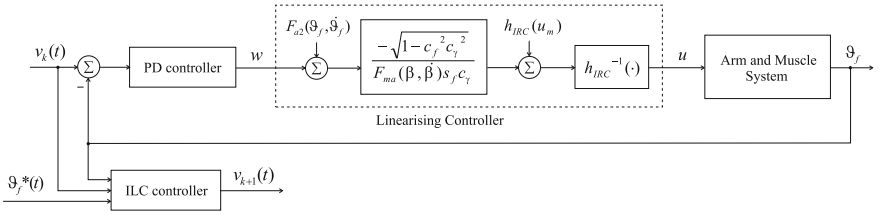

Fig. 4.12 Block diagram of the ILC system

$$v_{k+1}(z) = v_k(z) + Lz^{\lambda} e_k(z) \tag{4.34}$$

where L is a scalar gain, and λ is the phase-lead in samples. Figure 4.12 shows the overall control system consisting of the feedback control loop and the ILC law. Let $e(t) = \vartheta_f^*(t) - \vartheta_f(t)$ and hence using (4.34)

$$e_{k+1}(z) = e_k(z) - Lz^{\lambda} P(z) e_k(z) \tag{4.35}$$

and

$$P(z) = \frac{C(z)G(z)}{1 - C(z)G(z)} \tag{4.36}$$

where $G(z)$ and $C(z)$ are the discretized representations of (4.32) and (4.33) respectively.

The relationship

$$e_{k+1}(z) = e_k(z)\left(1 - LP(z)z^{\lambda}\right) \tag{4.37}$$

yields the monotonic trial-to-trial error convergence criterion

$$\left|1 - LP(e^{j\omega T_s})e^{j\omega\lambda T_s}\right| < 1 \tag{4.38}$$

for ω up to the Nyquist frequency. For a given frequency (4.38) is a sufficient condition for monotonic trial-to-trial error convergence. Furthermore the convergence speed is dictated by the magnitude of the left-hand side; if it is close to zero, convergence will occur in a single trial and if greater than one, divergence is likely to occur at that frequency.

Given the above considerations, L and λ are chosen such that the left-hand side of (4.38) is minimized to provide the fastest convergence over those frequencies present in the reference trajectory. Higher frequencies, or those at which plant uncertainty may cause the criterion to be violated, are removed through the use of a non-causal zero-phase filter applied to the error in the time between successive trials. The sample time used is $T_s = \frac{1}{40}s$, which corresponds to the frequency at which stimulation pulses are applied to the patient (see later in this chapter). This frequency is synchronized with the robotic control system and each pulse is produced with a delay of less than 10 μs. Next, the effect of varying the phase-lead is investigated

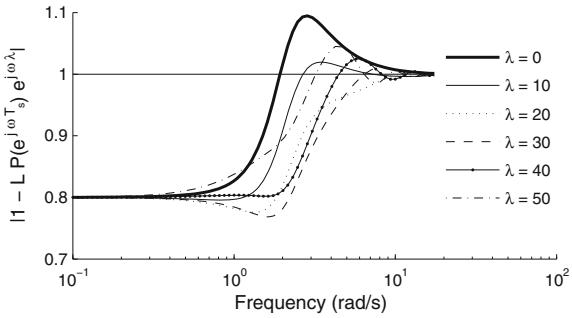

Fig. 4.13 Monotonic convergence criterion for the system with $\omega_b = 0.45\,\text{Hz}$ for $L = 0.2$ and various λ

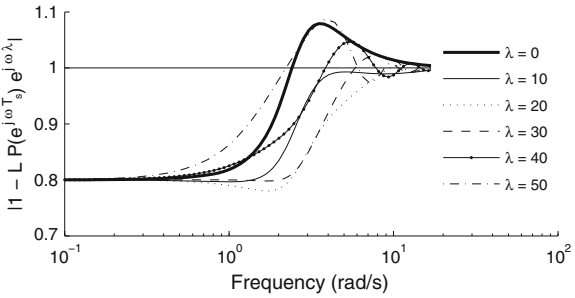

Fig. 4.14 Monotonic convergence criterion for the system with $\omega_b = 0.53\,\text{Hz}$ for $L = 0.2$ and various λ

for two of the five closed-loop system transfer-functions that were considered in the previous sub-section.

Figure 4.13 shows the monotonic convergence criterion (4.38) for the system with bandwidth $\omega_b = 0.45\,\text{Hz}$ for a variety of phase-lead values λ. Figure 4.14 shows the same criterion for the system with bandwidth $\omega_b = 0.53\,\text{Hz}$. A value of $L = 0.2$ has been chosen in both cases in order to produce an extremely robust system at the expense of convergence speed. Reducing L can be shown to increase robustness to model uncertainty over all frequencies, providing further support for this approach.

It can be established that choosing the phase-lead to maximize the convergence at a given frequency also achieves maximum robustness to gain and phase uncertainty at that frequency, which means that there is no compromise between robustness and convergence speed in selecting this parameter. Therefore the phase-lead will be selected to maximize the convergence over a suitable frequency range and a zero-phase filter implemented to ensure stability at all higher frequencies (this is advisable even if the convergence criterion is satisfied).

For general application, it is natural for this frequency range to correspond to the bandwidth of the system. The system with $\omega_b = 0.45\,\text{Hz}$ has maximum convergence over its bandwidth using a phase-lead of 30 samples (although a phase-lead of 20 samples produces greater stability over higher frequencies, which is an important factor if a zero-phase filter is not used). Similarly the system with $\omega_b = 0.53\,\text{Hz}$ has

maximum convergence over its bandwidth of 20 samples. Using these phase-lead values the system with the higher bandwidth has the property of monotonic convergence at greater frequencies than the system with lower bandwidth. For further discussion and guidelines on the choice of phase-lead and filter design, see, e.g., Freeman et al. (2005).

4.3.4 Adjoint ILC

The adjoint ILC law is given in z-transform form by

$$v_{k+1}(z) = v_k(z) + \beta P^*(z) e_k(z) \tag{4.39}$$

where $P^*(z)$ is the adjoint of the plant model used. An attractive feature of this law is that, with a sufficiently small scalar multiplier, β, it is guaranteed to satisfy the condition for monotonic convergence over all frequencies and hence ensure a satisfactory transient response. The monotonic convergence criterion is

$$\left|1 - \beta P(e^{j\omega T_s}) P^*(e^{j\omega T_s})\right| < 1 \tag{4.40}$$

which leads to

$$0 < \beta |P(e^{j\omega T_s})|^2 < 2 \tag{4.41}$$

for ω up to the Nyquist frequency. This ILC law has been found, with supporting experimental evidence, to provide a high level of robustness to model uncertainty (Freeman et al. 2005).

To examine the effect of the choice of gain in this ILC law, plots of the monotonic convergence condition (4.40) for the two systems examined in the last sub-section for a variety of β were constructed. Figure 4.15 shows the monotonic convergence criterion for the system with bandwidth $\omega_b = 0.45$ Hz. and Fig. 4.16 shows the same criterion for the system with bandwidth $\omega_b = 0.53$ Hz. Both systems satisfy the criterion for the values of β examined. For frequencies where the closed-loop system has a gain close to unity, approximate convergence will occur in a single trial for values of β close to one. In practice, however, β is chosen to be significantly lower in order to increase the system robustness at the expense of the convergence rate. As with the phase-lead law, the convergence rate that can be achieved at a given frequency is closely connected to the system bandwidth. This rate can be increased within a given range by convolving $P^*(z)$ with a zero-phase band-pass filter in (4.39) (see Freeman et al. 2005 for details). The same effect could be achieved by replacing $P^*(z)$ with the plant inverse $P^{-1}(z)$ and then using a low-pass filter. However, the increase in convergence speed is gained at the price of reduced robustness and therefore a zero-phase band-pass filter will not be used unless, in application, the convergence rate is found to be unacceptably low.

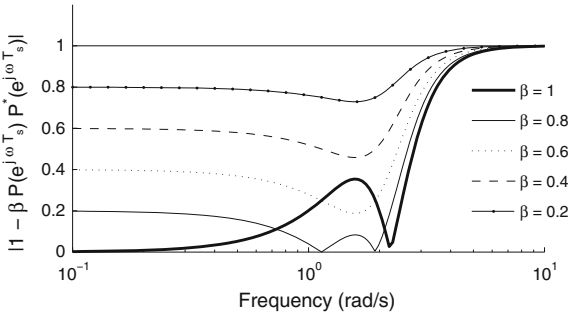

Fig. 4.15 Monotonic convergence criterion for $\omega_b = 0.45\,\text{Hz}$

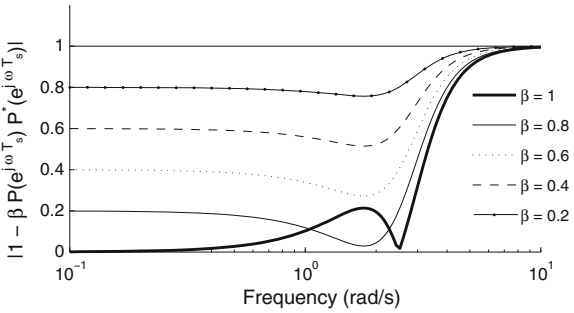

Fig. 4.16 Monotonic convergence criterion for $\omega_b = 0.53\,\text{Hz}$

4.4 Experimental Results with Unimpaired Subjects

The controllers of the previous section have been tested on 18 unimpaired subjects aged between 50 and 65 years (mean age 57 years, 10 months with standard deviation 5 years, 4 months). These subjects are age matched with the stroke patients to whom the control laws were later applied, generating the results detailed in the next section of this chapter. Representative results from a single subject are presented to enable detailed examination of performance. In addition, summary results of the performance of all subjects are included.

For each of the 18 unimpaired subjects tested the arm model was first identified using tests and procedures described in Freeman et al. (2007). These involved taking measurements of the arm, establishing its maximum range of movement and then fitting a circle to the trajectory traced out by the elbow, in order to provide γ (see Fig. 4.3) and the position of the shoulder joint. The arm was then held stationary while FES was applied to the triceps using a ramp signal, in order to produce the functions, $h_{IRC}(u)$ and $h_{LAD}(t)$, in the muscle model, using deconvolution and a nonlinear optimization procedure. Stimulation sequences and kinematic trajectories, imposed on the arm by the robot, were then applied and Least Mean Squares (LMS) optimization used to arrive at the remaining model parameters.

Figure 3.2 shows a schematic of the form of the reference signal used to produce the results in this section in relation to the position of the subject's shoulder joint.

The reference was set at an angle of 20° from the y axis but was individually calculated for each subject to extend their arm from 55 to 95 % of their total arm length over the course of the movement. Two trajectories were created by moving along this reference at two different speeds. Each trajectory started with a waiting period when it was set equal to the starting point of the reference. The 'slow' trajectory lasted for 12.5 s in total (a 5 s waiting period and a 7.5 s movement along the reference), and the 'fast' trajectory lasted for 10 s (a 5 s waiting period followed by a 5 s movement). The waiting period was included to allow the ILC update computation to be completed before the arm was required to move again. Before each trial began, the subject's arm was moved to the initial position by the robot and then released only when the trajectory started. The subjects were not shown the trajectory before or during the test.

The values of K_{B_2} and K_{M_2} that dictate the end-effector characteristic were set at 5.78 Nm/rad s^{-1} and 0.29 Nm/rad s^{-2}, respectively, since these created a natural feel to the system and allowed the chosen trajectories to be accomplished with moderate effort and without limiting the bandwidth excessively. For a typical identified value of b_{a3} this choice of gains gives $\frac{b_{a3}+K_{M_2}}{K_{B_2}} \approx 0.1$, which gives a closed-loop system bandwidth of approximately 0.45 Hz when calculated using the same muscle dynamics and controller tuning procedure as adopted previously. The values of $\omega_n = 0.85\pi$ and $b_{a3} = 0.271$ were identified for the subject whose experimental results are given in this section.

4.4.1 Linearizing PD Controller

The feedback controller gains were tuned for each subject. Two or three repetitions of the slow trajectory were used to fine-tune the gains given by the standard Zeigler-Nichols rules and these values were used for the duration of the tests. In the remainder of this section the PD controller gains are $K_p = 10$ and $K_d = 2$. The effect of the linearizing feedback controller in the absence of ILC can be seen by inspection of the first trial results.

4.4.2 Phase-Lead ILC

Figure 4.17 shows results obtained using the phase-lead ILC law for various values of λ. The slow trajectory is used together with $L = 0.2$. This learning gain has been chosen conservatively and hence speed of convergence has been sacrificed for greater robustness. From these results, the best performing phase-lead is for 35 samples, which is similar to that found by inspection of the monotonic convergence criterion for P_b, a system with similar bandwidth, shown in Fig. 4.13. The root mean

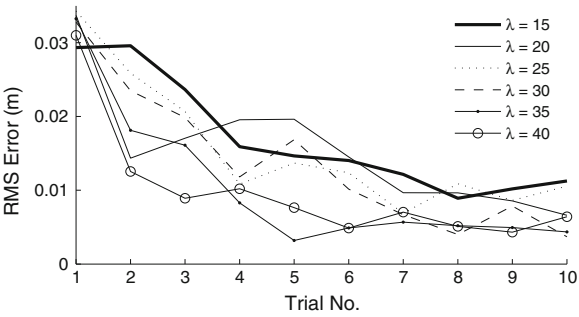

Fig. 4.17 Single subject phase-lead ILC results for the slow trajectory using $L = 0.2$ and various λ

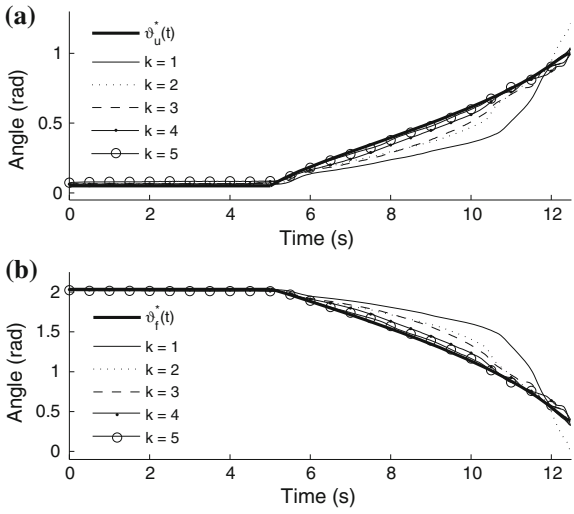

Fig. 4.18 Single subject experimental tracking of **a** $\vartheta_u^*(t)$ and **b** $\vartheta_f^*(t)$ for the slow trajectory using phase-lead ILC with $L = 0.2$ and $\lambda = 35$

square (RMS) error corresponding to this phase-lead converges to approximately 5 mm and has a minimum value of 3.2 mm.

Figure 4.18 shows the results obtained using $L = 0.2$ and $\lambda = 35$ in greater detail. It can be seen that during the first 5 trials the error reduces monotonically and the reference trajectory is tracked extremely well. This reflects the improvement in tracking accuracy that simple ILC laws can provide compared with the use of feedback controllers alone.

To examine the results further, Fig. 4.19 shows the associated stimulation input and ILC update. It can be seen from (a) that the stimulation applied during $k = 1$ saturates at 300 μs, but also further trials removes this effect and produces lower levels of stimulation. Use of ILC also leads to the application of stimulation during the initial 5 s waiting period before movement is required. Figure 4.19b shows that the updated v_k is converging to a fixed trajectory over repeated trials.

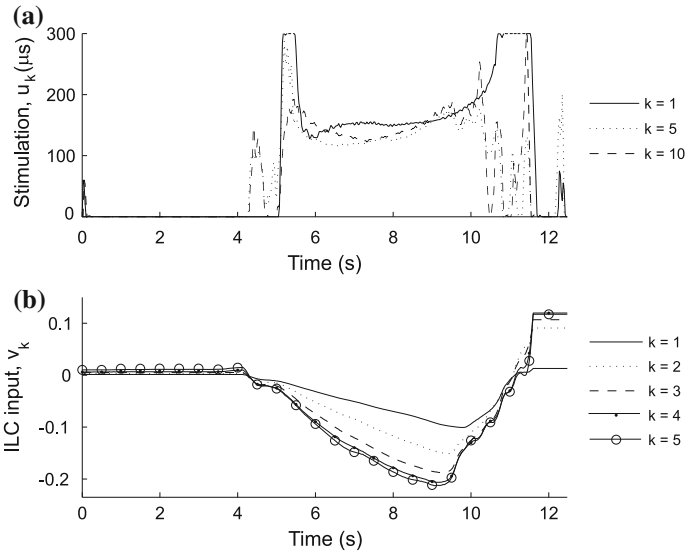

Fig. 4.19 Single subject experimental **a** stimulation and **b** updated input results for the slow trajectory using phase-lead ILC with $L = 0.2$ and $\lambda = 35$

4.4.3 Adjoint ILC

Figure 4.20 shows results obtained using the adjoint ILC law, where the slow trajectory is again used and $\beta = 0.2$. The plant model is labeled P and to examine the robustness of this ILC law the models P_a, P_c, P_d and P_e have also been used in its place, but model P_b has not been used due to its close similarity with P. It is clear that this ILC law is capable of exhibiting robustness to significant model uncertainty and produces minimum error and convergence rates comparable to the performance of its phase-lead counterpart. Use of the actual plant model results in convergence to approximately 5 mm in 4 trials and this level of error is maintained over the remaining trials.

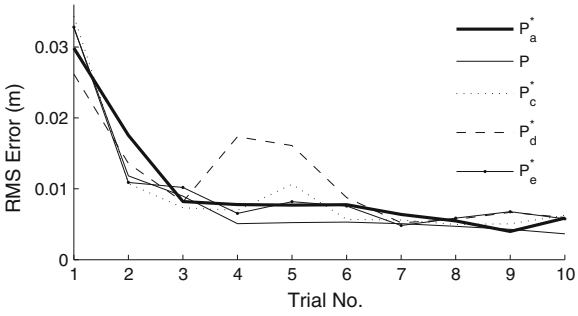

Fig. 4.20 Single subject adjoint ILC results using for the slow trajectory with $\beta = 0.2$ and various plant models

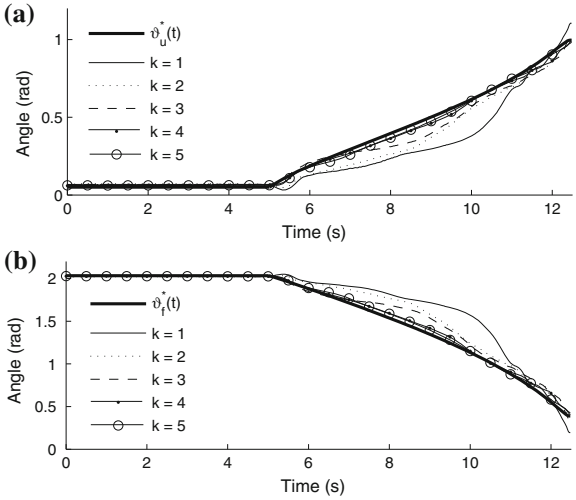

Fig. 4.21 Single subject experimental tracking of **a** $\vartheta_u^*(t)$ and **b** $\vartheta_f^*(t)$ using adjoint ILC for the slow trajectory with $\beta = 0.2$

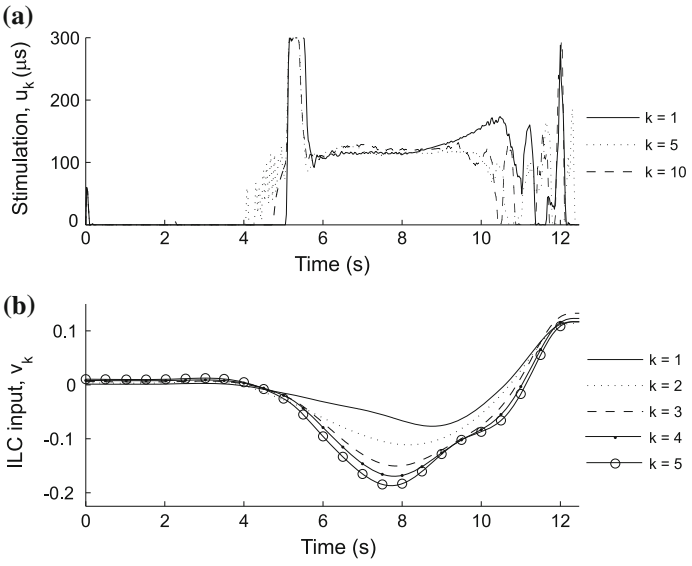

Fig. 4.22 Single subject experimental **a** stimulation and **b** updated input results using adjoint ILC for the slow trajectory with $\beta = 0.2$

Figure 4.21 shows tracking results using P over the first 5 trials and highlights the monotonicity of the convergence over the initial trials. Figure 4.22 shows the corresponding stimulation input and ILC update. It can be seen from (a) in this

figure that, as with the phase-lead law, adjoint ILC causes the stimulation to decrease from the level observed initially and leads to its application during the initial 5 s waiting period. Figure 4.22b illustrates the convergence of the ILC update to a similar trajectory as that observed with the phase-lead ILC applied.

4.4.4 Experimental Comparison

The performance of the phase-lead and adjoint ILC laws has been compared against NOILC defined by (2.28)–(2.31). A Kalman estimator has been used to provide the states of the linear plant approximation that are required in the implementation, derived using cost function error and state covariance weightings of 1 and 10 respectively. Figure 4.23 shows representative results using a variety of cost function error weighting values (it is the ratio of the weights that influences the optimal solution and hence R has been set at unity) compared with the use of the phase-lead and adjoint laws. It can be seen that the performance gained using NOILC is not able to exceed that of the simpler ILC laws for convergence over the 10 trials. Model-based ILC laws will, however, be required when non-planar tasks are considered in later chapters.

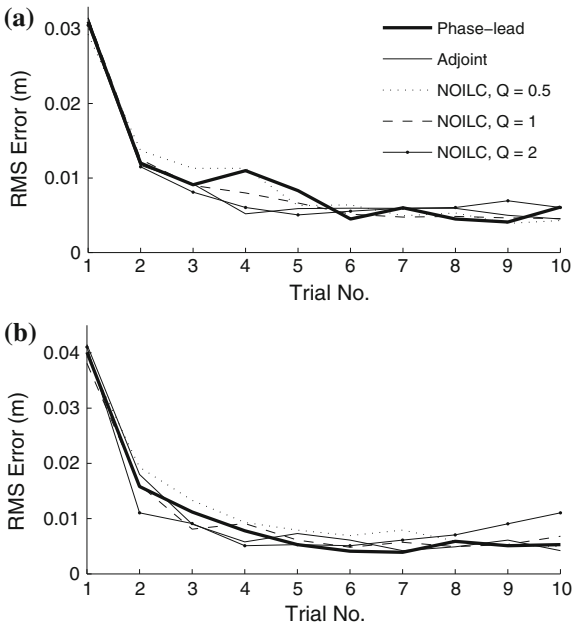

Fig. 4.23 Single subject comparison of phase-lead and adjoint algorithms with NOILC for **a** the slow trajectory, and **b** the fast trajectory

4.4.5 Results from Multiple Subjects

Given the similarity in performance of the phase-lead and adjoint ILC laws, group results are presented for the latter case only. Figure 4.24 shows results from the first four subjects tested. They relate to both (a) the slow trajectory, and (b) the fast trajectory. The results indicate that convergence can be achieved within 5 trials for both trajectories and an RMS tracking error of less than 10 mm over the course of the movement (and in some instances less than 5 mm) is possible in all cases.

Table 4.1 shows the mean and standard deviation of the RMS error obtained during the last trial, for all subjects tested. Trajectory 1 refers to the reference previously described, whilst trajectory 2 is a reference whose inclination from the y-axis is increased to 40°. The results confirm that the implemented ILC laws are capable of producing high levels of tracking accuracy.

These experimental results confirm that superior tracking performance has been achieved compared with alternative control methods that have been applied to the upper limb. These include the previous application of ILC (Dou et al. 1999) and also

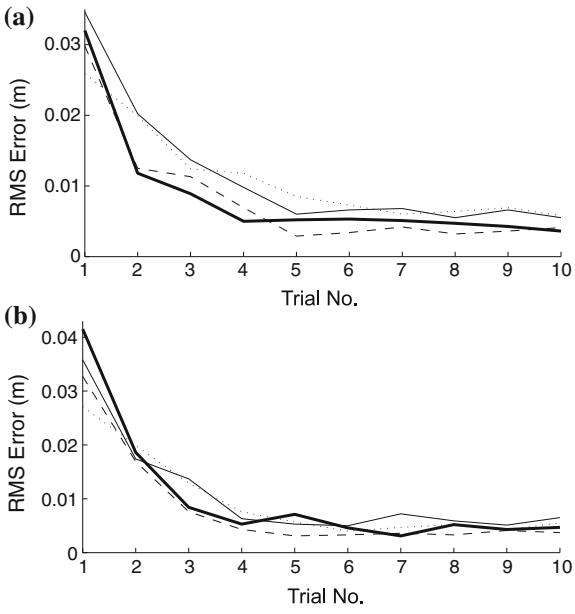

Fig. 4.24 Adjoint ILC results for **a** the slow trajectory, and **b** the fast trajectory, using $\beta = 0.2$ for four subjects

Table 4.1 Mean of last trial RMS error for all eighteen subjects (standard deviation in brackets)

Type	Mean of last trial RMS error/mm	
	Trajectory 1	Trajectory 2
Slow	9.41 (5.67)	10.22 (6.07)
Fast	12.18 (6.94)	12.93 (6.87)

both open-loop controllers, such as those considered in previous research (Davoodi and Andrews 2004; Popovic and Popovic 1998), and the limited number of closed-loop controllers that have been experimentally applied in this area, such as Lan et al. (1994). The major advantage of the ILC design, however, is the simplicity of tuning and the absence of any training experiments.

The simple structure ILC laws that have been examined also permit the degree of assistance to easily be changed via the use of a forgetting factor (see Freeman et al. 2005) which can also be used to promote voluntary effort when applied to stroke patients. Although ILC laws have moved beyond these relatively simple structure types and now encompass a wide range of (both linear and nonlinear) plant models and control law structures, the approach taken here was to apply ILC laws with the simplest structure which could meet the necessary performance requirements. When more than one muscle must be stimulated, as in later chapters, model-based ILC laws will be required.

In the next section, the results from a clinical trial with the ILC designs of this section are given based on the results in Hughes et al. (2009).

4.5 Clinical Results

4.5.1 Preliminaries and Patient Selection

A repeated-measures cross-sectional observational design was used in which patients attended the laboratory between eighteen and twenty-five occasions. All data collection was carried out by a single experienced investigator. A convenience sample of patients was recruited from the community. Criteria for inclusion were: adults over eighteen years who were more than six months post stroke, with a hemiparesis resulting in weakness of elbow extension, but with perceivable voluntary control of finger flexors, upper arm and shoulder muscles. In addition, when positioned in the robot they also needed to respond to surface FES applied to triceps brachii, resulting in elbow extension.

Patients were excluded from the study if they had uncontrolled epilepsy, required an interpreter, had any active device implant, e.g., pacemaker, implanted cardiac defibrillator, neuro-stimulator or drug infusion device, an allergy to sticking plaster/tape or alcohol wipes or any serious medical, psychological or cognitive impairment that, in the opinion of the investigators, would compromise safety or ability to comply with the study. Patients with any orthopaedic or neurological lesions affecting arm movement were also excluded.

Neither the workspace of the robotic arm, with link lengths 0.66 and 0.45 m, nor the size of the projected image 1.2 m by 0.8 m, restricted the patients for the range of trajectories used. The robot inertia mass and damping gains used were 1 $\mathrm{Nm}^{-1}\,\mathrm{s}^2$ and 15 Nm^{-1} s, respectively, i.e., the robot produced the effect that they the participants were moving a mass of 1 kg with viscous damping equal to 15 Nm^{-1} s. Participants

Table 4.2 Description of the three angles, length and duration of the trajectories

Angle	Length	Duration (s)
T1 (20 % internal rotation)	S (short—80 % of reach)	S (15)
T2 (midline)	M (medium 90 % of reach)	M (10)
T3 (20 % external rotation)	L (long 99 % of reach)	F (5)

were seated at the workstation at a height which allowed normal shoulder positioning; restraining seat belts were used to limit trunk movement, see Fig. 3.1. The patient's hemiplegic arm was placed in the robot arm holder with the hand curled around a padded vertical pillar. A semi-transparent perspex elliptical disc was positioned over the hand and forearm and attached to the top of the pillar. Prior to the treatment sessions, patients attended a preliminary session in which personalized trajectories were created and stimulation parameters and individual mathematical models of the arm were obtained.

To create personalized trajectories, patients were positioned in the robot and manually assisted to move their arm over their full available range of movement. These parameters extracted from the data collected were then used to define length of trajectories for each patient. Each trajectory extended from 55 to 80 % (short), 90 % (medium), or 99 % (long) of maximum reach. Trajectories were orientated in one of three directions (mid-line and 20 % of maximum range to either side). Trajectory tasks and were performed at three speeds (5, 10 and 15 s duration) and were the same for all patients. Trajectory details are summarized in Table 4.2 and the abbreviations for angle, length and duration used are defined.

As the next step, the level of comfortable maximum stimulation was identified for each patient and used as an upper limit in subsequent tests. A biomechanical model of the arm was then produced to describe movement in response to stimulation. The model and parameters were identified using a series of tests in which the robot moved the patients arm, with no voluntary action, about the workspace whilst applying low levels of FES (asymmetric, biphasic, 40 Hz fixed amplitude variable pulse width 0–300 μs with a resolution of 1 μs) through a CE marked commercially available stimulator. This biomechanical model was then used by the ILC law during all treatment sessions. The development and validation of this model is described in Freeman et al. (2009b).

4.5.2 Treatment Sessions

All patient s attended eighteen one hour treatment sessions and two attended an additional seven sessions. Three minutes of active assisted stretches were performed prior to and immediately after placing the arm in the robot. During sessions, FES was applied to the patient's triceps brachii muscle to assist them in completing tracking tasks. A task consisted of tracking one of a selection of twenty seven different

trajectories, 6 times (one subject could only manage 4) with a rest period of 15 s between each trial. The patients were positioned in the robot and a target area (diameter 60 mm) defined by a circle of LEDs with a central cross-hair was marked on the elliptical disc immediately above the hand and pillar.

After the initial setup, an overhead projector displayed an image of an elliptical path on to the perspex disc and an illuminated red dot moved along the trajectory at constant speed. The movement was clockwise for right and anticlockwise for left hemiplegics to ensure that the easier movement was associated with reaching and the same for both groups. The patient's arm was moved to the starting position by the robot. A 5 s "countdown" was visually displayed prior to the commencement of the tracking task. To perform the tracking, the patient was instructed to move their hand so that it kept pace with the moving red dot, keeping it within the circle of LEDs and as close as possible to the cross-hairs. To reinforce good performance and indicate error, the LEDs changed color; green when the tracking accuracy was within 25 mm, amber between 25–50 mm and red when the error exceeded 50 mm. The number of tracking tasks practised during each session was limited only by fatigue. In the time between each trial, the ILC law used kinematic and force data recorded during the previous trial, in conjunction with the biomechanical model of the arm, to update the FES applied during the next trial.

4.5.3 Outcome Measures

Outcome measures were collected by the same assessor. The primary measure for upper limb function was the ARAT (Carroll 1965). This was measured pre intervention (2 time-points for FMA), after session 18, and for 2 patients, post 25 sessions. The primary impairment measure was the ability to perform tracking tests (motor control). Patients were asked to perform four different tracking trajectories at the beginning and end of the treatment session using only voluntary action (no robotic assistance or FES), so any change in unassisted tracking ability could be measured. The trajectories, chosen to be easy enough for all patients to attempt, were, see Table 4.2, T1SS, T1MS, T2MS and T2SS conducted in the order given.

Movement, coordination and sensation of the upper limb were measured using FMA. Isometric force was assessed by locking the arm holder in a stationary position that was standardized for each participant, who was instructed to exert a force away from them in the sagittal plane for 5 s, before moving to the next direction in a clockwise fashion, see Fig. 4.25.

For each trajectory, the error between the cross-hair and the target was recorded at every time point using a sampling frequency of 1.6 kHz. Trajectory tracking performance was defined as the mean error value over the test duration. Peak values of the isometric force were obtained from three repetitions of each attempt for each direction and the mean calculated.

Statistical analysis was performed using the data analysis package SPSS *v*14.0. Descriptive statistics are presented for all outcome measures, where the baseline for

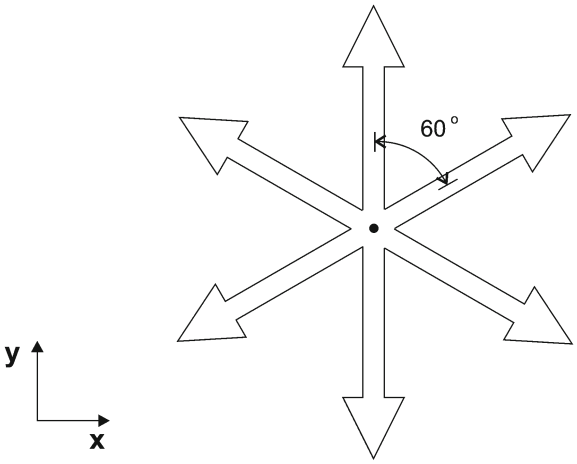

Fig. 4.25 Force measurement directions

clinical measures was taken as the mean of the 2 measurements pre intervention. Statistically significant changes in clinical measures and isometric force between baseline and session 18 were estimated using a paired *t* test. Changes in error tracking were estimated using summary measures, considered appropriate for a small sample (Matthews et al. 1990). Statistical significance of changes in tracking error were estimated using a one sample *t* test applied to the linear regression of error against session.

4.6 Results from the Clinical Trial Participants

After receiving ethical approval, five patients, three males and two females, were recruited and gave written consent. Their demographic characteristics are shown in Table 4.3 with a mean age of 52 years. These patients had suffered haemorrhagic or ischemic strokes ranging from 8 months to 8.4 years, mean 4 years, prior to recruitment to the study; three had a hemiparesis of the right side and two of the left.

Table 4.4 shows the clinical scores at baseline and after 18 sessions. A significant improvement was not identified for the ARAT, but was for the FMA.

4.6.1 Tracking Performance

To illustrate the effect of the stimulation in assisting tracking, Fig. 4.26a, b show typical changes in the angle of the shoulder and elbow during over the duration of a

Table 4.3 Demographic characteristics of the patients who took part in the study—TFS (time from stroke), ST (Stroke type) SH (side of hemiparesis) PDS (previous dominant side)

ID	Age (years)	Gender	TFS (years)	ST	SH	PDS
1	38	Male	2.8	Infarction	L	L
2	77	Female	8.4	Haemorrhage	L	R
3	41	Male	4.8	Infarction	R	R
4	55	Female	3.6	Haemorrhage	R	R
5	51	Male	0.7	Unknown	R	L

Table 4.4 Normative (normal score) and sample mean (SD) of baseline (Before) and after 18 sessions (After) for clinical outcome measures

Outcome measure (n = 5)	Before (SD)	After (SD)	Change (SD)
Normal score			P-value [95 % CI]
ARAT	4.00 (1.46)	3.40 (0.55)	−0.60 (1.19)
57(0)			0.32 [0.88, −2.08]
FMA (motor)	12.90 (3.36)	15.40 (4.28)	2.50 (1.58)
60(0)			0.02 [4.46, 0.54]

Mean change (SD) and 95 % Confidence Interval [95 % CI], expressed as the absolute value change during the 18 intervention sessions is also shown

T1SS trajectory. The solid line shows the ideal movements that would be required to complete the trajectory successfully; the dotted-dashed line represents unassisted movement, and the dash-dotted line shows movement assisted by FES. Figure 4.26c shows the FES pulse-width that is applied using ILC in order to produce these assisted movements. During the 5s "countdown" period, before the target movement starts, there is minimal stimulation. On the reach component of the trajectory (5–12.5 s) stimulation increases rapidly. Also there is a delay period of approximately 2 s between the stimulation peak and the peak shoulder and elbow angle, associated with the biomechanical response to stimulation. The robot provided a low level of assistance (60 Nm^{-1}), which was effectively only noticeable when the tracking error was greater than 5 cm. The data in Table 4.5 shows the change in the slope is significant for three out of the four tested trajectories: T1SS, T1MS and T2MS.

4.6.2 Isometric Force

Table 4.6 shows mean and maximum isometric force generated in six different directions (0°, 60°, 120°, 180°, 240°, 300°) recorded for (i) a sample of eight 50+ years

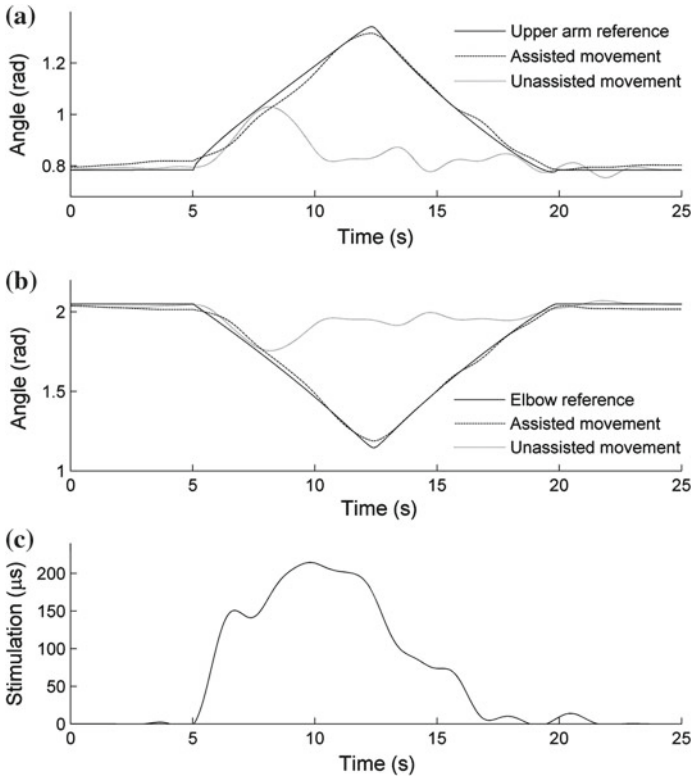

Fig. 4.26 Tracking performance plots

Table 4.5 Error tracking data across all patients for baseline and post 18 sessions, the slope of the line of best fit

Trajectory (n = 5)	Slope	P value [95 % CI]
T1SS	−3.302	0.03 [−0.0033, −0.0003]
T1MS	−3.165	0.03 [0.0044, −0.0000]
T2MS	−2.821	0.05 [−0.0043, −0.000]
T2SS	−2.270	0.09 [−0.0035, 0.0003]

old neurologically unimpaired right-handed participants and (ii) the five stroke patients' mean (SD) isometric force values at baseline (before) and after 18 sessions (after) corrected for side of hemiplegia. The direction in which the angle is measured is reversed depending on the side of hemiplegia to allow comparison across all participants. Mean (SD) change of isometric force, level of significance (paired t-test) and 95 % CI is also shown.

For unimpaired participants the isometric force varied with direction: strongest at 0°, 120° and 240° and weakest in the 60° and 300° directions. For stroke patients the isometric force also varied with direction; for both the pre and post intervention the strongest was at 120° and 180° and weakest in the 60° and 0°. The largest gains

Table 4.6 Mean (SD) and range [Min–Max] isometric force (N) generated by neurologically unimpaired participants and for stroke patients at Baseline and Post Treatment (18 sessions)

Angle	Normal Mean (SD) [Min–Max]	Baseline Mean (SD) [Min–Max]	Post Treatment Baseline [Min–Max]	PT-B (SD) P-value [95 % CI]
0°	81.75 (8.39)	35.58 (12.41)	12.82 (9.70)	
	[71.22–92.48]	[24.06–54.83]	[26.96–68.33]	0.04 [24.87, 0.78]
60°	48.41 (18.41)	33.35 (12.40)	37.93 (12.68)	4.58 (2.77)
	[20.13–81.38]	[25.67–54.86]	[27.53–59.92]	0.02 [19.44, 2.81]
120°	73.19 (19.18)	[31.60–93.24]	57.28 (18.40)	[34.56–79.70]
	68.41 (24.21)	[40.61–97.75]	11.13 (6.69)	0.02 [19.44, 2.81]
180°	72.21 (13.87)	53.21 (6.60)	66.42 (6.23)	13.21 (12.22)
	[54.10–95.78]	[43.71–60.53]	[61.33–74.86]	0.07 [28.39, −1.96]
240°	71.46 (19.41)	40.61 (8.64)	51.66 (10.46)	11.05 (6.18)
	[40.52–93.69]	[31.13–52.66]	[38.82–67.88]	0.02 [18.73, 3.37]
300°	61.41 (18.89)	38.08 (12.74)	56.20 (11.69)	18.11 (3.36)
	[33.79–88.68]	[24.35–53.84]	[42.05–71.65]	0.00 [22.28, 13.94]

Mean change (SD), during the 18 treatment sessions, level of statistical significance (Paired *t*-test) and 95 % CI is also shown

in force were made in the 300° and 180° directions and the smallest in the 60° and 240° directions; changes in force data across the group are significant in all but the 180° direction.

For each patient the mean isometric force results for each assessment are shown in Fig. 4.27. Each of the stroke patient's data are superimposed on data results from the unimpaired sample; the mean of eight participants (dark) and the strongest individual (light grey). In most cases the axis along which the principal changes in isometric force occurred reflected the side of hemiplegia; in left hemiplegics, patients 1 and 2, this was from bottom left to top right, for right hemiplegics, patients 3, 4 and 5, from top left to bottom right. Further force changes were evident after 25 sessions, but in a reduced number of directions compared to session 18; the improvements were seen in 3 directions, as opposed to all 6, for patient 3, and 4 directions, as opposed to 6, for patient 5.

4.6.3 Percentage Maximum Changes in the Level of Stimulation Used over Time

The assisted trajectory tracking tasks used during the intervention were selected based on clinical need. As such they were not necessarily used in every session, but could also have been used more than once. Figure 4.28 shows data recorded during the assisted T1 SS task for all patients when used. Where the task was repeated in the same session, data from the first performance is shown. For each trial the mean error

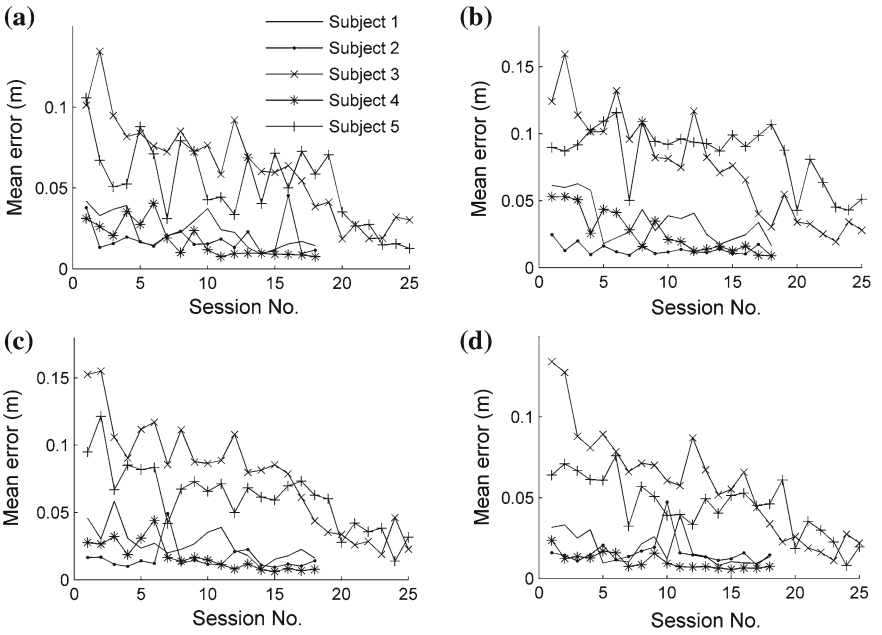

Fig. 4.27 Changes in tracking error data for each patient for each unassisted trajectory performed at the beginning of each treatment session, **a** T1SS, **b** T1MS, **c** T2MS, **d** T2SS

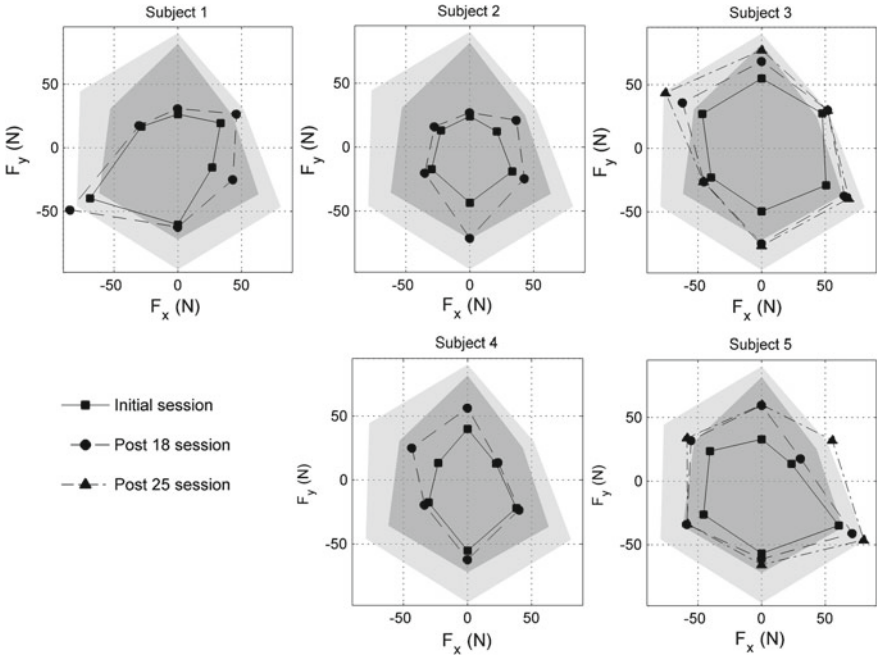

Fig. 4.28 Mean isometric force for each stroke patient: initially, post 18 and post 25 sessions

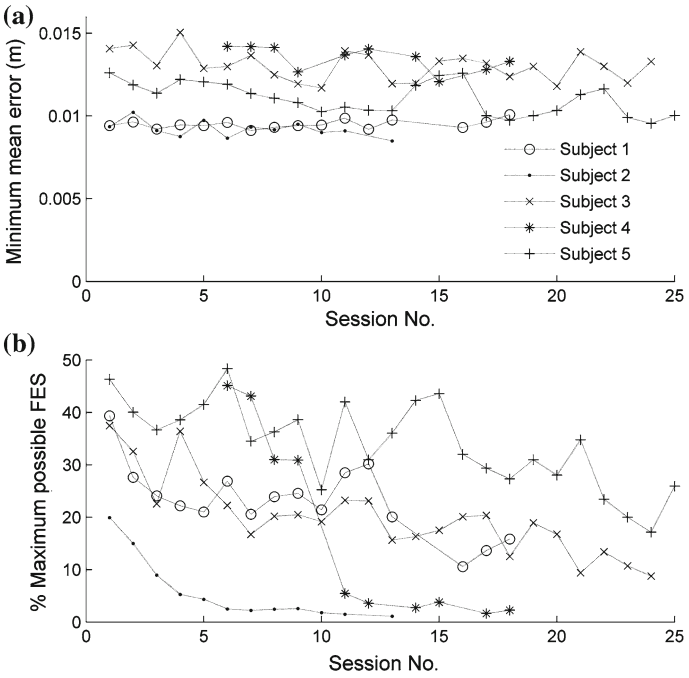

Fig. 4.29 Data recorded for all patients during the FES assisted T1 SS tracking task showing **a** error in tracking, **b** % max stimulation used

was calculated and the minimum over all trials is displayed in Fig. 4.29, from which the mean error over the sessions is between 15 and 8 mm, and does not decrease over time. Figure 4.29 shows the percentage of maximum stimulation required to correct the tracking error in the most accurate trial. For all patients the FES required decreased over the 18 sessions.

4.7 Overview of the Clinical Trial Results

The study whose results are given in the previous section has identified changes in clinical outcome measures, error tracking, isometric muscle force and percentage maximum level of stimulation required to correct error in five chronic stroke patients as a result of an intervention using FES mediated by ILC. The intervention consisted of either 18 or 25 sessions during which patients practiced planar reaching tasks augmented by responsive FES of the triceps brachii muscle.

Clinical trial results show a statistically significant improvement in tracking ability, a reduction in upper limb impairment measured by the FMA but the ARAT increased. This non-significant change observed in the ARAT was anticipated because this measure assesses hand function and activities requiring both reaching and

raising of the arm. The intervention involved only stimulation of triceps, during 2D tracking tasks requiring elbow and shoulder movement during which the forearm was supported. The change in unassisted error tracking for all patients over all trajectories was not monotonic, reflecting individual variations in day-to-day motor control, but was significant for three out of the four trajectories (T1SS, T1 MS, T2MS).

In terms of directional variation in isometric force, the results show that the stroke patients' mean isometric force data was less in all directions compared with the neurologically intact participants' mean. Both stroke and neurologically intact participants were weaker in some directions than in others. The directional variation in stroke patients' isometric data, both baseline and post treatment, closely reflects the pattern of variation occurring in neurologically intact participants. This is true for all directions excluding 0°, this being the second weakest direction for stroke patients and the strongest for neurologically unimpaired people. When other directions are considered, similarities emerge; the next strongest directions include 120°, 180° and 240°, then 300°. The weakest direction for all patients is 60°. Differences in orientation appear therefore to have a large effect on the ability to generate isometric force.

Figure 4.28 demonstrates that all the patient's isometric force data increased over the 18 sessions and improved further over the extra 7 sessions and that this change was significant for five out of the six directions tested. The gain in force over the intervention might be predicted to be greatest in the 0° direction i.e., directly away from the body as the triceps brachii was stimulated in the intervention. This was not the case. Overall, patients' isometric force increased most in the direction of 300°, then in 180° and then in 0°. The gains were smallest in the direction in which patients were weakest (60°). Improvements in force reflected individual impairments including the side of hemiplegia.

The discussion above would imply that for stroke patients the gains in isometric force were most marked in directions requiring the use of pectoralis major, a powerful shoulder adductor as well as triceps brachii and biceps brachii. A change in triceps brachii force would be expected, but the reason for a change in the biceps brachii force is less clear. Co-activation, observed during motor learning, may increase joint stiffness and stability to improve performance. A future study could investigate whether unintended co-activation resulting from the practice of new tasks leads to an increase in the biceps brachii strength.

Figure 4.29 shows that during the intervention using FES mediated by ILC, the error tracking remained within a close range (<150 mm) whilst the FES required to achieve it reduced over the course of the intervention period. It has been suggested that the mechanisms for the recovery of voluntary power after using FES are due to effects on peripheral muscle (strength, fitness, length and spasticity) or central mechanisms (cortical or segmental reorganization and modification of Hebb synapses) (Rushton 2003).

4.7.1 Limitations of the Clinical Trial

The results obtained demonstrate significant improvements in unassisted error tracking, isometric force and reduction of impairments as measured on the upper limb FMA motor scale. To verify these results the intervention will need to be applied to a larger sample of patients. As there was no control group the degree to which the observed changes were related to movement practice or to FES mediated by ILC cannot be separated. Any future trials should address this limitation by having a control group using the robot without electrical stimulation and increasing the robotic assistance to provide similar levels of tracking accuracy.

Weakness has been found to be the main contributor to activity limitation in other studies (Ada et al. 2006). The improvements in isometric force and reductions in other impairments have not, however, translated into improvements in function as measured by the ARAT in this initial trial. Subsequent research should therefore focus on stimulating more muscles (e.g., anterior deltoid) and relaxing the horizontal forearm constraints to allow a greater range of movement in three dimensions. Such research is the subject of the remainder of this monograph.

References

Ada L, O'Dwyer N, O'Neill E (2006) Relation between spasticity, weakness and contracture of the elbow flexors and upper limb activity after stroke: an observational study. Disabil Rehabil 28(13–14):891–897

Baratta R, Solomonow M (1990) The dynamic response model of nine different skeletal muscles. IEEE Trans Biomed Eng 37:243–251

Carroll D (1965) A quantitative test for upper extremity function. J Chronic Disabil 18:479–491

Colgate JE, Hogan N (1988) Robust control of dynamically interacting systems. Int J Control 48(1):65–88

Davoodi R, Andrews BJ (2004) Fuzzy logic control of FES rowing exercise in paraplegia. IEEE Trans Biomed Eng 51(3):541–543

Dou H, Tan KK, Lee TH, Zhou Z (1999) Iterative learning control of human limbs via functional electrical stimulation. Control Eng Pract 7(3):315–325

Freeman CT, Lewin PL, Rogers E (2005) Experimental evaluation of iterative learning control algorithms for non-minimum phase plants. Int J Control 78(11):826–846

Freeman CT, Hughes A-M, Burridge JH, Chappell PH, Lewin PL, Rogers E (2007) An experimental facility for the application of iterative learning control as an intervention aid to stroke rehabilitation. Meas + Control: J Inst Meas Control 40(1):20–23

Freeman CT, Hughes A-M, Burridge JH, Chappell PH, Lewin PL, Rogers E (2009a) A robotic workstation for stroke rehabilitation of the upper extremity using FES. Med Eng Phys 31(3):364–373

Freeman CT, Hughes A-M, Burridge JH, Chappell PH, Lewin PL, Rogers E (2009b) A model of the upper extremity using FES for stroke rehabilitation. J Biomech Eng 131(3):031011–031023

Freeman CT, Hughes A-M, Burridge JH, Chappell PH, Lewin PL, Rogers E (2009c) Iterative learning control of FES applied to the upper extremity for rehabilitation. Control Eng Pract 17(3):368–381

Hughes A-M, Freeman CT, Burridge JH, Chappell PH, Lewin PL, Rogers E (2009) Feasibility of iterative learning control mediated by functional electrical stimulation for reaching after stroke. Neurorehabil Neural Repair 23(6):559–568

Krebs HI, Hogan N, Aisen ML, Volpe BT (1998) Robot-aided neurorehabilitation. IEEE Trans Rehabil Eng 6:75–87

Lan N, Feng H-Q, Crago PE (1994) Neural network generation of muscle stimulation patterns for control of arm movements. IEEE Trans Rehabil Eng 2(4):213–224

Le F, Markovsky I, Freeman CT, Rogers E (2010) Identification of electrically stimulated muscle models of stroke patients. Control Eng Pract 18(4):396–407

Le F, Markovsky I, Freeman CT, Rogers E (2012) Recursive identification of hammerstein systems with application to electrically stimulated muscle. Control Eng Pract 20(4):386–396

Loureiro R, Amirabdollahian F, Topping M, Driessen B, Harwin W (2004) Upper limb mediated stroke therapy—GENTLE/s approach. J Auton Robot 15(1):35–51

Lum PS, Burgar CG, Shor PC (2004) Evidence for improved muscle activation patterns after retraining of reaching movements with the MIME robotic system in subjects with post-stroke Hemiparesis. IEEE Trans Neural Syst Rehabil Eng 12(2):186–194

Matthews JNS, Altman D, Campbell MJ, Royston P (1990) Analysis of serial measurements in medical research. Br Med J (Clinical Research Ed.) 300(6719):230–235

Popovic D, Popovic M (1998) Tuning of a nonanalytical hierarchical control system for reaching with FES. IEEE Trans Biomed Eng 45(2):203–212

Rushton DN (2003) Functional electrical stimulation and rehabilitation—an hypothesis. Med Eng Phys 1:75–78

Shue G, Crago PE, Chizeck HJ (1995) Muscle-joint models incorporating activation dynamics, moment-angle, and moment-velocity properties. IEEE Trans Biomed Eng 42(2):213–223

Siciliano B, Villani L (1999) Robot force control. Kluwer Academic Publishers, Boston

Chapter 5
Iterative Learning Control of the Unconstrained Upper Limb

Building on the planar results of the previous chapter, an extension to a 3D task is developed where the ability to lift the arm is also rehabilitated. As stroke patients have difficulty lifting their affected arm, a gravity unweighting robot is used and the development again leads to a clinical trial. The analysis is extended to compensate for muscle fatigue.

5.1 Robotic System

In the work described in the previous chapter, the patient's forearm is constrained to lie in a horizontal plane and the next stage is to consider a wider range of more functional movements, which more closely resemble the tasks necessary for daily living (Hughes et al. 2009) and are aligned with the activity-based ARAT measures. This chapter develops the previous model of the arm to remove the planar forearm constraint, permitting unconstrained movement, and applies three ILC laws to the subsequent system, including one to compensate for muscle fatigue. First, the development of the robotic systems used is described in this section taken, in part, from Freeman et al. (2011).

To provide assistance in the completion of unconstrained 3D upper limb reaching movements, FES must, as in the planar case of the previous chapter, be applied using a controlled environment to reduce fatigue and ensure safety and comfort across a broad spectrum of patient abilities. Many exoskeletal robotic systems exist that are capable of providing such support, although very few have been combined with FES and fewer still with model-based FES control schemes. The research described in this chapter uses a commercially available device, but the ILC laws may be applied to a range of such supports.

C.T. Freeman et al., *Iterative Learning Control for Electrical Stimulation and Stroke Rehabilitation*, SpringerBriefs in Control, Automation and Robotics, DOI 10.1007/978-1-4471-6726-6_5

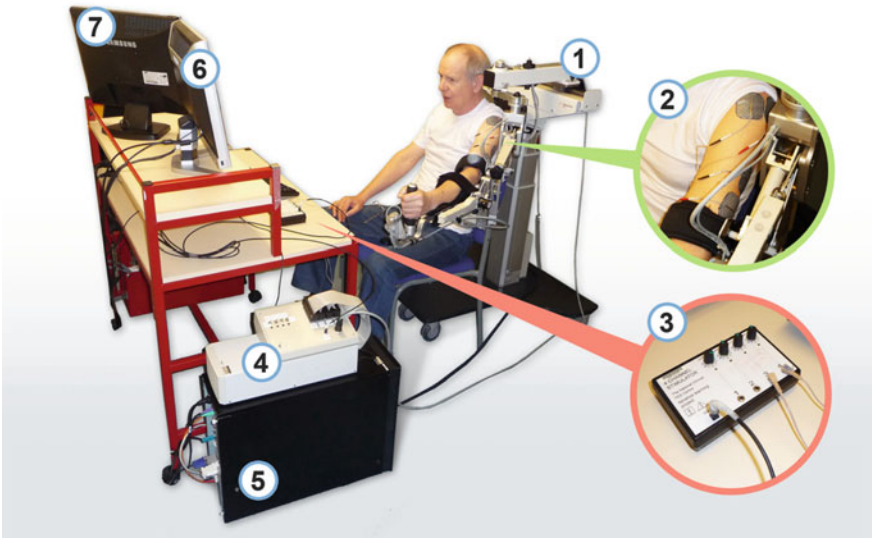

Fig. 5.1 3D ILC system components: (*1*) unweighing robotic device, (*2*) surface electrodes on triceps and anterior deltoid, (*3*) FES module, (*4*) real-time processor and interface module, (*5*) PC, (*6*) monitor displaying task, and (*7*) operator monitor

The mechanical exoskeleton employed is shown in Fig. 5.1 and has two springs incorporated in the mechanism to provide support to overcome gravity. This passive unweighing device allows patients to focus practice on the impaired muscles rather than those acting against gravity. Whilst it is supplied with its own broad range of virtual reality tasks, these are not suitable for control law evaluation and a custom task display system has instead been developed.

The patient is seated with their impaired arm strapped into the mechanical unweighing device, whose segmental lengths and degree of anti-gravity support are adjusted for each person. Joint positional data provided by resolvers mounted on the support mechanism are transferred to the interface module, which connects external devices to the real-time hardware.

In application, the FES electrodes are attached to the patient's anterior deltoid and triceps muscles in accordance with clinical guidelines and are connected to a FES module that is, in turn, connected to the interface module. The clinical operator uses a graphical user interface (GUI) to enter data and initiate tests necessary for the generation of a suitable reaching task and information required for the FES control law. Once the task is set up, FES control algorithms are calculated automatically using a graphical simulation environment with access to control toolboxes and downloaded to a dedicated single-board controller. The task is displayed using custom-made virtual reality software, whilst the FES based control law simultaneously provides assistive stimulation to enable its accurate completion. The components of the system are next described in detail.

5.1.1 Mechanical Support

Armeo (Hocoma AG, Zurich, Switzerland) is a commercially available upper extremity therapy system that combines a passive arm support with intensive task-oriented exercises presented in a virtual reality environment. The mechanical support alone is used in the research described in this chapter. Each joint is aligned in either the horizontal or vertical plane, which is measured using a resolver. Moreover, whilst the FES laws and other system components developed in this chapter may in principle be applied using any system (passive or robotic) capable of providing support and kinematic information, the movement constraints and kinetic properties imposed influence the dynamic model used.

5.1.2 Biomechanical Dynamic Model

The biomechanical system consists of the human arm and exoskeleton mechanical support system shown in Fig. 5.2a. Figure 5.2b shows the kinematic structure of the exoskeleton support, for which the joint variables are assembled into the vector $q_a = [\theta_1, \theta_2, \theta_3, \theta_3', \theta_4, \theta_5]^T$ and correspond to the measured joint angles. Also the parallelogram structure of the upper arm section results in $\theta_3 = \theta_3'$.

Figure 5.2c shows the human arm and since it is strapped to the support there exists a unique bijective transformation between their coordinate sets, given by $q_u = f_a(q_a)$, where

$$q_u = [\vartheta_a, \vartheta_b, \vartheta_c, \vartheta_d, \vartheta_e]^T$$

contains the anthropomorphic variables shown in this figure. Using this relationship, application of Lagrangian analysis produces a dynamic model of the combined robotic and human arm systems given in the anthropomorphic coordinates as

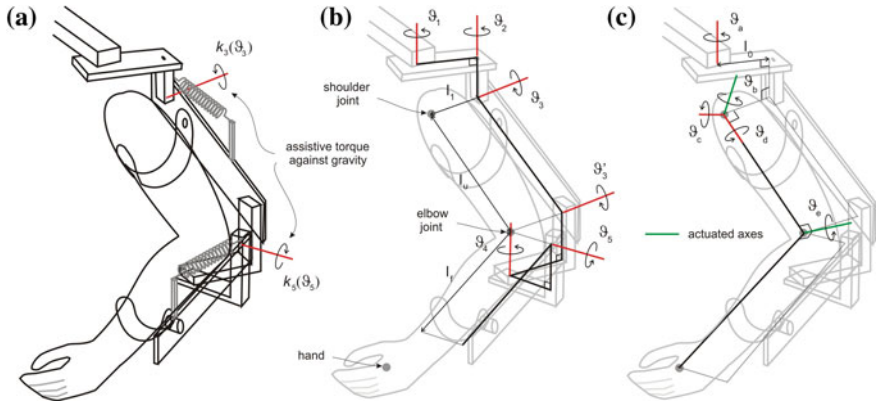

Fig. 5.2 Kinematic system relationships, **a** combined system, **b** Armeo support, and **c** human arm

$$B_u(q_u)\ddot{q}_u + C_u(q_u, \dot{q}_u)\dot{q}_u + F_u(q_u, \dot{q}_u) + G_u(q_u) + K_u(q_u) = \tau_u(u, q_u, \dot{q}_u) - J_u^T(q_u)h \quad (5.1)$$

where B_u, $C_u \in \mathbb{R}^{5\times5}$ are the inertial and Coriolis matrices, respectively, for the 3D system, $G_u \in \mathbb{R}^5$ is the vector of moments produced by gravity, and $K_u \in \mathbb{R}^5$ is the vector of moments produced by the unweighing action, where Freeman et al. (2011) gives a full description of the individual components.

The non-conservative forces assume the same form as in the planar case in the previous chapter and hence

$$F_u(q_u, \dot{q}_u) = \left[\, F_a\left(\vartheta_a, \dot{\vartheta}_a\right) \ldots F_e\left(\vartheta_e, \dot{\vartheta}_e\right) \right]^T$$

whose components incorporate friction and spasticity. Also the vector due to stimulated muscle in (5.1) takes the form

$$\tau_u(u, q_u, \dot{q}_u) = \left[\, 0\ \tau_b\left(u_b, \vartheta_b, \dot{\vartheta}_b\right)\ 0\ 0\ \tau_e\left(u_e, \vartheta_e, \dot{\vartheta}_e\right) \right]^T$$

where $u_b(t)$ and $u_e(t)$ are the electrical stimulation sequences applied to the triceps and anterior deltoid muscles, respectively, and $u = [u_a, u_b, u_c, u_d, u_e]^T$. Moreover, h represents a vector of external forces and torques applied by the therapist using a handle mounted on a sensor attached to the robotic support and is only used during identification tests.

The model (5.1) is used by the FES control law to calculate a control vector that results in accurate tracking of a reference trajectory. Since assistive torque is applied about the ϑ_b and ϑ_e axes only, the system is underactuated. When applied during the treatment of patients, the control law assists tracking about ϑ_b and ϑ_e alone, and, in response to clinical guidelines, it is assumed that the patient has sufficient control over the remaining axes to adequately perform the task.

5.1.3 FES Module

The FES system can deliver 4 channels of stimulation, each comprising a sequence of bi-phasic pulses at 40 Hz. The frequency, amplitude, pulsewidth range and bi-phasic characteristic have been chosen to achieve a smooth muscle contraction, see de Kroon et al. (2005), McNeal et al. (1986) for a comparison of the effects of the stimulation parameters. The control hardware produces a series of 5 V amplitude, 40 Hz pulses with the required pulsewidth for each channel. Each of them is then optically isolated and fed to the amplification stage of a battery powered commercial stimulator to result in the desired bi-phasic characteristic and voltage amplitude. In response to safety requirements, the pulsewidth and hence the energy supplied to the arm is limited by the control software and by components within the modified stimulator. The amplification level used for each channel is set prior to each treatment session by applying a stimulation signal with pulsewidth 350 μs and then the voltage is slowly increased until the maximum comfortable level is reached.

5.1.4 Software Systems

In contrast to the planar case of the previous chapter, it is not feasible to display a real world tracking task in 3D and therefore a virtual task is displayed to the patient to ensure clarity, with provision for additional visual instructions and performance feedback. The patient's screen runs a 3D virtual reality environment that displays a graphic of their arm in real-time, together with the trajectory tracking task, and is shown in Fig. 5.3. The aim of the tracking task is for the patient to follow a sphere that travels along the trajectory at various speeds, whilst ILC laws, designed using the biomechanical system, regulate the assistive FES stimulation required for their completion. The graphic of the patient's hand changes color to indicate their current error level. Feedback of performance is also given by an error percentage score displayed after each set of trials. A graphic of the initial arm position is displayed to ensure accurate resetting of the system at the start of each trial.

Custom reference trajectories are generated for each patient, producing tracking tasks that extend the arm out in front of the patient in response to clinical need, which were calculated using their identified workspace to establish the maximal arm extension directly in front of them and out to their affected side. By interpolating between these two points a third intermediate point is then generated. Each reference starts from an initial point close to the patient's body and extends 60, 80 and 100 % of the distance to one of these points. The task comprises reaching out to one of the end-point locations, with the fixed trajectories for each of the five joints generated by scaling a third-order ramp signal of 10 s duration and adding an offset to ensure that it smoothly connects the required start and end joint angles. This results in the vector of reference trajectories

$$q_u^*(t) = \left[\vartheta_a^*(t) \ \vartheta_b^*(t) \ \vartheta_c^*(t) \ \vartheta_d^*(t) \ \vartheta_e^*(t) \right]^T$$

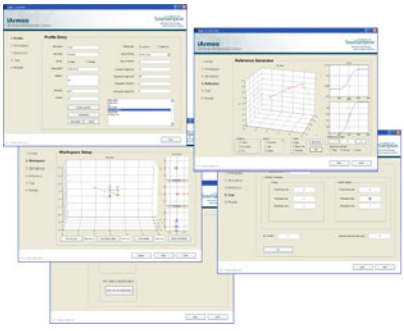

Screen for Physiotherapists:
System Configuration and Training Sessions

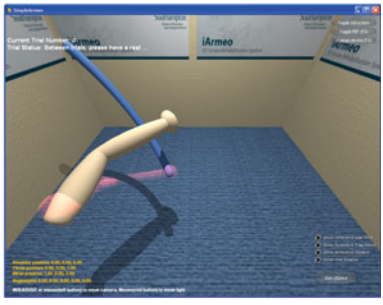

Screen for Patients:
Realtime 3D Graphic Environment

Fig. 5.3 Screen shots of the software system

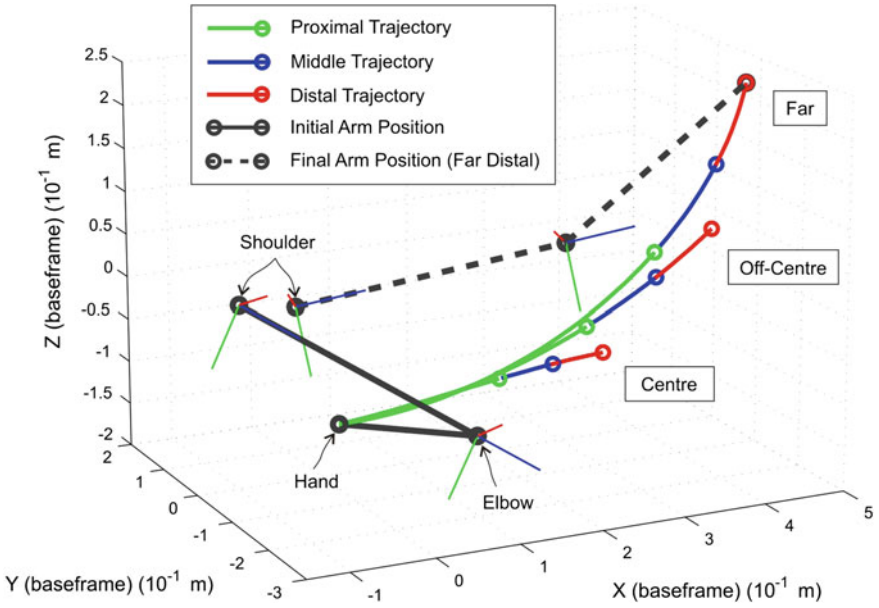

Fig. 5.4 Reference trajectories for the 3D rehabilitation system

where the presence of non-fixed $\vartheta_a^*(t)$, $\vartheta_c^*(t)$, and $\vartheta_d^*(t)$ components makes the task more natural to the patients, who can use their remaining voluntary effort to move these joints. An example of the reaching tasks used during testing and in clinical trials is given in Fig. 5.4.

5.2 ILC Design

Two ILC designs are used, starting with the phase-lead law of the previous chapter (see also (4.34)),

$$v_{k+1}(t) = v_k(t) + L_g e_k(t + \lambda), \ \lambda > 0 \tag{5.2}$$

where

$$e_k(t) = q_u^*(t) - q_{u,k}(t). \tag{5.3}$$

In this 3D case the system is treated as two SISO systems, i.e., the control and movement of forearm and upper arm can be achieved independently of each other. Since FES is applied only about ϑ_b and ϑ_e, L is multiplied by the matrix

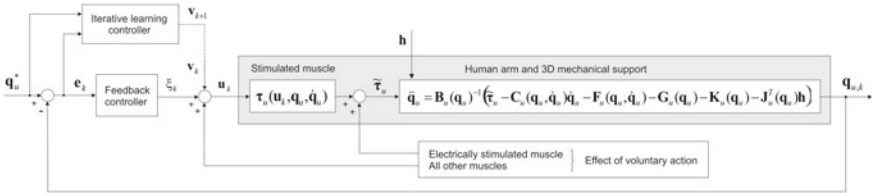

Fig. 5.5 Block diagram representation of the ILC control scheme for the 3D rehabilitation system

$$\begin{bmatrix} 0 & 0 & 0 & 0 & 0 \\ 0 & 1 & 0 & 0 & 0 \\ 0 & 0 & 0 & 0 & 0 \\ 0 & 0 & 0 & 0 & 0 \\ 0 & 0 & 0 & 0 & 1 \end{bmatrix}$$

As illustrated in Fig. 5.5, the ILC law operates in conjunction with a feedback controller given by $\frac{\xi_k(s)}{e_k(s)} = C(s)$ that provides baseline tracking and disturbance rejection. In operation the phase-lead ILC law performs best when the system approximates a simple time-delay and with an appropriately tuned feedback controller can ensure rapid convergence over initial trials. As in the previous chapter, the problem of high frequency components gradually increasing when a large number of trials are performed can always be addressed through use of a zero-phase filter applied to the error or control input, however, the low number of trials performed means that it is unnecessary in the present application. In contrast to phase-lead, Newton ILC (Lin et al. 2006) (2.36)–(2.42) uses the full model in the calculation of the next trial input.

5.2.1 Experimental Results with Unimpaired Subjects

The phase-lead and Newton ILC laws were experimentally implemented using six unimpaired participants as an essential step in obtaining ethical approval for patient trials. Representative results and summary statistics are given in this section. Each participant was seated in the robot, which was adjusted to their individual arm dimensions. Electrodes were positioned over their triceps and anterior deltoid muscles in such a way that maximum movement was generated through application of FES. The stimulation amplitude and maximum pulsewidth were adjusted to be within comfortable limits. As described above, the model of the human arm includes two person-dependent parameters that define the position of the anterior deltoid axis, which is fixed with respect to the shoulder as shown in Fig. 5.2c. These were determined before the experiments commenced by applying FES to the anterior deltoid and recording the resulting movements of the human arm. Since the rotation of the human upper arm should then be about the anterior deltoid axis, see Fig. 5.2c, this

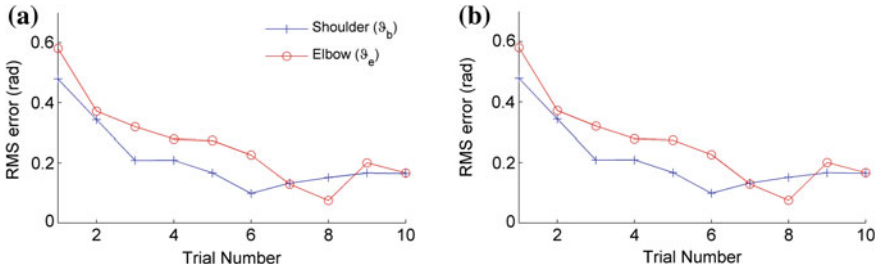

Fig. 5.6 RMS error plots for **a** participant 1 and **b** participant 2 using phase-lead ILC

axis was identified by fitting a plane to the elbow position by least mean squares optimization. The vector perpendicular to the plane, which is also through the pivot, then equates to the required anterior deltoid axis (Freeman et al. 2011).

Figure 5.6 gives tracking performance results for two participants with the phase-lead ILC law. The RMS error is given for both ϑ_b and ϑ_e over 10 trials, where for trial k

$$\mathrm{RMS}_{i,k} = \sqrt{\frac{1}{T+1}\sum_{t=0}^{T}\left(\vartheta_i^*(t) - \vartheta_{i,k}(t)\right)^2}, \quad i = b, e \tag{5.4}$$

where $T+1$ is the number of samples in the discrete representations of the reference $\vartheta_i^*(t)$ and recorded joint angle sequence $\vartheta_i(t)$. Due to the kinematic redundancy of the task, this is a more reliable measure than the Cartesian end-point error, which was used in the planar case.

In this unimpaired study, the tracking error reduces quickly and maintains a low level as the trials progress. In some cases the RMS error increases slightly in later trials because the participant's triceps started to suffer from fatigue but the ILC was quickly able to modify the stimulation to maintain a low error. Figure 5.7 shows tracking performance for the same two participants, illustrating close reference tracking for both controlled angles.

Table 5.1 gives summary statistics for 6 unimpaired participants. Each participant undertook ILC trials using two trajectories, the first moved their arm out in front of them and the second moved it out and to their side. The average RMS error was calculated for each trajectory and the mean and standard deviation calculated across participants. These calculations were then repeated using the lowest RMS error recorded for each trajectory.

Figure 5.8 shows error norm results over 10 trials of the Newton ILC law for two participants, using a long off-center and a medium off-center trajectory. The results are representative of all the tasks tested and confirm that accurate tracking is achieved within very few trials. The NOILC weighting matrices used in these tests were $Q = 30I$ and $R = I$ respectively. Figure 5.9 shows representative input, output, and error signals recorded on trial 8 for one participant and confirm that a high level

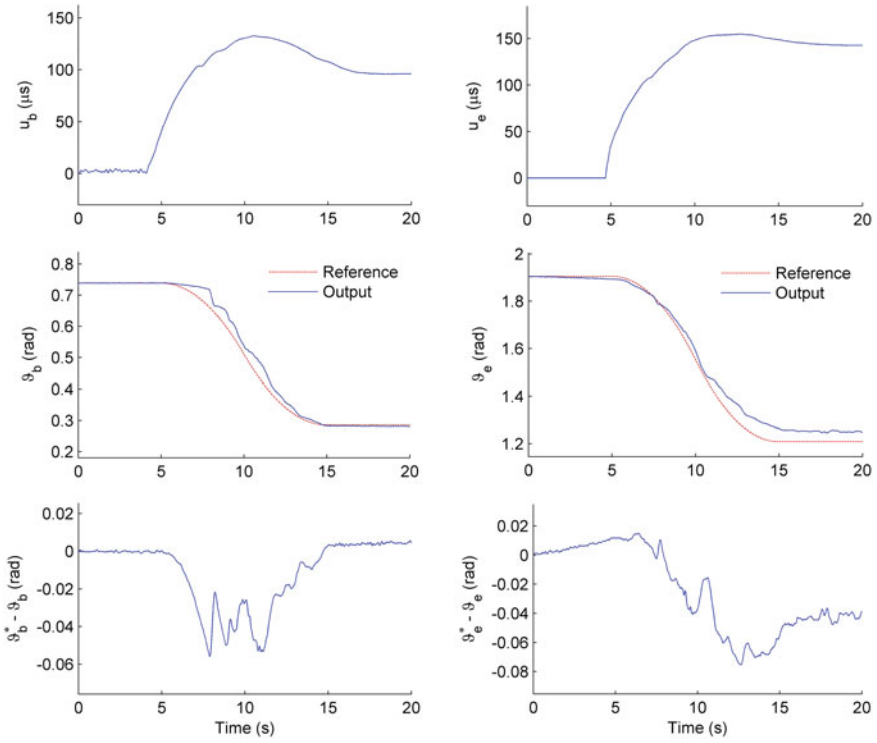

Fig. 5.7 Tracking performance for participant 1 on trial 6. Five second padding is applied at the beginning and end of each reaching movement

Table 5.1 Mean (standard deviation) RMS error for 6 unimpaired participants undertaking two trajectory tracking exercises using the 3D robot system with no voluntary assistance

		Trajectory 1	Trajectory 2
Shoulder RMS error (rad)	Best trial only	0.2415 (0.0693)	0.0574 (0.0557)
	Mean of first 6 trials	0.0949 (0.0906)	0.1691 (0.1609)
Elbow RMS error (rad)	Best trial only	0.0721 (0.0700)	0.0837 (0.0900)
	Mean of first 6 trials	0.1480 (0.1327)	0.2189 (0.1723)

of tracking performance is achieved with an input signal that is not excessive. The theoretical property of monotonic trial-to-trial convergence to zero tracking error is degraded due to inaccuracies in the human arm model, motivating development of more accurate identification procedures, and future use of on-line and recursive techniques. Such identifications routines, however, must be suitable for application within the restrictive conditions of clinical trials, where there is limited set-up time, little opportunity to repeat measurements and satisfactory results for a wide range of patients and changing physiological conditions are required.

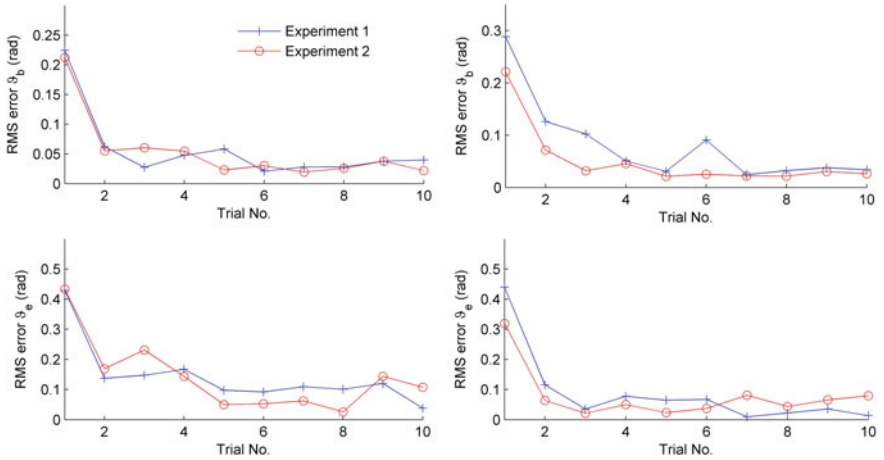

Fig. 5.8 RMS error plots for 2 participants using Newton ILC, subject 1, *left-hand plots*, subject 2, *right-hand plots*

5.2.2 Clinical Trial

The results in this section are, in the main, from Meadmore et al. (2012), which also details how the patients were recruited to the study and ethical approval obtained. On completion of these steps, the five patients chosen (three men and two women) were aged between 33 and 67 years ($M = 52.6$, $SD = 15.27$) and had suffered ischemic strokes, between 6 years 6 months and 11 months prior to recruitment to the study ($M = 3$ years 10 months, $SD = 2$ years); four had a hemiparesis of the left side and one of the right. All patients were right-side dominant prior to their stroke and all complied with the study protocol, i.e., attended all sessions. During each intervention session patients spent 40–50 min practising reaching movements.

In advance of the intervention sessions, two assessments, four weeks apart, were completed to establish baseline performance for three clinical outcome measures, with a final assessment one or two days later. Assessments of the upper limb consisted of the FMA and ARAT outcome measures, assessing impairment and function respectively. Eighteen possible reference trajectories were used; each of these could be in one of three orientations relating to space in front and to the hemiplegic side (center, off-center and far), one of three lengths (proximal, middle, and distal) and one of two speeds (5 and 10 s duration).

5.2.3 Unassisted Tracking Tasks

Patients completed four unassisted tracking tasks immediately following set up and at the end of each session. These tasks involved tracking a slowly moving sphere

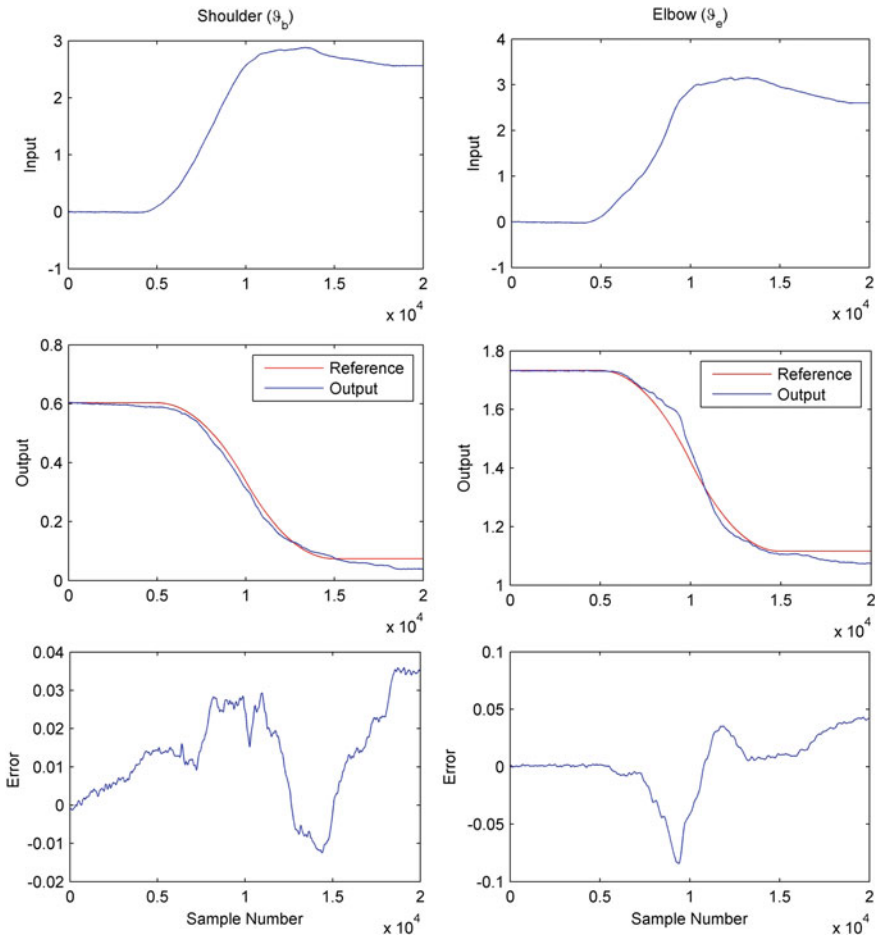

Fig. 5.9 Tracking performance of Newton ILC

along the far distal, far middle, off-center middle, and center distal trajectories of 10 s duration. Patients attempted each unassisted tracking trajectory once, i.e., each task consisted of one trial, with no FES assistance. For each task, there was a five-second countdown prior to the commencement of each trial, presented both visually and verbally.

One measure of tracking performance that can be compared across different tasks is the RMS of the tracking error, which for joint j is given by (5.4). Once evaluated, this number was divided by the norm of the reference trajectory for the same joint, calculated using the same formula, and the result subtracted from 1. Hence performance score of 1 corresponded to perfect tracking and a negative value indicates a movement away from the desired trajectory.

Assisted tracking tasks were selected according to clinical need and hence some trajectories may have been used more than once or not at all. During each task, FES was applied to the muscles to assist the patient's tracking. For three of the patients, the triceps and anterior deltoid were trained simultaneously (patients 1, 3, and 5). However, for two patients (2 and 4), an adverse response was observed when both muscles were stimulated, i.e., a flexor synergy was observed, most likely related to spasticity. In these cases, FES was mainly applied to one muscle at time, e.g., stimulation of triceps and then anterior deltoid.

In each task, patients completed 6 trials tracking the same trajectory. A 15 s rest period between trials was designed to reduce fatigue and was extended if necessary. During this period a graphic was presented illustrating tracking performance for the trial just completed and the optimal stimulation signals for application in the next trial were also computed in this time period.

Patients started each movement from the same initial position, which was determined at the start of the first trial and completed between 4 and 6 trials depending on fatigue, where control action to suppress this effect is considered in the next section of this chapter. For each trial tracking performance was measured, as described above, and the percentage of maximum FES applied was calculated by dividing the norm of the FES by the norm of the maximum stimulation that could be applied. Examples of these signals are shown in Fig. 5.10, which also illustrates ILC correcting the applied FES to result in accurate tracking.

The data from the two pre-intervention assessment sessions were tested for differences using a t-test and then averaged for baseline performance. A one-tailed,

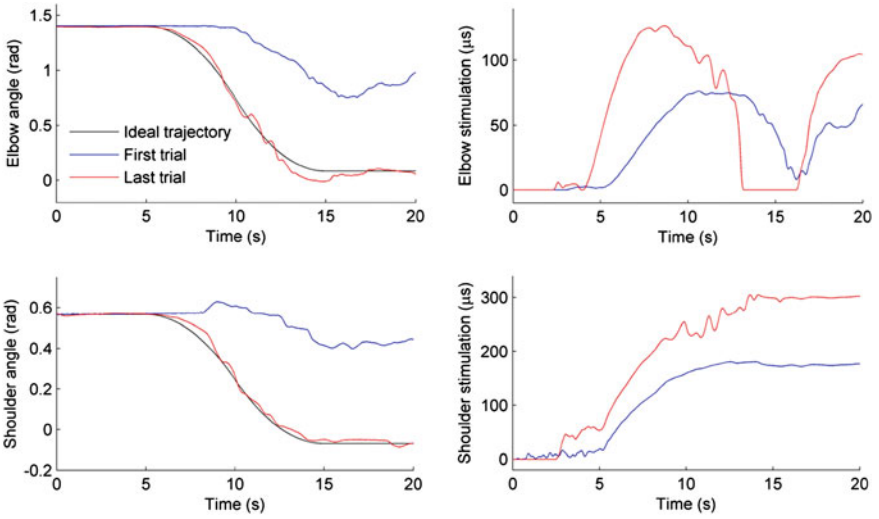

Fig. 5.10 Example of ILC correcting tracking: Elbow and shoulder tracking is shown on first and last trial (*left-hand column*), together with corresponding applied FES (*right-hand column*). Five second padding is applied at beginning and end

paired t-test, with a significance level of $p < 0.05$, was used to compare baseline and post-intervention FMA and ARAT outcome measures. An improvement of 10 % of the total number of points available for these measures was considered a clinically relevant improvement (van der Lee et al. 2001). The maximum score for the FMA (motor component) was 66 and the maximum score for the ARAT was 57. In line with previous work (Hughes et al. 2009), changes in assisted and unassisted performance were analyzed by calculating best-fit linear regression slopes of performance against session number for each patient, and applying one-sample t-tests. Significance was associated with a value of $p < 0.05$.

The clinical scores for the FMA and ARAT at baseline and after 18 intervention sessions are shown in Tables 5.2 and 5.3 respectively. There were no significant differences between the two baseline assessment sessions for the FMA, $t(4) = -2.08$, $p = 0.11$, or ARAT, $t(4) = -1.83$, $p = 0.14$. A significant improvement was found from baseline to post-intervention for the FMA, $t(4) = -4.54$, $p = 0.001$, with all patients showing an improvement on the motor sub-test of this assessment.

This improvement was above the suggested 10 % increase for clinical relevance in 3 of the 5 patients, although overall the 14 % change was not statistically different from 10 %, $t(4) = 1.32$, $p = 0.26$. No changes were found for the ARAT, $t(4) = -0.34$, $p = 0.37$. Thus, this rehabilitation system reduced motor impairment of the upper arm in stroke patients but this did not transfer to functional improvements as assessed by the ARAT.

Table 5.2 FMA at baseline and post-intervention sessions

P.Id	Baseline (pre-1, pre-2) average	Post	Change (%)
1	(7, 12) 9.5	20	16
2	(19, 19) 19	33	21
3	(28, 34) 31	44	20
4	(15, 15) 16	21	8
5	(42, 42) 42	46	6
Mean (SD)	23.5 (12.95)	32.8 (12.28)	14

P.Id Patient identification number

Table 5.3 ARAT at baseline and post-intervention sessions

P.Id	Baseline (pre-1, pre-2) average	Post	Change (%)
1	(0, 0) 0	1	16
2	(4, 10) 7	10	21
3	(9, 9) 9	10	20
4	(3, 5) 4	0	8
5	(11, 13) 12	13	6
Mean (SD)	6.4 (12.95)	6.8 (5.89)	14

P.Id Patient identification number

5.2.4 Unassisted Tracking Performance

Figure 5.11 illustrates unassisted tracking performance for the elbow as a function of session, for each patient and task. Similar patterns of performance were found for the shoulder. Best-fitting regression lines were calculated for each combination of patient, task, and muscle, giving 40 slopes in total, and one-tailed t-tests found that the slopes, collapsed across all patients, were reliably positive for each of the four unassisted tasks for both the shoulder and the elbow (Meadmore et al. 2012).

The slopes computed were significantly different from zero, showing that tracking accuracy, i.e., error between arm position and target, improved over the course of the intervention for both shoulder and elbow movements. Moreover, the mean slopes correspond (Meadmore et al. 2012) to performance increases of between 49 and 93 % over the course of the intervention, thereby confirming significant improvement.

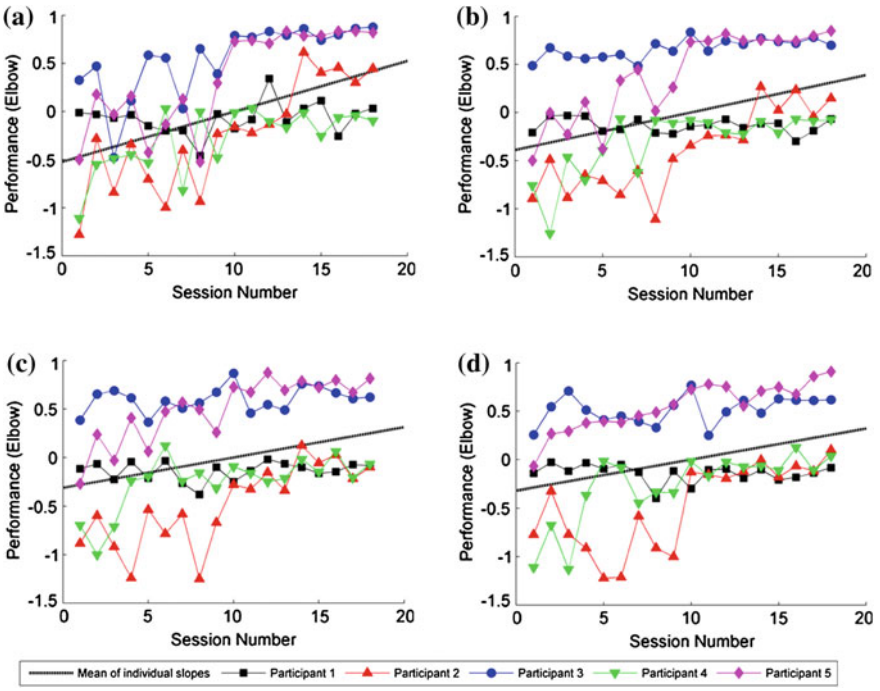

Fig. 5.11 Unassisted tracking performance for the elbow as a function of session, for each patient and unassisted task. Panel **a** shows tracking performance for the center-distal task; Panel **b** shows tracking performance for the off-center-middle task; Panel **c** shows tracking performance for the far middle task; Panel **d** shows tracking performance for the far distal task. 1 = perfect tracking performance. Best fitting regression slopes were calculated for each combination of patient, muscle and task, with mean slopes (across participants) shown

5.2.5 Assisted Tracking Performance

Tracking performance measures and the percentage of maximum stimulation applied were calculated using the final trial in each task and were averaged across tasks in each session. As shown in Fig. 5.12, for both the shoulder and the elbow, patients tracking performance became more accurate over the 18 sessions and the percentage maximum stimulation decreased. Best-fitting regression lines were calculated for each patient and muscle, and one-tailed, one-sample t-tests found that the slopes collapsed across all patients and were statistically significant for each muscle.

These results suggest that the amount of movement produced by the FES, for both the triceps and anterior deltoid, increased over the intervention. To further qualify this, the tracking performance from the final trial in each task was divided by the corresponding percentage maximum stimulation, and averaged across tasks in each session. The slopes of the best-fitting regression lines were found to be significantly positive (Meadmore et al. 2012), confirming that over the intervention a greater amount of performance was elicited per unit of FES applied.

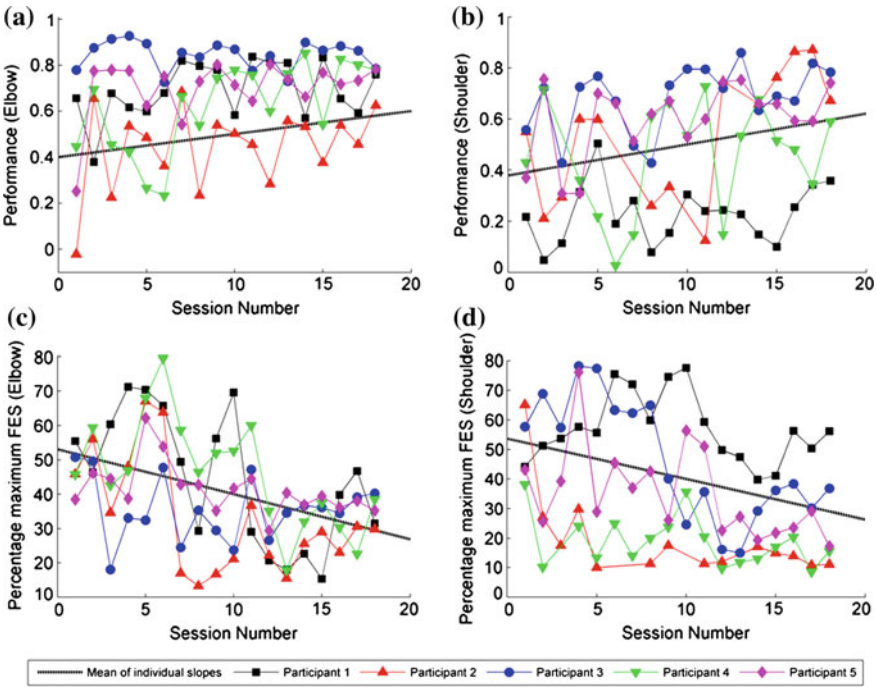

Fig. 5.12 Panel **a** and **b** show tracking performance in the assisted tasks over sessions for the elbow and the shoulder respectively; Panel **c** and **d** show the percentage maximum stimulation applied to the triceps and anterior deltoid respectively, over sessions. Best fitting regression slopes were calculated for each combination of patient and muscle, with mean slopes (across participants) shown

5.2.6 Discussion

The main aims of the study were to investigate the feasibility and effectiveness of a novel 3D stroke rehabilitation platform for the upper limb that combines FES mediated by ILC. This system uses the most advanced model-based FES control laws that have been employed clinically in upper arm stroke rehabilitation, and comprises a substantial development beyond the results in the previous chapter for planar tasks. The effectiveness of FES is suggested to be most beneficial when combined with a patient's own voluntary intention to move. The ILC component was employed to optimize the potential benefit of such intention. Three key findings confirmed feasibility and effectiveness from baseline to post-intervention: a clinically significant improvement in the FMA; an improvement in unassisted tracking required for accurate assisted tracking. Tracking performance in the assisted tasks was more accurate than tracking in the unassisted tasks. In addition, a reduction in the amount of FES applied to the muscles and an increase in the accuracy of assisted tracking was confirmed. Further tests are required to determine the relative contribution of muscle strength and voluntary control to improved tracking performance and thereby explain the reduction in FES.

These performance measures indicate that training the triceps and anterior deltoid improved movement of the upper limb in five stroke patients. However, the observed motor improvement did not transfer to functional improvements, as measured by the ARAT. This is consistent with previous work, with a number of systematic reviews, e.g. Kwakkel et al. (2008), reporting that robotic therapy reduces motor impairment but does not improve functional impairment. The ability to use the hand is an integral component of the ARAT and other functional outcome measures. As only the triceps and anterior deltoid muscles were trained, this may explain why no change was found on this outcome measure. This finding implies that to observe changes in functional outcome measures, future work should extend the application of this intervention to the hand and wrist. This issue is discussed again in the next chapter.

The findings of this study were also in line with those of the previous chapter, in which ILC mediated FES was used to assist stroke patients in planar reaching movements. Specifically, Hughes et al. (2009) found an increase in tracking performance, a reduction in applied FES, and a marginal improvement in FMA scores. The observed improvements in the FMA scores were greater in the current compared to the previous study. Furthermore, the observed FMA improvement was greater than 10 %, indicating a trend towards clinical relevance (van der Lee et al. 2001). One possible reason for the difference in results is that the intervention in this study trained two muscles in 3D space, whereas the previous intervention trained only the triceps in 2D space. Alternatively, the patients in this study had higher initial FMA scores and this may have contributed to the differences found.

5.3 Muscle Fatigue

If muscle fatigue arises in robotic-assisted stroke rehabilitation then this often means that the session must be stopped. In control systems terms, the question that arises is: is it possible to augment an ILC control law to prevent or lessen the effects of muscle fatigue? This section gives some preliminary results in this area based on a form of cascade control. The evaluation of the resulting control scheme is by simulation using a model constructed from patient data from the clinical trials of the previous section.

The material in this section focuses on control system design and hence the muscle model used is an approximation that captures many of the characteristics of FES stimulated muscle, including the force-length and force-velocity properties, nonlinear recruitment and contraction dynamics, where the steady-state torque, T_m, produced by the static nonlinearity with input u is represented by

$$T_m = c_1 \left| \frac{e^{c_1 u} - 1}{e^{c_2 u} + c_3} \right| \tag{5.5}$$

where c_1, c_2 and c_3 are muscle dependent parameters to be determined and u denotes the externally applied stimulation impulse. As previously in this monograph, the linear activation part converting T_m to the resultant torque τ generated by the muscle is modeled as a critically damped second-order linear system with undamped natural frequency ω_n.

Considerable effort has been directed towards modeling and control of fatigued muscles but not in the rehabilitation domain. The objective in this section is to include a term, or model, to represent the effects of fatigue on the performance and enhance or, augment, the control system to lessen or overcome its effects. Modeling of fatigue has been considered in Riener et al. (1996), Riener and Fuhr (1998), where the fatigue dynamics were found to be dependent on activation level, stimulation frequency and recovery. Other research (Abbas and Chizeck 1995; Lan 2002) has established that the effects of fatigue can be represented by multiplying the isometric force produced by the fatigue-free model by a time-varying parameter of the form

$$F(t) = F_0(1 - k_f t) \tag{5.6}$$

where F_0 is the steady-state fatigue-free isometric force and $k_f > 0$ is the rate of fatigue, i.e., the force decays with time in the presence of fatigue.

For ILC based stroke rehabilitation, it is necessary to take account of the repeated trials and hence the fatigue model used is

$$F_k(t) = F_0(1 - k_f t)\lambda^k, \quad |\lambda| < 1 \tag{5.7}$$

where λ governs the influence of the fatigue from trial-to-trial. The premise is that the larger k_f and λ the greater the effects of fatigue on the muscle output. Both of these factors are muscle-dependent and therefore have to be estimated for each patient.

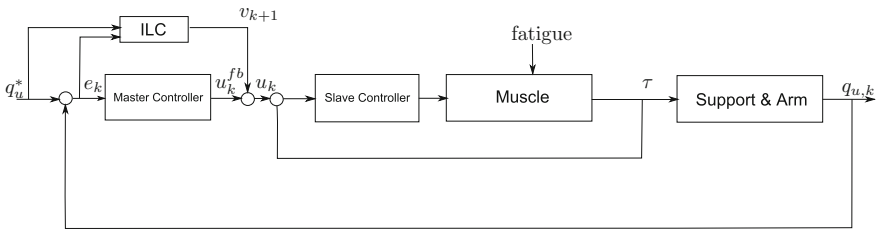

Fig. 5.13 Cascade control of the supported human arm and muscle system

The control scheme developed in what follows is shown in Fig. 5.13 where the effects of fatigue are represented as a disturbance on the muscle and regulated by a feedback loop placed around the muscle model and the controller in this loop is termed the slave.

In this arrangement, q_u^* is the reference vector, $q_{u,k}$ the measured output vector, u_k^{fb} and v_{k+1}, are the outputs of the master controller and the ILC law on the kth trial, respectively, and $u_k = u_k^{fb} + v_{k+1}$ is the input to the muscle control loop. This is a form of cascade control, which has also been the subject of other ILC research outside the healthcare domain. For example, in Tan et al. (2012) the convergence of cascaded ILC was addressed, where two ILC loops are cascaded. Other research on the use of ILC plus feedback control for high-precision tracking performance has been reported, e.g., Huang et al. (2014). For ease of presentation, this scheme will be referred to as cascade control where relevant in the rest of this section. Development follows, in the main, (Xu et al. 2013, 2014).

Figure 5.13 is a form cascade control arrangement where the slave controller is a proportional gain in each of the two channels and the master controller is PD. Control design consists of first designing a feedback linearizing control input for the slave controller muscle inner loop and applying ILC to the resulting system. These are detailed next, starting with the linearizing controller where trial-to-trial updating is not present and hence the trial variable is omitted for ease of presentation.

The remainder of this section considers the case when the slave controller is a proportional gain in each of the two channels and the master controller is PD as in previous work (Freeman et al. 2012). In this first work, the aim is to establish if muscle fatigue can be compensated for by augmenting the scheme used in the previous research reported in Freeman et al. (2012), Meadmore et al. (2012). Moreover, there is a strong case for initially considering the simplest possible addition to the existing scheme and hence the forms of the master and slave controllers considered. Other possibilities, such as adding ILC to the inner loop, i.e., the slave controller loop, or other choices for the master and/or slave controller, are left as topics for future research, see also the conclusions chapter of this monograph.

Given the selection of the master controller, the tasks are to first construct a feedback linearizing control input for the feedback inner loop that includes the slave controller and then design the ILC. The muscle model can be written in state-space form as

$$\dot{\boldsymbol{x}}_{\boldsymbol{i}} = \begin{bmatrix} 0 & 1 \\ -\omega_n^2 & -2\omega_n \end{bmatrix} \boldsymbol{x}_i + \begin{bmatrix} 0 \\ 1 \end{bmatrix} h_{IRC,i}(u_i)$$

$$\tau_i = \begin{bmatrix} \omega_n^2 & 0 \end{bmatrix} \boldsymbol{x}_i, \; i = b, e \tag{5.8}$$

where for each i $x_i = \begin{bmatrix} x_{i,1} & x_{i,2} \end{bmatrix}^T$ is the state vector, u_i is the applied stimulation impulse and τ_i the generated muscle torque respectively. If $h_{IRC,i}(u_i), i = b, e$, is assumed known and monotonic, its static gain characteristic can be canceled by including its inverse as a gain term and the linearizing controller is

$$\boldsymbol{u} = \begin{bmatrix} u_b \\ u_e \end{bmatrix} = \begin{bmatrix} h_{IRC,b}^{-1}(\omega_n^2 x_{b,1} + 2\omega_n x_{b,2} + \frac{v_b'}{\omega_n^2}) \\ h_{IRC,e}^{-1}(\omega_n^2 x_{e,1} + 2\omega_n x_{e,2} + \frac{v_e'}{\omega_n^2}) \end{bmatrix} \tag{5.9}$$

where v_b' and v_e' denote the required muscle torque output to be designed.

Applying this controller cancels the static nonlinearity and next the slave controller is designed. This master/slave control structure provides a more flexible structure than the single loop control methods, which could lead to faster system response. Hence its use as a preliminary controller prior to ILC design for this application area. As there is no need to realize accurate tracking in the inner loop, a proportional controller in each channel is used.

The slave controller gain is selected using trial-and-error and the master controller as in Freeman et al. (2012), with general guidance suggesting that in order to avoid resonance minimal difference between the gains of slave and master controllers is desirable. It follows from simple block algebra that the slave controller loop dynamics are described by the transfer-function matrix

$$\boldsymbol{G}_{muscle}(s) = \begin{bmatrix} \frac{K_{P_b}^s}{s^2 + K_{P_b}^s} & 0 \\ 0 & \frac{K_{P_e}^s}{s^2 + K_{P_e}^s} \end{bmatrix} \tag{5.10}$$

where $K_{p_b}^s$ and $K_{p_e}^s$ are the proportional gains defining the slave controller. Also the inputs to the controlled muscle model (5.10) are the calculated torques from the master controller together with the torques generated by the ILC law, giving

$$v_b' = K_{P_b}^m(\vartheta_b^* - \vartheta_b) + K_{D_b}^m(\dot{\vartheta}_b^* - \dot{\vartheta}_b) + v_b \tag{5.11}$$

$$v_e' = K_{P_e}^m(\vartheta_e^* - \vartheta_e) + K_{D_e}^m(\dot{\vartheta}_e^* - \dot{\vartheta}_e) + v_e \tag{5.12}$$

where v_b and v_e are the outputs from the ILC law and $K_{P_i}, K_{D_i}, i = b, e$, are the gains for the PD master controller.

A number of methods are available in the non-ILC literature for tuning the slave controller to achieve good performance, as described in, for example, Skogestad

and Postlewaite (2005). The reason for introducing the slave controller loop is to "pre-compensate" the plant to obtain faster response rather than achieving 'perfect tracking'. As such, a simple trial and error design method is used but further research could be directed to this task once it is established that there is merit in using this overall approach, i.e., introduce a control loop around the muscle model to compensate for fatigue.

Once the controllers developed above are applied, the resulting dynamics are described by the state-space model

$$\begin{aligned} \dot{\boldsymbol{x}} &= \boldsymbol{f}(\boldsymbol{x}, \boldsymbol{u}) \\ \boldsymbol{y} &= \boldsymbol{h}(\boldsymbol{x}) = \left[\vartheta_b \ \vartheta_e \right]^T \end{aligned} \tag{5.13}$$

where

$$\boldsymbol{x} = \left[q_u^T \ \dot{q}_u^T \ \boldsymbol{x}_b^T \ \boldsymbol{x}_e^T \right]^T$$

and

$$\boldsymbol{f}(\boldsymbol{x}) = \begin{bmatrix} \dot{q}_u \\ p_1(q_u, \dot{q}_u) \\ p_2(q_u, \dot{q}_u) + ((\boldsymbol{B}_u q_u)^{-1})_{2,2} \ K^s_{P_b} x_{b,1} \\ p_3(q_u, \dot{q}_u) \\ p_4(q_u, \dot{q}_u) \\ p_5(q_u, \dot{q}_u) + (\boldsymbol{B}_u(q_u)^{-1})_{5,5} \ K^s_{P_e} x_{e,1} \\ x_{b,2} \\ -K^s_{P_1} x_{b,1} + u_b \\ x_{e,2} \\ -K^s_{P_2} x_{e,1} + u_e \end{bmatrix} \tag{5.14}$$

with

$$\boldsymbol{p}(q_u, \dot{q}_u) = -\boldsymbol{B}_u^{-1}(q_u) \left(\boldsymbol{C}_u(q_u, \dot{q}_u)\dot{q}_u + \boldsymbol{F}_u(q_u, \dot{q}_u) + \boldsymbol{G}_u(q_u) + \boldsymbol{K}_u(q_u) \right) \tag{5.15}$$

where the control laws for u_b and u_e are given in (5.9), (5.11) and (5.12). The remaining task is the design of the ILC law for v_b and v_e in (5.11) and (5.12), which is detailed next.

One obvious option at this stage is to again apply phase-lead ILC as in the planar task of Chap. 4, i.e., design a phase-lead ILC law for each of the muscles. This was considered but, as expected, the performance achieved was inferior to that for the planar case. Moreover, for other 3D tasks it will be required to stimulate more than two muscles and it is to be expected that the increase in dynamic complexity will require the design of more advanced ILC laws. This motivates the decision to consider model-based design, where as an exemplar Newton ILC, see (2.36)–(2.42), is used. In the next section the merits of this design over gradient-based alternatives for this application are discussed.

The overall control law on trial $k + 1$ can now be stated as

$$\begin{aligned}\boldsymbol{u}_{k+1} &= \begin{bmatrix} u_{b,k+1} \\ u_{e,k+1} \end{bmatrix} \\ &= \begin{bmatrix} h_{IRC,b}^{-1}(\omega_n^2 x_{b,1,k+1} + 2\omega_n x_{b,2,k+1} + A) \\ h_{IRC,e}^{-1}(\omega_n^2 x_{e,1,k+1} + 2\omega_n x_{e,2,k+1} + B) \end{bmatrix} \end{aligned} \tag{5.16}$$

$$A = \frac{K_{P_b}^m(\vartheta_b^* - \vartheta_{b,k+1}) + K_{D_b}^m(\dot{\vartheta}_b^* - \dot{\vartheta}_{b,k+1}) + v_{b,k} + \Delta v_{b,k+1}}{\omega_n^2}$$

$$B = \frac{K_{P_e}^m(\vartheta_e^* - \vartheta_{e,k+1}) + K_{D_e}^m(\dot{\vartheta}_e^* - \dot{\vartheta}_{e,k+1}) + v_{e,k} + \Delta v_{e,k+1}}{\omega_n^2}$$

where $\Delta \boldsymbol{v}_{k+1} = \left[\Delta v_{b,k+1} \ \Delta v_{e,k+1} \right]^T$ are computed by Newton ILC. Moreover, the stability of this design can be determined under mild conditions by analyzing the Lipshitiz properties of the plant and the convergence properties of Newton ILC laws, see Xu et al. (2014).

5.3.1 Performance Evaluation

An extensive simulation evaluation of the performance of the control system designed in the previous section has been undertaken (Xu et al. 2013). The parameters for the controlled system, i.e., the uncontrolled system dynamics, are from those collected in clinical trials (Meadmore et al. 2012). The reference trajectories ϑ_b^* and ϑ_e^* also come from Meadmore et al. (2012), see Fig. 5.14, corresponding to lifting and extending the upper arm and forearm over a period of 6 s. Variation is permissible in the uncontrolled joint angles ϑ_a, ϑ_c and ϑ_d. The sampling frequency is 400 Hz. Two general comparative control performance issues are addressed: (i) the ILC design developed in this chapter and (ii) the new ILC design against previous designs where no representation of fatigue was included.

These are treated in turn below where to provide a common basis for comparison the proportional gains for the slave controller were set as $K_{P_2}^s = 450$, $K_{P_5}^s = 600$ for both triceps and anterior deltoid, and the gains of the PD feedback controller are chosen as $K_{P_b}^m = 100$, $K_{D_e}^m = 5$ and $K_{P_e}^m = 200$, $K_{D_e}^m = 1$, respectively. The weighting matrices in the NOILC cost function used as part of the Newton design were $\boldsymbol{Q} = 5 \times 10^4 I$ and $\boldsymbol{R} = I$.

In the case of performance under (i) above, the evaluation is over 6 trials where previous work including clinical trials has shown that ILC mediated FES has most effect after a relatively small number of trials (Hughes et al. 2009). The 2-norm values of the tracking error, i.e., computed along each trial and plotted against trial number, for ϑ_b and ϑ_e are shown in Fig. 5.15. On the first trial only the slave controller has an effect on the 2-norm for this trial, i.e., no ILC action is applied. On subsequent trials

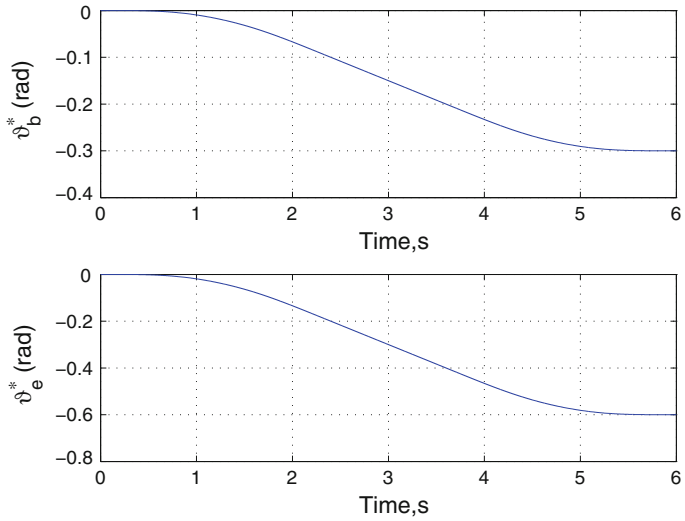

Fig. 5.14 Reference trajectories used for the 3D rehabilitation system fatigue simulations

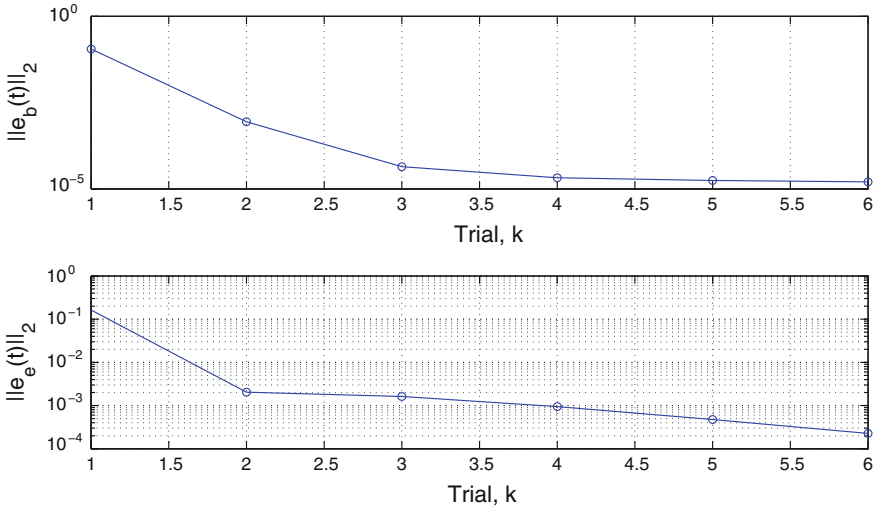

Fig. 5.15 Convergence of tracking error with Newton ILC

the ILC law starts to 'learn' from previous trial error and the tracking performance is significantly improved.

The tracking performance of both joints on the 6th trial are shown in Fig. 5.16 and demonstrate excellent trajectory tracking. Figures 5.17 and 5.18 show the tracking errors for the controlled joint angles ϑ_b and ϑ_e, respectively, where the use of ILC gives a tracking accuracy of 10^{-4} *rad* after the first trial.

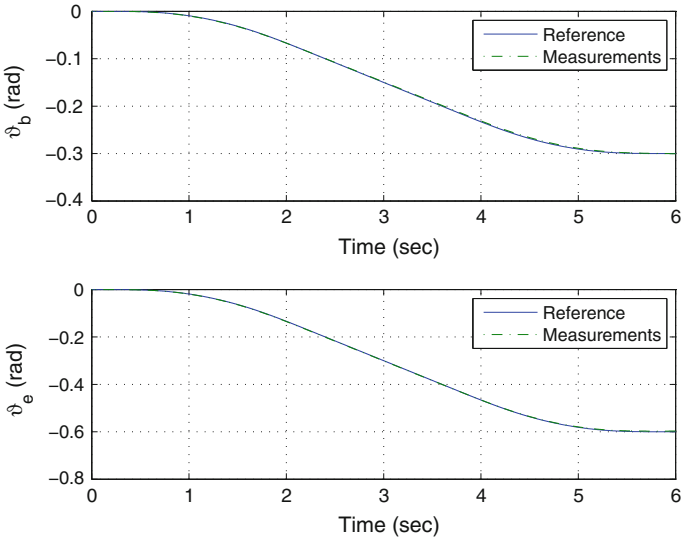

Fig. 5.16 Trajectory tracking for Newton method-based ILC on trial 6

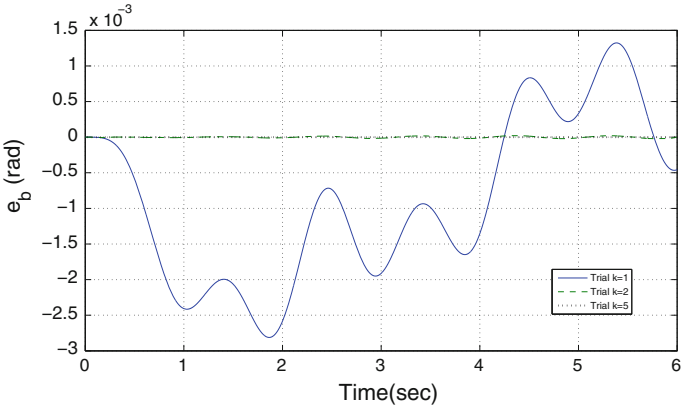

Fig. 5.17 Trajectory tracking error for ϑ_b, $k = 1, 2, 5$

An alternative to Newton ILC would be to combine slave control loop with gradient-based ILC. This would require up to fourth order derivatives of both the reference signal and the measured signal in comparison to first-order derivatives of both signals in Newton ILC. Moreover, much better tracking performance and more rapid convergence within fewer trials is achieved with this nonlinear ILC law.

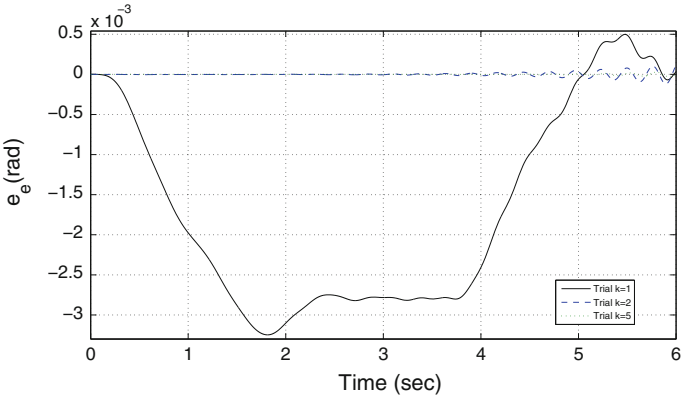

Fig. 5.18 Trajectory tracking error for ϑ_e, $k = 1, 2, 5$

The model (5.6) includes terms to model fatigue during the execution of a trial and from trial-to-trial. In the results given below, the latter factor is fixed by setting $\lambda = 0.99$ and hence the torque from the muscles decreases at a rate of 1 % between successive trials. The robustness of the control law to modeling error is examined by introducing a time-varying modeling mismatch corresponding to the fatigue rates $k_f = \frac{1}{30}, \frac{1}{10}$ for both joints respectively. First the performance of slave control loop alone, i.e., no ILC, is evaluated.

Figure 5.19 shows the tracking characteristics of the slave controller loop as the muscle force is decreased due to fatigue introduced by varying k_f. The reference trajectories for both joints are still tracked, but tracking is partly lost for the fatigue rate $k_f = \frac{1}{10}$.

The results in these last two figures correspond strongly with other results (Jezernik et al. 2014; Dimitra 2005) where the control of FES based muscle stimulation is considered. This previous work and the results in this section strongly suggest that direct feedback control to counter the effects of muscle fatigue can give movement tracking in the presence of decreasing muscle torque but larger inputs are required to compensate for this loss. If repeated trials are made then the 2 norm of the error will increase with each one in the presence of fatigue.

To examine the performance of slave control loop with Newton ILC, the simulation has again been run for 6 trials with a fatigue rate of 1 % from trial-to-trial and a fatigue rate of 10 % during the trial. For the Newton ILC the inner loop NOILC computation iteration number was set at 10. This simulation replicates the case when the patient attempts the tracking for 6 trials and for each trial 10 iterations are required to update the input to be applied on the next trial. Figure 5.20 shows the trajectory tracking, which, in contrast to the slave control loop alone, exhibits fast trial-to-trial convergence and Fig. 5.21 shows the corresponding 2-norm errors.

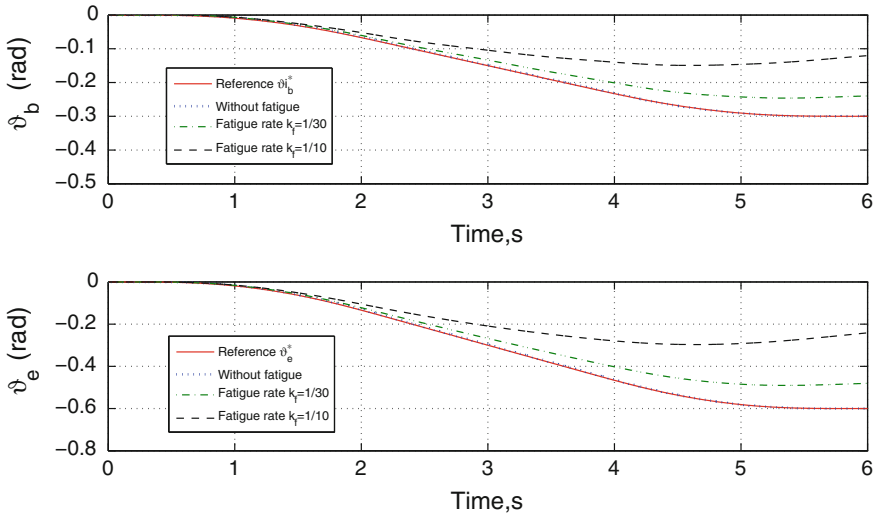

Fig. 5.19 Trajectory tracking performance for different fatigue rates

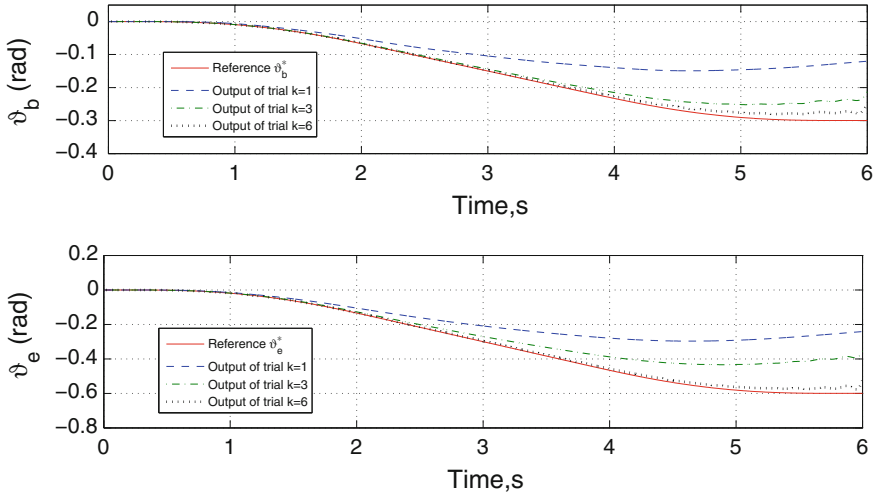

Fig. 5.20 ILC trajectory tracking with 10 %/s fatigue rate during a trial and 1 % trial fatigue rate from trial-to-trial

Compared to Fig. 5.15 where no representation for fatigue is included, Fig. 5.21 shows much poorer tracking accuracy due to the existence of fatigue. This confirms that muscle fatigue can have a very serious effect on performance and that the use of ILC can be effective. To support this last assertion, the stimulation levels required to generate the results in the previous figure are again within the limits discussed above (Fig. 5.22).

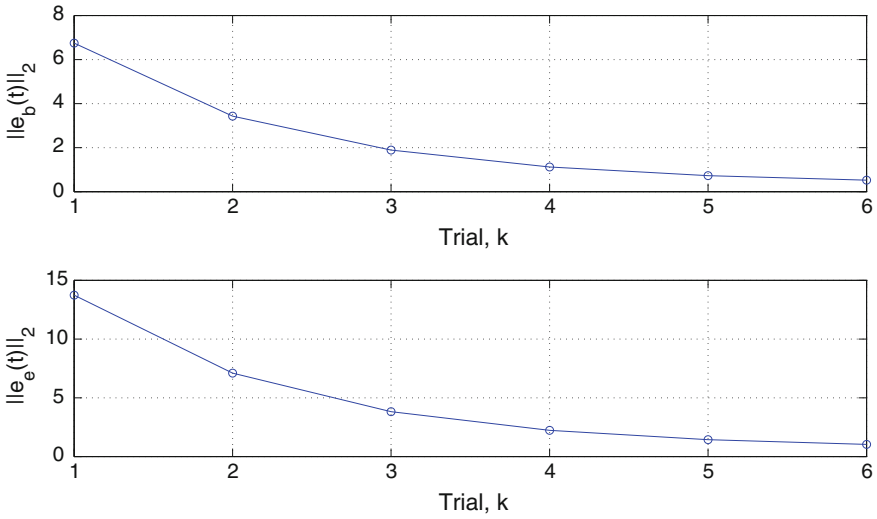

Fig. 5.21 2-norm tracking error of cascade control and Newton ILC in the presence of fatigue

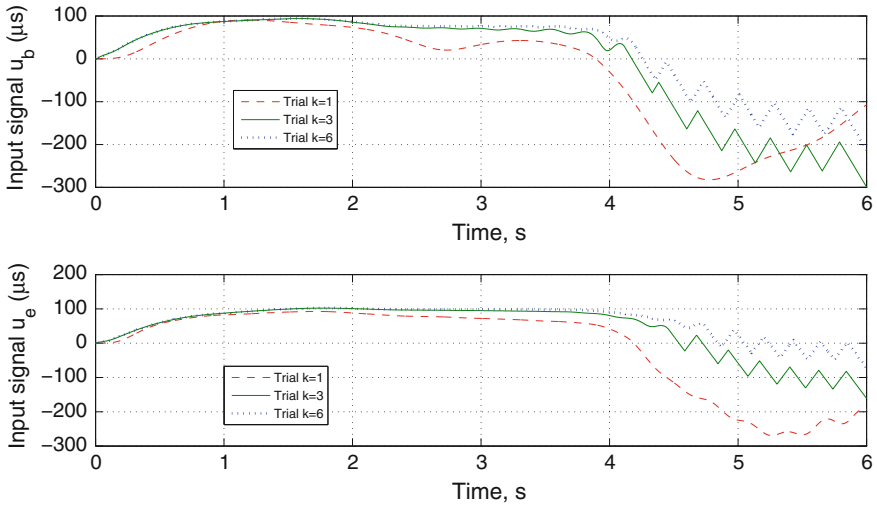

Fig. 5.22 Stimulation input with fatigue and ILC applied for trial 6

The results in the last three figures demonstrate the improvement in both tracking accuracy and fatigue resistance possible when Newton ILC is applied instead of feedback control action alone. As expected, both of these properties are not guaranteed if the muscle output torque drops to a low value, as shown in Fig. 5.23 where a moderate increase of the 2-norm tracking error is observed in both joints after 13 trials. On trial 31, there has been a 13 % trial-to-trial decay of the muscle torque before the

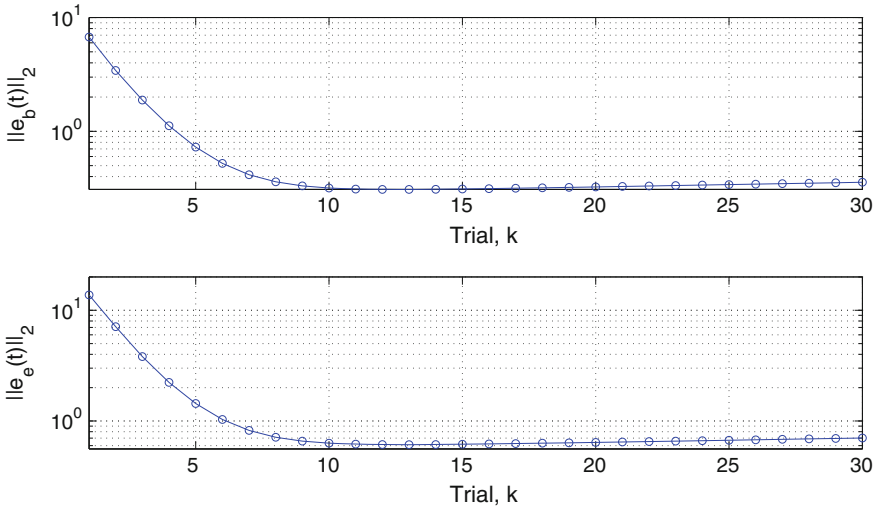

Fig. 5.23 Convergence characteristics of cascade control plus ILC with a fatigued muscle. These plots show an initial reduction in the 2-norm tracking error up to the 13th trial, followed by a moderate divergence as the muscle fatigue increases

start of this trial and the muscle continues to fatigue along the trial, resulting in a 73 % loss of the original muscle torque. This torque decay with continue with further trials and the previous tracking is no longer ensured, leading to a gradual divergence of the error.

It is unlikely that the health professional supervising the session would allow this number of trials to take place but there is still interest in terms of ILC design generally where in applications it can arise that the error is decreasing monotonically from trial-to-trial but then begins to arise again on subsequent trials, see Longman (2000) where this is termed 'long-term stability'. Comparing Figs. 5.15 and 5.23 confirms that this could also arise in the stroke rehabilitation application.

The zero-phase filter

$$H(z) = \frac{0.0095 + 0.0095z^{-1}}{1 - 0.981z^{-1}} \tag{5.17}$$

was applied to u_{k+1} before it is summed with the cascade controller torque. The pass and stop-band cutoff frequencies were 0.5 Hz with a maximum pass-band attenuation of 1 dB and 10 Hz and minimum stop-band attenuation 20 dB. Figure 5.24 shows the resulting 2-norm tracking error over 30 trials, with the case without this filter added also given for comparison purposes. With the filter added the onset of 'long-term stability' problems is delayed for both joints. Again, it must be stressed that an actual session with a patient would not reach the number of trials before the onset of this problem.

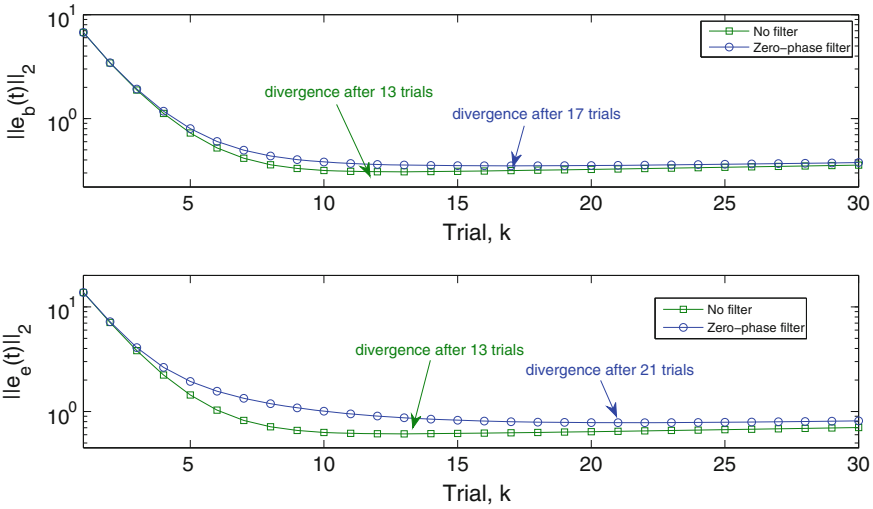

Fig. 5.24 2-norm trial-to-trial error with and without the zero-phase filter added over 30 trials

The results of this simulation study confirm that the control arrangement used is capable of representing and compensating for the effects of muscle fatigue in this area. Much further work remains to be done on control systems design/evaluation before clinical trials can be considered. For example, the results in this chapter have used simple structure master and slave controllers where the objective was to make the simplest possible changes to clinically trialed designs.

One possible aspect to examine here is to add ILC to the inner loop. Also the question of assigning the relative effort of the master and slave controllers should be addressed, together with the use of alternatives to Newton-based ILC. Further research is also required on the fatigue model itself. An alternative approach to representing the effects of fatigue in this ILC application is to treat it as a trial-dependent disturbance and aim to design a trial dependent learning gain. Some results on this approach in the engineering literature can be found in, e.g., Chen and Moore (2002).

References

Abbas JJ, Chizeck HJ (1995) Neural network control of functional neuromuscular systems: computer simulation studies. IEEE Trans Biomed Eng 42(11):1117–1127

Chen YQ, Moore KL (2002) Harnessing the nonrepetitiveness in iterative learning control. In: Proceedings of the 41st IEEE conference on decision and control, pp 3350–3355

de Kroon JR, Ijzerman MJ, Lankhorst GJ, Zilvold G (2005) Relation between stimulation characteristics and clinical outcome in studies using electrical stimulation to improve motor control of upper extremity in stroke. J Rehabil Med 35:65–74

Dimitra B (2005) Feedback control of a high level upper extremity neuroprosthesis. Ph.D. thesis, Case Western Reverse University

Freeman CT, Tong D, Meadmore KL, Cai Z, Rogers E, Hughes A-M, Burridge JH (2011) Phase-lead iterative learning control algorithms for functional electrical stimulation based stroke rehabilitation. Proc Inst Mech Eng Part I 22(5):850–859

Freeman CT, Rogers E, Hughes A-M, Burridge JH, Meadmore KL (2012) Iterative learning control in health care: electrical stimulation and robotic-assisted upper-limb stroke rehabilitation. IEEE Control Syst Mag 32(1):18–43

Huang D, Xu J-X, Venkataramanan V, Huynh TCT (2014) High-performance tracking of piezoelectric positioning stage using current-cycle iterative learning control with gain scheduling. IEEE Trans Ind Electron 61(2):1085–1098

Hughes A-M, Freeman CT, Burridge JH, Chappell PH, Lewin PL, Rogers E (2009) Feasibility of iterative learning control mediated by functional electrical stimulation for reaching after stroke. Neurorehabilitation Neural Repair 23(6):559–568

Jezernik S, Wassink RG, Keller T (2014) Sliding mode closed-loop control of FES: controlling the shank movement. IEEE Trans Biomed Eng 51(2):263–272

Kwakkel G, Kollen BJ, Krebs HI (2008) Effects of robot-assisted therapy on upper limb recovery after stroke: a systematic review. Neurorehabilitation Neural Repair 22:111–121

Lan N (2002) Stability analysis for postural control in a two-joint limb system. IEEE Trans Neural Syst Rehabil Eng 10(4):249–259

Lin T, Owens DH, Hatonen J (2006) Newton method based iterative learning control for discrete non-linear systems. Int J Control 79(10):1263–1276

Longman RW (2000) Iterative learning control and repetitive control for engineering practice. Int J Control 73(10):930–954

McNeal D, Baker LL, McCaffrey S, Lopez J (1986) Subject preference for pulse frequency with cutaneous stimulation of the quadriceps. In: Proceedings of the 9th annual conference of the rehabilitation engineering society of North America, pp 273–275

Meadmore KL, Hughes A-M, Freeman CT, Cai Z, Tong D, Burridge JH, Rogers E (2012) Functional electrical stimulation mediated by iterative learning control and 3D robotics reduces motor impairment in chronic stroke. J Neuroeng Rehabil. doi:10.1186/1743-0003-9-32

Riener R, Fuhr T (1998) Patient-driven control of FES-supported standing up: a simulation study. IEEE Trans Rehabil Eng 6(2):113–124

Riener R, Quinternt J, Schmidt G (1996) Biomechanical model of the human knee evaluated by muscular stimulation. J Biomech 29(9):1157–1167

Skogestad S, Postlewaite I (2005) Multivariable feedback control: analysis and design. Wiley, New York

Tan Y, Dai H-H, Huang D, Xu J-X (2012) Unified iterative learning control schemes for nonlinear dynamic systems with nonlinear input uncertainties. Automatica 48(12):3173–3182

van der Lee JH, De Groot V, Beckerman H, Wagenaar RC, Lankhorst GJ, Bouter LM (2001) The intra- and interrater reliability of the action research arm test: a practical test of upper extremity function in patients with stroke. Arch Phys Med Rehabil 82(1):14–19

Xu W, Chu B, Rogers E (2013) Cascade based iterative learning control of robotic-assisted upper extremity stroke rehabilitation. In: Proceedings of the 52nd IEEE conference on decision and control, pp 6688–6693

Xu W, Chu B, Rogers E (2014) Iterative learning control for robotic-assisted upper limb stroke rehabilitation in the presence of muscle fatigue. Control Eng Pract 31:63–72

Chapter 6
Goal-Oriented Stroke Rehabilitation

Building on work reported in previous chapters, the system developed and evaluated in this chapter includes stimulation of the wrist and hand extensors. This directly targets activities of daily living, comprising real-world tasks that require manipulation of objects using the hand and wrist.

6.1 System Overview

The research on combining ILC and FES for upper limb rehabilitation described in the preceding chapters used planar light tracking tasks or Virtual Reality (VR) 3D object tracking, incorporating explicit reference trajectories for the patient to follow. To directly target activities of daily living, the system in this chapter assists patients to complete real-world tasks that require manipulation of objects using the hand and arm. Support against gravity is provided for the patient's arm using a commercially available passive spring support. Tracking of the patient's arm and hand movements is achieved using a Kinect motion capture device and wrist electrogoniometers. An optional data glove is also used for collection of finger movement, where required. Since no explicit reference trajectory is shown to the patient, the ILC scheme (Freeman et al. 2013) employs principles from motor control to deliver the optimum FES assistance.

The Kinect greatly facilitates non-invasive motion capture by providing a free software development kit and pre-calibrated 'out of the box' hardware, which has vastly reduced the associated hardware and software cost (Clark et al. 2012). The Kinect is a small ($0.30 \times 0.08 \times 0.06$ m), lightweight (1.4 kg) device incorporating a video camera with an infra-red source and an infra-red sensor. The infra-red sensor measures the reflection of infra-red light by objects in front of the camera and calculates 3D position data for those objects. Recent accuracy tests have indicated that the device is capable of calculating position data with an accuracy of approximately

C.T. Freeman et al., *Iterative Learning Control for Electrical Stimulation and Stroke Rehabilitation*, SpringerBriefs in Control, Automation and Robotics, DOI 10.1007/978-1-4471-6726-6_6

1 cm (Dutta 2012). The software supplied with the Kinect uses pattern recognition to detect landmarks of interest, such as limb segments and joint estimations.

In the system developed in this chapter, the Kinect is used to capture joint center locations for the shoulder, elbow and wrist for the calculation of shoulder and elbow joint angles. It is not possible to use the Kinect for the calculation of wrist and hand joint angles due to accuracy limitations in hand tracking when the device is at the distance required to produce a large enough field of view for all the other segments. Instead, an electrogoniometer is included to collect wrist angle data and an optional data glove can be used to capture individual finger joint angle data.

FES surface electrodes are positioned over the patient's anterior deltoid, triceps and wrist and hand extensor muscles, with placement following clinical guidelines. A series of 5 V, 40 Hz pulses are produced by the control hardware for each channel and amplified by a four-channel electrical stimulator to generate a bi-phasic signal which achieves a smooth muscle contraction (de Kroon et al. 2005). For safety, the maximum pulsewidth that can be applied to any channel is limited within the control software and also by the stimulator. Prior to any session, the amplification level for each channel is set by applying a constant stimulation signal with pulsewidth 300 μs from the control hardware and slowly increasing the voltage until the maximum comfortable level is reached. During subsequent tests the pulsewidth is limited to 300 μs.

The electrode array is formed by 5×8 elements that can each be routed to one of four FES channels through use of custom made controlled multiplexor hardware, comprising an Arduino board and shift register array. For each required hand and wrist posture, the optimal electrode sites and associated FES pulsewidths are selected during initial tests through a search procedure involving local linear model identification and gradient-descent optimization. The sites are then fixed during subsequent experiments, with the pulsewidth amplitudes controlled by ILC. Figure 6.1 shows the electrode array and data glove and the control system block diagram is again that of Fig. 5.5.

The system software incorporates tracking of the patient's movement with the control schemes implemented to mediate the FES in real-time. A custom made C++ application is used to read the arm and hand positions from the Kinect, electrogoniometer and (if used) data glove. Position data are then transferred to the real-time

Fig. 6.1 Electrode array with data glove and electrogoniometer used for stimulating and tracking hand and wrist movement

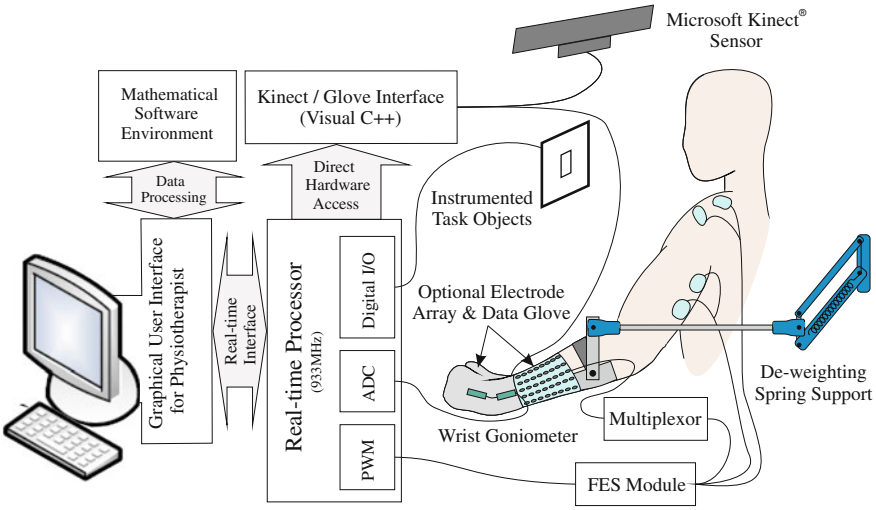

Fig. 6.2 Signal flow diagram

control hardware (dSPACE ds1103) that implements ILC laws involving embedded dynamic models of the arm. Outputs of the control law comprise pulse-width modulated (PWM) signals for each of the FES stimulator channels, together with RS232 serial data to control the electrode array. Digital inputs and outputs are also employed to interface with the instrumented task objects. Figure 6.2 shows a signal flow diagram.

A graphical user interface (GUI) has been developed to enable the user to customize control parameters, implement the FES control, collect position outcome data, select the task details to be performed and review performance after each session.

6.2 Control Design and Evaluation

6.2.1 Human Arm Model

A dynamic model of the arm-support system incorporates a biomechanical description of the human arm and a representation of the SaeboMAS spring support. Position values for the shoulder, elbow and wrist joint centers are calculated using the Kinect. To assist the FES actuated control law, a simplified model of the arm is used for the calculation of joint angles. Figure 6.3 shows the kinematic model of the human arm.

Spasticity in stroke patients often restricts flexion of the shoulder in the anteroposterior plane, extension of the elbow and extension of the wrist and fingers (Levin 1996). Therefore, the anterior deltoid, triceps and wrist and hand extensor muscles were selected for stimulation. It is assumed that stimulation applied to the triceps produces movement about an axis perpendicular to the upper and forearm segments

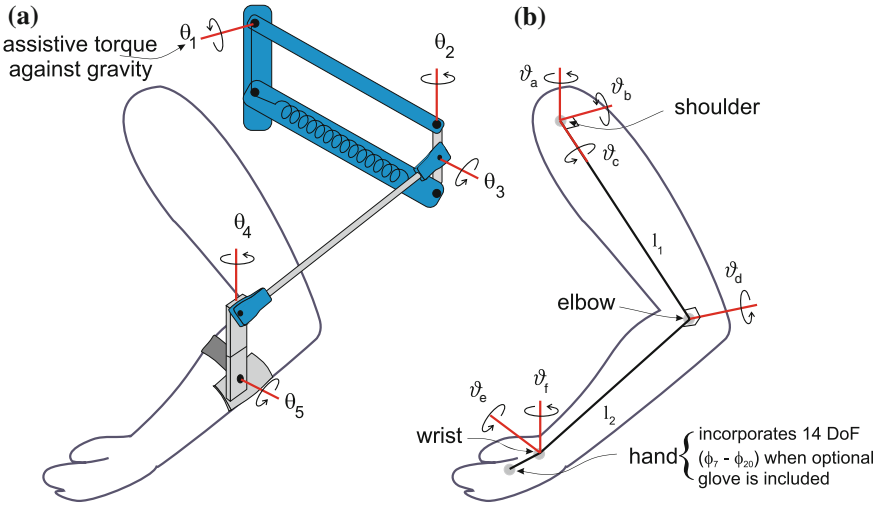

Fig. 6.3 Kinematic model of the **a** SaeboMAS support and **b** human arm

and that stimulation applied to the wrist and hand extensors produces movement about an axis that is fixed with respect to the forearm. For the anterior deltoid it is assumed that stimulation produces movement about an axis that is fixed with respect to the shoulder and determined by two rotation transformations. These comprise rotations around the z-axis by β and around the x-axis by γ. Identification of β and γ is described below.

The dynamic model of the human arm is

$$B_h(q_u)\,\ddot{q}_u + C_h(q_u,\dot{q}_u)\,\dot{q}_u + F_h(q_u,\dot{q}_u) + G_h(q_u) + K_h(q_u) = \tau(u,q_u,\dot{q}_u) - J_h^T(q_u)\,h_h \tag{6.1}$$

$$q_u = \left[\,\vartheta_a\ \vartheta_b\ \vartheta_c\ \vartheta_d\ \vartheta_e\ \vartheta_f\,\right]^T$$

where $B_h(\cdot)$ and $C_h(\cdot)$ are 6×6 inertial and Coriolis matrices, respectively, $F_h(\cdot)$ and $G_h(\cdot)$ are friction and gravitational vectors and $\tau(\cdot)$ comprises the moments produced through application of FES. These moments are of the form

$$\tau(u,q_u,\dot{q}_u) = \left[\,\tau_a(\vartheta_a,\dot{\vartheta}_a,u_a)\ 0\ 0\ \tau_d(\vartheta_d,\dot{\vartheta}_d,u_d)\ \tau_e(\vartheta_e,\dot{\vartheta}_e,u_e)\ 0\,\right]^T$$

where $u_a(t)$, $u_d(t)$ and $u_e(t)$ represent the electrical stimulation applied to the anterior deltoid, triceps and wrist and hand extensor muscles, respectively, with $u = \left[\,u_a\ 0\ 0\ u_d\ u_e\ 0\,\right]^T$ and the same muscle model as in the previous chapters. Finally, h is a vector of externally applied force and torque comprising components h_s due to the spring support and h_h due to interaction with objects and $J_h(\cdot)$ is the system Jacobian.

The SaeboMAS support structure dynamics are of the form

$$B_s(q_r)\ddot{q}_r + C_s(q_r, \dot{q}_r)\dot{q}_r + F_s(q_r, \dot{q}_r) + G_s(q_r) + K_s(q_r) = -J_s^T(q_r)h_s \quad (6.2)$$

where $B_s(\cdot)$ and $C_s(\cdot)$ are 5×5 inertial and Coriolis matrices and

$$q_r = \begin{bmatrix} \theta_1 & \theta_2 & \dots & \theta_5 \end{bmatrix}^T$$

represents the angles of the spring support. In addition, $J_s(\cdot)$ is the system Jacobian, and $F_s(\cdot)$ and $G_s(\cdot)$ are friction and gravitational vectors. The vector $K_s(\cdot)$ comprises the moments produced through gravity compensation provided by the spring, which takes the form $\begin{bmatrix} k_1(\theta_1) & 0 & 0 & 0 & 0 \end{bmatrix}^T$. Also the rigid connection between structures gives rise to a bijective mapping between q_u and q_r and hence the combined model is given by

$$B(q_u)\ddot{q}_u + C(q_u, \dot{q}_u)\dot{q}_u + F(q_u, \dot{q}_u) + G(q_u) + K(q_u) = \tau(u, q_u, \dot{q}_u) - J^T(q_u)h \quad (6.3)$$

This model of the arm is used by the FES control law to produce an input signal that results in accurate completion of the tasks. During trials incorporating FES, the law assists tracking about ϑ_a, ϑ_d and ϑ_e alone, and it is assumed that the patient has sufficient control over the remaining axes to adequately perform the task. Due to the complexity of identifying the parameters in a full dynamic model of the hand and wrist, the array element identification procedure uses stimulation and angular output data from the glove to construct a linear model linking these variables (Freeman 2014). The resulting representation is then integrated with a simpler model of the hand and wrist (Soska et al. 2013) detailed next.

6.2.2 Hand and Wrist Model

A possible control scheme for the hand and wrist is shown Fig. 6.4. In control terms, this is a highly coupled system with each joint actuated by at least two muscle groups: flexor and extensors. Furthermore, most of the hand muscles are either bi-articular or multi-articular, i.e., they actuate simultaneously two or more joints. The muscles of the hand are divided into two groups: intrinsic i.e., originate solely in the hand and extrinsic, i.e., located proximally in the forearm. Although it is possible to stimulate individual intrinsic and extrinsic muscles of the hand, e.g., using embedded electrodes, in most of the FES systems considered in the literature only the extrinsic muscles are stimulated. The approach taken in this monograph is to investigate feasibility of surface electrode array stimulation of extrinsic muscles, which hence avoids the need for surgery and makes the approach cost effective and suitable for widespread uptake. A simplified model of the hand is developed next and used in control law design.

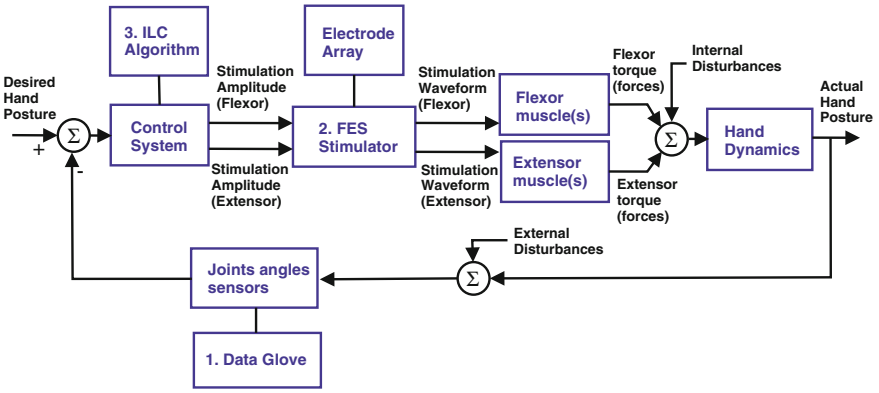

Fig. 6.4 FES schematic for hand and wrist rehabilitation

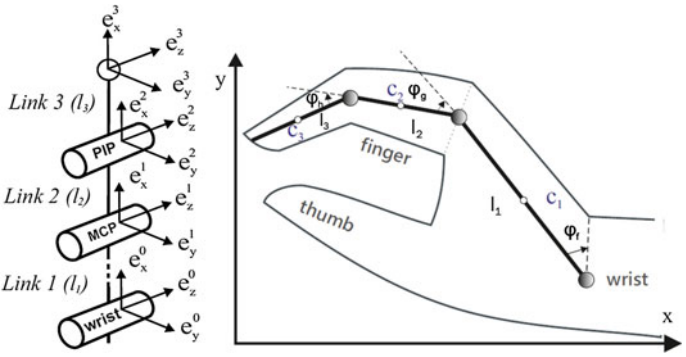

Fig. 6.5 Planar hand model

The model developed includes a single composite finger, representing the combined action of four fingers, wrist and neglects the thumb orientation. The finger and wrist are modeled as a 3-link rigid body system, consisting of 3 active revolute joints as shown in Fig. 6.5. This still provides an accurate representation of the hand since 42 % of the functional movements of the hand involve the four fingers moving together (Ingram et al. 2008). Link 1 represents the II-V Metacarpal bones connected by the wrist joint, Links 2 and 3 represent proximal and middle phalangeals of the finger connected by the Metacarpal-Phalangeal joint (MCP) and Proximal-Interphalangeal joint (PIP) respectively.

The dynamic model of the finger/wrist is formulated using Lagrangian analysis and can be written in the form

$$B_f(q_f)\ddot{q}_f + C_f(q_f, \dot{q}_f) + G_f(q_f) + F_f(q_f, \dot{q}_f) = \tau_f(u, q_f, \dot{q}_f) \qquad (6.4)$$

where $B_f(q_f)$ is the inertia matrix, $C_f(q_f, \dot{q}_f)$ denotes the centrifugal and Coriolis forces, $G_f(q_f)$ is the vector representing gravitational force and the generalized co-ordinates are $q_f = \begin{bmatrix} \vartheta_f & \vartheta_g & \vartheta_h \end{bmatrix}^T$. During purely horizontal movement of the finger, gravity can be neglected.

The inertia matrix is

$$B_f(q) = \begin{bmatrix} b_{11} & b_{12} & b_{13} \\ b_{21} & b_{22} & b_{23} \\ b_{31} & b_{23} & b_{33} \end{bmatrix}$$

where

$$\begin{aligned}
b_{11} &= m_1 c_1^2 + m_2 l_1^2 + m_2 c_2^2 + 2m_2 l_1 c_2 \cos\vartheta_g + m_3 l_1^2 \\
&\quad + m_3 l_2^2 + 2m_3 l_1 l_2 \cos\vartheta_g + 2m_3 l_1 c_3 \cos(\vartheta_g + \vartheta_h) \\
&\quad + 2m_3 l_2 c_3 \cos\vartheta_h + m_3 c_3^2 + J_1 + J_2 + J_3 \\
b_{12} &= m_2(c_2^2 + l_1 c_2 \cos\vartheta_g) + m_3 l_2^2 + m_3 c_3^2 + m_3 l_1 l_2 \cos\vartheta_g \\
&\quad + m_3 l_1 c_3 \cos(\vartheta_g + \vartheta_h) + 2m_3 l_2 c_3 \cos\vartheta_h + J_2 + J_3 \\
b_{13} &= m_3 c_3^2 + m_3 l_1 c_3 \cos(\vartheta_g + \vartheta_h) + m_3 l_2 c_3 \cos\vartheta_h + J_3 \\
b_{22} &= m_2 c_2^2 + m_3 l_2^2 + m_3 c_3^2 + m_3 l_2 c_3 \cos\vartheta_h + J_3 \\
b_{23} &= m_3 c_3^2 + m_3 l_2 c_3 \cos\vartheta_h + J_3 \\
b_{33} &= m_3 c_3^2 + J_3
\end{aligned}$$

where $m_1 = 0.3\,\text{kg}$, $m_2 = 0.015\,\text{kg}$, $m_3 = 0.009\,\text{kg}$ are the masses, $J_1 = 5 \times 10^{-4}$, $J_2 = 5 \times 10^{-6}$, $J_3 = 3 \times 10^{-6}$ are inertias ($\text{kg}\,\text{m}^2$) and the assumed lengths (m) are $l_1 = 0.08$, $l_2 = 0.05$, $l_3 = 0.048$ and $c_i = 0.5 l_i,\ i = 1, 2, 3$.

The entries in $C_f(q_f, \dot{q}_f)$ are

$$\begin{aligned}
c_{11} &= -[m_3 c_3 l_1 s_{23} + m_3 c_3 l_2 \sin\vartheta_h](2\dot{\vartheta}_f\dot{\vartheta}_h + 2\dot{\vartheta}_g\dot{\vartheta}_h + \dot{\vartheta}_h^2) \\
&\quad - [(m_2 l_1 c_2 + m_3 l_1 l_2)\sin\vartheta_g + m_3 l_1 c_3 s_{12}](2\dot{\vartheta}_f\dot{\vartheta}_g + \dot{\vartheta}_g^2) \\
c_{21} &= [(m_2 c_2 l_1 + m_3 l_1 l_2)\sin\Theta_2 + m_3 c_3 l_2 s_{23}]\dot{\vartheta}_h^2 \\
&\quad - m_3 c_3 l_2 \sin\vartheta_h(2\dot{\vartheta}_g\dot{\vartheta}_h + \dot{\vartheta}_g^2) \\
c_{31} &= [m_3 c_3 l_2 \sin\vartheta_g + m_3 c_3 l_1 s_{23}]\dot{\vartheta}_g^2 + m_3 c_3 l_2 \sin(2\dot{\vartheta}_g\dot{\vartheta}_f + \dot{\vartheta}_f^2)
\end{aligned}$$

where $s_{i,j} = \sin(\vartheta_i + \vartheta_j)$. Also τ_f is the vector of moments produced by the application of FES and $F_f(q_f, \dot{q}_f)$ is the vector of frictional components acting about each joint of the form

$$F_f(q_f, \dot{q}_f) = \begin{bmatrix} k_1(\vartheta_{0,f} - \vartheta_f) - b_1\dot{\vartheta_f} \\ k_2(\vartheta_{0,g} - \vartheta_g) - b_2\dot{\vartheta_g} \\ k_3(\vartheta_{0,h} - \vartheta_h) - b_3\dot{\vartheta_h} \end{bmatrix} \tag{6.5}$$

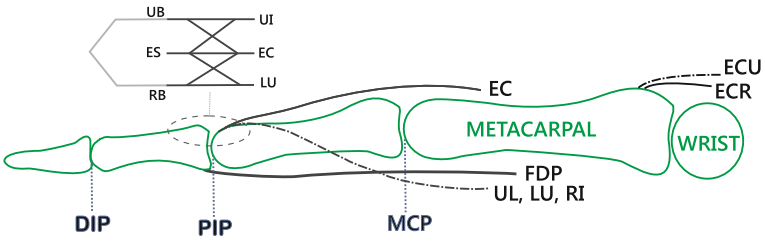

Fig. 6.6 The musculo-tendon structure of the wrist and finger

where $b_1 = 0.05$, $b_2 = 0.014$, and $b_3 = 0.01$ are the viscous friction coefficients (Ns/m). It is assumed that the muscle groups that actuate each joint produce a stiffness that can be represented by a spring with zero elongation at the initial position $\vartheta_{0,f} = \frac{2\pi}{3}$, $\vartheta_{0,g} = \frac{\pi}{2}$, $\vartheta_{0,h} = \frac{\pi}{3}$ and stiffness coefficients $k_1 = 6.5$, $k_2 = 0.9$, $k_3 = 0.8$ (N/m).

Figure 6.6 shows the musculoskeletal structure of the finger and wrist included in the model. The wrist joint is assumed to be actuated by three extensor muscles: Extensor Communis (EC), Extensor Carpi Radialis Longus (ECR) and Extensor Carpi Ulnaris (ECU). The muscles of the finger act through a complex tendon network, termed the extensor mechanism. This network is approximated by a longitudinally symmetric tendon rhombus, consisting of active and the passive tendons, as also shown in Fig. 6.6.

The extensor mechanism of the finger is modeled in the same manner as Theodorou et al. (2011) and includes 5 active tendons, driven by independently controlled muscles: the Flexor Digitorum Profundus (FDP), the Extensor Digitorum Communis (EC), the Ulnar and Radial Interosseous (UI and RI), the Lumbrical muscle (LU), and 3 passive tendons: the Radial Band (RB) the Ulnar Band (UB) and the Extensor Slip (ES).

Electrically stimulated muscles of the hand contract, generating pulling forces that produce finger/wrist movement. The transformation from muscle force vector, y, with dimension m to the p-dimensional net joint torque, τ_f, at the finger/wrist joints can be defined as in Valero-Cuevas (2009), yielding

$$\tau_f(u, q_f, \dot{q}_f) = R(q_f)y(u, q_f, \dot{q}_f) \tag{6.6}$$

where

$$R(q_f) = \begin{bmatrix} r_{11} & \dots & r_{1m} \\ \vdots & \ddots & \vdots \\ r_{p1} & \dots & r_{pm} \end{bmatrix} \tag{6.7}$$

$$y(u, q_f, \dot{q}_f) = \begin{bmatrix} y_1(u_1, l_1, \dot{l}_1) \\ \vdots \\ y_m(u_m, l_m, \dot{l}_m) \end{bmatrix} \tag{6.8}$$

and each entry in $R(q_f)$ is the signed scalar moment arm value that transforms a muscle force into torques at the various joints it crosses. Moreover, entry $r_{i,j}$ in $R(q_f)$ can be evaluated by differentiating the excursion (displacement) E of the jth tendon with respect to the ith joint angle, i.e.,

$$r_{1,j} = \frac{\partial E_j(\vartheta_f)}{\partial \vartheta_f}, \quad r_{2,j} = \frac{\partial E_j(\vartheta_g)}{\partial \vartheta_g}, \quad r_{3,j} = \frac{\partial E_j(\vartheta_h)}{\partial \vartheta_h}, \quad j = 1, \ldots, m \tag{6.9}$$

Excursion of the FDP is modeled (Landsmeer 1955) as

$$E^{\text{tendon}} = \vartheta d^{\text{tendon}} + 2y^{\text{tendon}} \left(1 - \frac{\vartheta/2}{\tan \vartheta/2}\right) \tag{6.10}$$

where d^{tendon} is the distance from the straight section of the tendon to the tendon constraint along the line perpendicular to the axis of the bone and ϑ is the corresponding angle rotation. The term y^{tendon} is the distance along the axis of the bone from the end of the straight section of the tendon to the joint center.

Tendon excursion of the EC is a function of the wrist and MCP with the addition of the displacement, transformed to the PIP joint through the extensor mechanism

$$E^{EC} = -r_1^{EC}\vartheta_f - r_2^{EC}\vartheta_g + L(E_1, E_2, E_3) \tag{6.11}$$

where

$$E_1 = E^{ES}, \quad E_2 = E^{UB}, \quad E_3 = E^{RB} \tag{6.12}$$

and the execution function $L(E_1, E_2, E_3)$ is defined as

$$L(E_1, E_2, E_3) = \sum_{i=1}^{3} w_i E_i = 0, \quad w_i > 0, \quad j = 1, 2, 3 \tag{6.13}$$

The excursions of the remaining tendons are each modeled as a second-order polynomial approximation of (6.10) as $(b^{\text{tendon}} + h^{\text{tendon}}\vartheta)\vartheta$, where b^{tendon} and h^{tendon} are constants. Also the tendon excursions can be expressed as functions of the finger extension/flexion angles ϑ_g and ϑ_h as

$$\begin{aligned}
E^{FDP} &= \sum_{i=2}^{3} \vartheta_h^{FDP} + 2y_h^{FDP}\left(1 - \frac{\vartheta_h/2}{\tan \vartheta_h/2}\right) \\
E^{ES} &= -r^{ES}\vartheta_h \\
E_{RB} &= -(b^{RB} + h^{RB}\vartheta_h)\vartheta_h \\
E_{UB} &= -(b^{UB} + h^{UB}\vartheta_h)\vartheta_h \\
E^{RI} &= (b^{RI} + h^{RI}\vartheta_g)\vartheta_g + E^{UB} \\
E^{UI} &= (b^{UI} + h^{UI}\vartheta_g)\vartheta_g + E^{UB}
\end{aligned}$$

$$\begin{aligned} E^{LU} &= (b^{LU} + h^{LU}\vartheta_g)\vartheta_g + E^{RB} - E^{FDP} \\ E^{ECU} &= (b^{ECU} + h^{ECU}\vartheta_f)\vartheta_f \\ E^{ECR} &= (b^{ECR} + h^{ECR}\vartheta_f)\vartheta_f \end{aligned} \tag{6.14}$$

Hence applying (6.9), each column of the moment arm matrix $R(q_f)$ represents the moment arm vector corresponding to each muscle and therefore

$$R(q_f) = \begin{bmatrix} R^{FDP} & R^{LU} & R^{UI} & R^{RI} & R^{EC} & R^{ECR} & R^{ECU} \end{bmatrix} \tag{6.15}$$

where

$$R^{FDP} = \begin{bmatrix} 0 \\ d_1^{FDP} + y_1^{FDP}\left(\frac{\sin\vartheta_g - \vartheta_g}{2\sin^2\vartheta_g}\right) \\ d_2^{FDP} + y_2^{FDP}\left(\frac{\sin\vartheta_h - \vartheta_h}{2\sin^2\vartheta_h}\right) \end{bmatrix}$$

$$R^{LU} = \begin{bmatrix} 0 \\ b^{LU} + 2h^{LU}\vartheta_g - R^{FDP}_{\vartheta_g} \\ -b^{RB} - 2h^{RB}\vartheta_h - R^{FDP}_{\vartheta_h} \end{bmatrix}$$

$$R^{UI} = \begin{bmatrix} 0 \\ b^{LU} + 2h^{LU}\vartheta_g \\ -b^{UB} - 2h^{UB}\vartheta_h \end{bmatrix}$$

$$R^{EC} = \begin{bmatrix} -r_1^{EC} \\ -r_2^{EC} \\ -w_1 r^{ES} + w_2 R^{UB}_{\vartheta_h} + w_3 R^{RB}_{\vartheta_h} \end{bmatrix}$$

and

$$R^{UB}_{\vartheta_h} = -(b^{UB} + 2h^{UB}\vartheta_h) \tag{6.16}$$

$$R^{RB}_{\vartheta_h} = -(b^{RB} + 2h^{RB}\vartheta_h) \tag{6.17}$$

Also

$$R^{ECR} = \begin{bmatrix} b^{ECR} + 2h^{ECR} & 0 & 0 \end{bmatrix}^T \tag{6.18}$$

and

$$R^{ECU} = \begin{bmatrix} b^{ECU} + 2h^{ECU} & 0 & 0 \end{bmatrix}^T \tag{6.19}$$

Table 6.1 Torques acting about the joints

Tendon–joint type	d	y	r	h	b
EC—extrinsic (wrist)	–	–	14.12	–	–
ECR—extrinsic (wrist)	–	–	–	−11.72	1.14
ECU—extrinsic (wrist)	–	–	–	−8.51	1.55
FDP—extrinsic (MCP)	8.32	8.32	–	–	–
RI—extrinsic (MCP)	–	–	–	−1.29	5.62
UI—intrinsic (MCP)	–	–	–	−8.16	18.76
LU—intrinsic (MCP)	–	–	–	−2.17	12.53
EC (MCP)	–	–	8.3	–	–
FDP (PIP)	5.76	7.5	–	–	–
ES—intrinsic (PIP)	–	–	2.92	–	–
RB—intrinsic (PIP)	–	–	–	−0.47	2.54
UB—intrinsic (PIP)	–	–	–	0.57	1.7

Using (6.6), the torque acting about a joint can be calculated as a function of the force in each muscle and the current joint angle vector, see Table 6.1.

Each element of the muscle force vector $y(u, q_f, \dot{q}_f)$ is formed from the moment produced by the application of the FES signal $u_j(t)$ to the jth stimulated muscle with

$$u = \begin{bmatrix} u_1 \ \dots \ u_m \end{bmatrix}^T \tag{6.20}$$

and using the muscle model (4.12)

$$y_i(u_i(t), q_f, \dot{q}_f) = g_i(u_i, t) \times F_{m,i}(q_f, \dot{q}_f), \ i = 1, \dots, m \tag{6.21}$$

in which the Hammerstein structure $g_i(u_i, t)$ is composed of a static nonlinearity g_{IRC_i} followed by linear dynamics with state-space model matrices

$$\{M_{A,i}, M_{B,i}, M_{C,i}\}, \ i = 1, \dots, m.$$

Using (6.4) the relationship between the applied stimulation and the joint angles can be written as the state-space model

$$\begin{aligned} \dot{x}(t) &= f(x(t), u(t)) \\ q_f(t) &= h(x(t)) \end{aligned} \tag{6.22}$$

where

$$f(x(t),u(t)) = \begin{bmatrix} \dot{q}_f \\ B_f^{-1}(q_f)X(q_f,\dot{q}_f) \\ M_{A,1}x_1 \\ \vdots \\ M_{A,p},x_p \end{bmatrix} + \begin{bmatrix} 0 \\ 0 \\ M_{B,1},g_1(u_1) \\ \vdots \\ M_{B,p}g_p(u_p) \end{bmatrix}$$
$$h(x(t)) = \begin{bmatrix} I\ 0\ 0\ 0 \end{bmatrix} \tag{6.23}$$

where

$$x = \begin{bmatrix} q_f^T\ \dot{q}_f^T\ x_1^T\ \dots\ x_j^T \end{bmatrix}^T$$

and the ith row of $X(q_f,\dot{q}_f)$ is

$$R_i(q_f)M_{C,i}x_i F_{m,i}(q_f,\dot{q}_f) - C_{f,i}(q_f,\dot{q}_f) - F_{f,i}(q_f,\dot{q}_f),\ i = 1,\dots,m$$

The nonlinear differential state-space model (6.22) in the ILC setting can now be discretized to result in a description of the form (2.36), i.e.,

$$\begin{aligned} x_k(p+1) &= f(x_k(p),u_k(p)) \\ q_{f,k}(p) &= h(x_k(p)) \end{aligned} \tag{6.24}$$

Defining

$$\begin{aligned} u_k &= \begin{bmatrix} u_k^T(0)\ u_k^T(1)\ \dots\ u_k^T(T-1) \end{bmatrix}^T \\ q_{f,k} &= \begin{bmatrix} q_{f,k}^T(1)\ q_k^T(2)\ \dots\ q_{f,k}^T(T) \end{bmatrix}^T \end{aligned}$$

the relationships between the input and output time series can be written in algebraic terms as

$$\begin{aligned} q_{f,k}(1) &= h(x_k(1)) = h(f(x_k(0),u_k(0))) \\ &= g_1(x_k(0),u_k(0))) \\ &\vdots \\ q_{f,k}(T) &= h(x_k(T)) = h(f(x_k(T-1),u_k(T-1)) \\ &= g_T(x_k(0),u_k(0),u_k(1),\dots,u_k(T-1)) \end{aligned}$$

Hence, assuming $x_k(0) = 0$, (6.24) can be represented by

$$q_{f,k} = g(u_k) \tag{6.25}$$

where

$$g(\cdot) = \left[g_1^T(\cdot)\ g_2^T(\cdot)\ \ldots\ g_T^T(\cdot) \right]^T$$

To control hand posture, it is necessary to specify the joint positions at a fixed number $M \leq T$ of sample instants $1 \leq n_1 \leq n_2 \leq n_M$ and take these to be

$$q^* = \left[q^*(0)^T\ q^*(1)^T\ \ldots\ q^*(M-1)^T \right]^T$$

Also the form of ILC used can be considered as an iterative numerical solution to the problem of finding a control input that solves the problem

$$\min_u J(u) \ \text{ subject to } \ \Lambda u \leq b,\ J(u) = ||q^* - \Phi g(u)||_2^2 \tag{6.26}$$

where $J(u)$ is the point-to-point error norm and the $pM \times pT$ matrix Φ has block entries

$$\Phi_{i,j} = \begin{cases} I, & j = n_i,\ i = 1, 2, \ldots, M \\ 0, & \text{otherwise} \end{cases}$$

Given that each FES input must be bounded, i.e., $u_{\min} \leq u_i \leq u_{\max}$, it is necessary to impose vector inequality constraints of the form

$$\Lambda u \leq b$$

where

$$\Lambda = \left[-I\ I \right]^T$$
$$b = \left[u_{\min}\ \ldots\ u_{\min}\ u_{\max}\ \ldots\ u_{\max} \right]^T$$

In the absence of the constraint, the Newton ILC design is

$$\begin{aligned} u_{k+1} &= u_k - \nabla^2 J(u_k)^{-1} \nabla J(u_k) \\ &= u_k + (\Phi g^{'}(u_k))^{\dagger}(q^* - \Phi g(u_k)) \end{aligned} \tag{6.27}$$

where † denotes the generalized matrix inverse, $g^{'} = \frac{\delta g(u_k)}{\delta u_k}$ and in the ILC setting $\Phi g(u_k)$ is replaced by the point-to-point error $e_k = q^* - q_{f,k}$. The descent direction term in (6.27) is the solution, $\overline{u}$, to

$$\min_{\overline{u}} ||\overline{u}||_2^2, \ \text{ subject to } \ \Phi g^{'}(u_k)\overline{u} = e_k \tag{6.28}$$

Hence applying the constraint $\Lambda u_{k+1} \leq b$, which translates to $\Lambda \overline{u} \leq b - \lambda u_k$, gives the solution of (6.26) as

$$u_{k+1} = u_k + \Delta u_k \tag{6.29}$$

where Δu_k is the solution of

$$\min_{\overline{u}} ||\overline{u}||_2^2, \text{ subject to } \begin{cases} \Phi g^{'}(u_k)\overline{u} = e_k \\ \Lambda \overline{u} \leq b - \Lambda u_k \end{cases} \tag{6.30}$$

Using results in Freeman and Tan (2012), this last problem can be solved by applying the gradient method to

$$\min_{u} ||y_r - \Phi y_k - \Phi g^{'}(u_k)u||_2^2 \text{ subject to } \Lambda u \leq b - \Lambda u_k \tag{6.31}$$

using the barrier method with update

$$u_{j+1} = u_j + \alpha(\Phi g^{'}(u_k))^T - \frac{1}{\tau_j}\Lambda^T d \tag{6.32}$$

applied to $\Phi g^{'}(u_k)$ where the elements, d_i, of d are

$$d_i = \frac{1}{b_i - \Lambda_i^T(u_j + u_k)} \tag{6.33}$$

This iteration is performed multiple times between trials k and $k+1$ to generate the discrete term Δu_k used in (6.29). The parameter τ_j is increased at each inter-trial iteration update j in order to reach the hard constraint, as detailed in Freeman and Tan (2012). Moreover, there are no intensive matrix calculations required in (6.32) since $w = g^{'}(u_k)v$ corresponds to the linear time-varying system

$$\begin{aligned} \tilde{x}(p+1) &= A(p)\tilde{x}(p) + B(p)v(p) \\ w(p) &= C(p)\tilde{x}(p) \end{aligned} \tag{6.34}$$

where $A(p)$, $B(p)$ and $C(p)$ are computed as in (2.41). Also the term $w = (g^{'}(u_k))^T v$ has state-space model

$$\begin{aligned} \tilde{x}(p+1) &= A^T(p)\tilde{x}(p) + C^T(p)v(T-1-p) \\ w(T-1-p) &= B^T(p)\tilde{x}(p) \end{aligned} \tag{6.35}$$

Convergence and robustness properties of this algorithm have been developed in Freeman and Tan (2012) where it is shown that convergence to zero error requires that $\Phi g^{'}(u_k)$ has full row-rank. Hence point-to-point locations can be chosen to recover feasibility in the presence of a highly coupled interaction matrix $R(q_f)$.

As a simulation example, consider the case when the sampling frequency is 100 Hz and the clinically relevant task is to move the hand from an initial flexed position to the position defined (angles in radians) by $\vartheta_f = 1.57$, $\vartheta_g = 0.47$ and $\vartheta_h = 0.21$, respectively, which represents opening the hand to grasp an object. Two separate cases are considered: (a) stimulation applied to all muscles and (b) only intrinsic

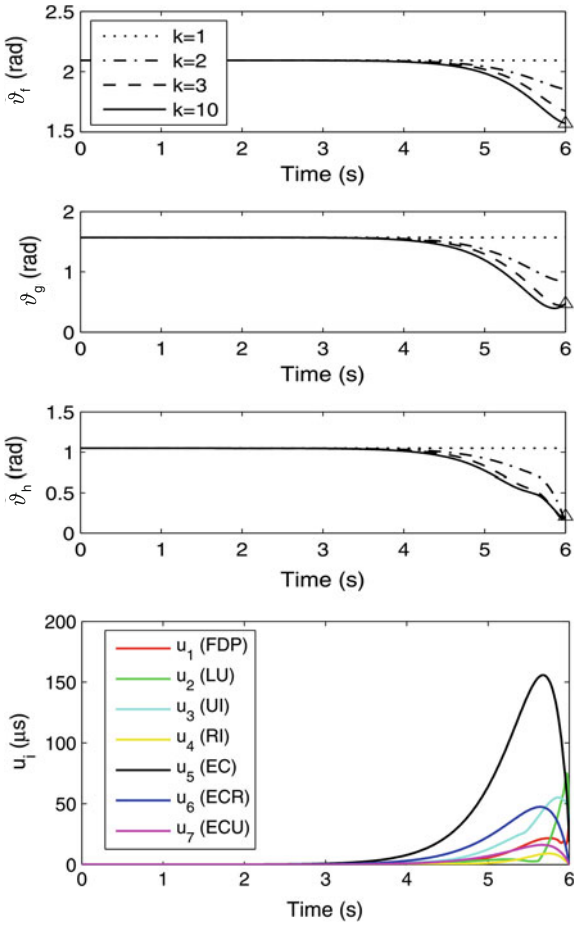

Fig. 6.7 Stimulation of extrinsic and intrinsic muscles using Newton point-to-point ILC with an inequality constraint against trial number

muscles are stimulated. The stimulation limits of $u_{\min} = 0$ and $u_{\max} = 350$ μs are imposed and the results given in Figs. 6.7, 6.8, 6.9 and 6.10 confirm that a wide variety of point-to-point movements can be achieved by intrinsic muscle stimulation but requires higher levels of stimulation. Figures 6.7 and 6.9 show the joint trajectories over 10 trials and the FES input on the final trial. As seen in Figs. 6.8 and 6.10 error convergence results in high accuracy tracking within a few trials.

The simulation results in these four figures confirm the potential of assisted movement using the muscles stimulated but there is the possibility of increased input norms and hence the possibility of fatigue, especially for the EC muscle.

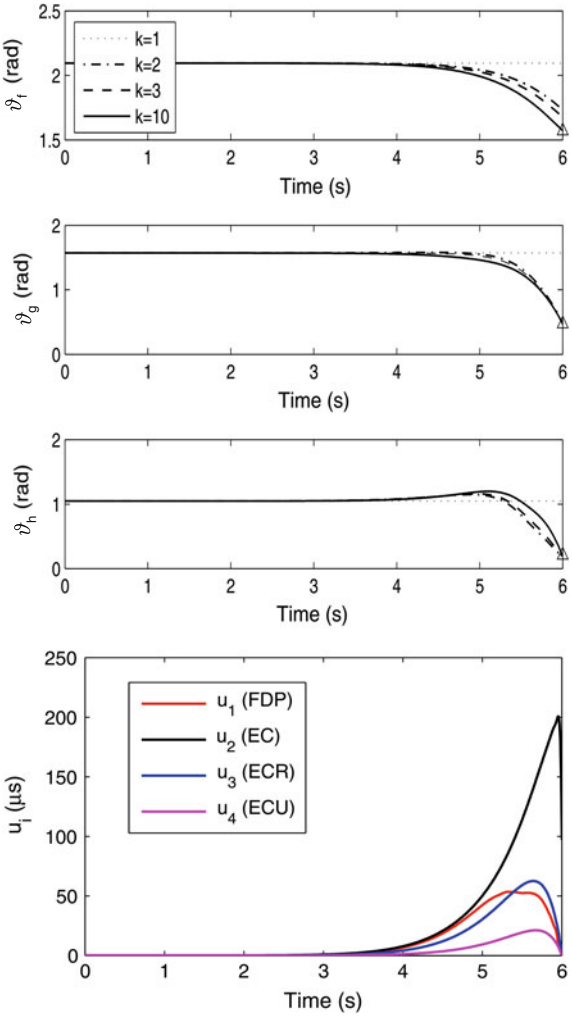

Fig. 6.8 Stimulation of extrinsic muscles using Newton point-to-point ILC with an inequality constraint against trial number

6.2.3 Model Identification

The FES control laws are designed using a dynamic model of the combined human arm and mechanical support. This dynamic model requires the two parameters, β and γ, which define the anterior deltoid axis, which were determined by applying a ramped 10 s FES signal to the anterior deltoid and recording the associated movement of the patient's elbow. It is assumed that the spring support cancels the effect of gravity and therefore the stimulation only produces movement about the anterior deltoid axis. A plane is fitted to the elbow positions that were collected whilst the stimulation was applied, which were then used to determine β and γ.

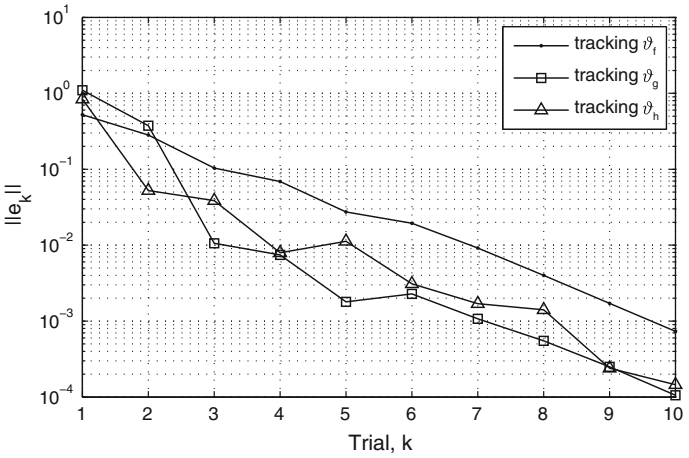

Fig. 6.9 Stimulation of extrinsic and intrinsic muscles using Newton point-to-point ILC against trial number

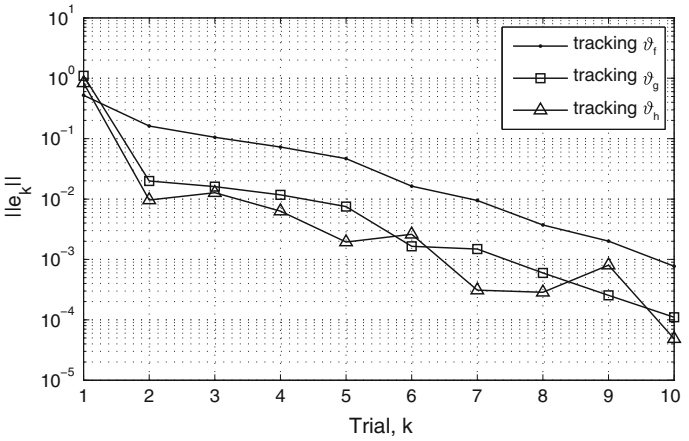

Fig. 6.10 Stimulation of extrinsic muscles using Newton point-to-point ILC with inequality constraints: error norm against trial number

6.2.4 FES Control

The control law is used to assist tracking of reference trajectories that are extracted for the shoulder, elbow and wrist joints. Control is implemented (Exell et al. 2013) for the pulse width inputs $u_a(t)$, $u_d(t)$ and $u_e(t)$ in the input vector $u(t)$. The outputs controlled by the system are the entries $\vartheta_a(t)$, $\vartheta_d(t)$ and $\vartheta_e(t)$ of vector $q_u(t)$, which track the corresponding $\vartheta_a^*(t)$, $\vartheta_d^*(t)$ and $\vartheta_e^*(t)$ of $q_u^*(t)$ containing the joint angle

reference trajectories for each task. Joint angles not controlled by the system can either be assumed fixed and removed, or treated as disturbances.

Application of dynamic model based ILC will be required but the construction of such a model is a non-trivial task. Hence the results given in the rest of this chapter use phase-lead ILC (4.34), where the results obtained will also be useful for comparison in due course of performance relative to full dynamic model based design. The phase-lead ILC law employed has the form

$$v_{k+1}(t) = v_k(t) + L_g e_k(t + \lambda) \tag{6.36}$$

where $\lambda > 0$ is the phase-lead term and v_{k+1} is added to the feedback control output to produce stimulation update u_{k+1}. Moreover, the joint error e_k is calculated using

$$e_k(t) = q_u^*(t) - q_{u,k}(t) \tag{6.37}$$

Since only the joint angles (ϑ_a, ϑ_d and ϑ_e) are controlled, the matrix

$$L_g = L\text{diag}\{1\ 0\ 0\ 1\ 1\ 0\}$$

where $L > 0$ is a scalar but this matrix could also be formed by choosing different values of L for the two stimulated joint angles.

The reference trajectories for the clinical trial whose results are reported in the next section were constructed from tests with unimpaired participants undertaking the functional tasks detailed in the next section. Reference data for the three controlled joint angles and tasks were scaled to the size and reach of each patient. Variation in the joint angles ϑ_b and ϑ_c is allowed by the system since only ϑ_a, ϑ_d and ϑ_e are controlled. Tasks were included in the system that are functionally relevant to daily reach and grasp tasks and offer a range of movement challenges in 3D space. The tasks that form each rehabilitation session are selected by the physiotherapist, based on the individual requirements of the patient.

6.3 Clinical Results

6.3.1 Experiments with Unimpaired Subjects

The results in this section are taken, in part from Meadmore et al. (2013, 2014). Evolving from the previous systems that used planar light tracking, Chap. 4, or virtual reality 3D object tracking tasks, Chap. 5, the system in this chapter uses functionally relevant real world tasks. The particular tasks used were: (1) switching a low light switch (shoulder height), (2) switching a high light switch (head height), (3) closing a drawer (shoulder height), (4) stabilizing an object on a table with the affected arm whilst manipulating the object with the unaffected arm, (5) repositioning a

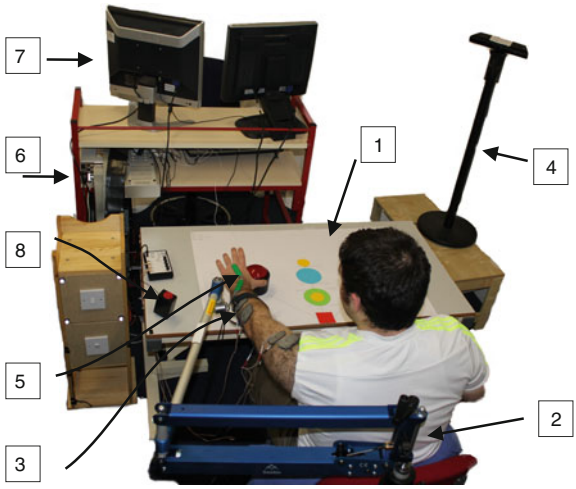

Fig. 6.11 The components of the workstation. (*1*) Task display; (*2*) SaeboMAS arm support; (*3*) Surface electrodes and arrays on anterior deltoid, triceps and wrist extensor muscles; (*4*) Kinect; (*5*) goniometer; (*6*) control algorithm hardware and software; (*7*) operator monitor; (*8*) stop button

drink-sized object on a table, (6) pressing buttons positioned on a table. All of the task endpoints were scaled for each patient's arm length and shoulder height such that the reference joint angle signals result in the desired positioning of the hand for the task.

Figure 6.11 shows the workstation set up for the functional tasks; the tasks were selected so that they incorporate different aspects of reaching, grasping and manipulating objects at varying elevation ranging from table to head height.

Entries (1)–(6) in this figure are detailed above and in operation the therapist uses the operator monitor interface (7) to select appropriate tasks and monitor training. The therapist also has an over-ride stop button (8) that can be used to terminate trials with immediate effect.

The tasks used were functional reach and grasp tasks performed in everyday life, designed to span the workspace and offer a range of reaching challenges requiring different amounts of shoulder, elbow and wrist extension. Five main tasks were used; closing a drawer, switching on a light switch, stabilizing an object, button pressing and repositioning an object. The objects were placed at different percentages of arm length (60, 75, 80, 95 %) away from the participants glenohumeral joint, see Fig. 6.12, directly in line with this joint, 45 % across body, or 45 % to the hemiplegic side. As illustrated in Fig. 6.12, the light switch was located at two different heights (low $-90°$ and high $-115°$ of elevation). The table was positioned at a distance of 45 % of arm length away from the glenohumeral joint and 35 cm below the arm when the arm was held 90 % horizontal to the shoulder.

In each session, participants repeatedly practiced functional tasks with real objects with assistance from FES. Participants were positioned at the workstation and the arm being tested was loosely strapped into the dynamic mobile arm support system. The arm support was adjusted such that the participant received enough support that it felt as though the arm were floating but that the hand could rest easily on the table

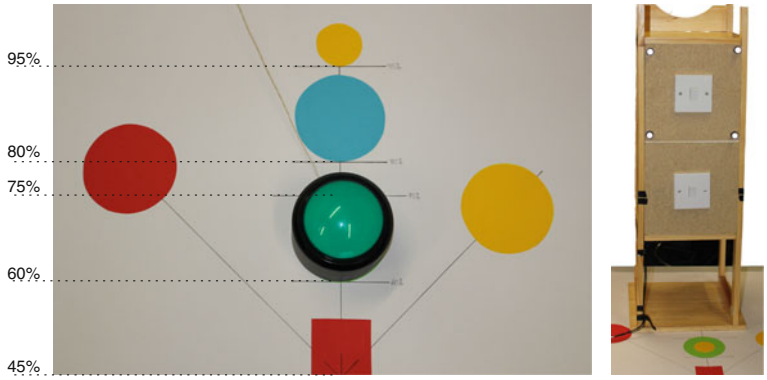

Fig. 6.12 Functional tasks that performed during rehabilitation

top. Movement produced by FES in the anterior deltoid, triceps and wrist extensors was established. Maximum stimulation levels were identified for all muscles and used as an upper limit for participant comfort and safety. Parameters necessary for the model of the arm were also identified. The custom graphical user interface was used by the therapist to perform the subsequent tests.

During training, the therapist selected the tasks to be trained, where these were chosen to challenge the participant but also such that completion was not unrealistic. Each task was typically repeated 6 times. Participants always started each task with their hand resting on the red square, see Fig. 6.12, in front of their shoulder and the therapist gave a verbal three-second countdown prior to the commencement of each trial. During each task, FES was applied to the anterior deltoid, triceps and wrist extensor muscles in order to assist performance of the movement. Patients were instructed to always try to move their arm to complete the task themselves. The FES was mediated by ILC to facilitate the movement of their arm over the 6 trials of the selected task.

At the beginning and end of each session, participants also completed five unassisted tasks: four button pushing tasks (located at 60 or 80 % of reach in line with the shoulder, or at 75 % of reach, 45 % across body or 45 % to the hemiplegic side), and the high light switch task (located at 75 % of reach and 110 % of elevation). The unassisted tasks consisted of one trial only.

Joint angles, timings and error magnitudes between the participants arm movement and the reference movement were recorded for each task. These provided a measure of accuracy for each muscle group for unassisted tasks, i.e., movements without FES, and assisted tasks. Unassisted performance was measured at the beginning and end of each training session so that changes in unassisted performance could be mapped over time. In addition, the change in error for each muscle group could be measured across the 6 trials of each assisted task. This gave an indication of whether the ILC was successfully reducing error in performance. As in the previous clinical trials, FMA and ARAT were administered to assess upper limb impairment

and function. These assessments were conducted by an independent assessor pre and post the 18 training sessions. As noted above, detailed results are given in Meadmore et al. (2013, 2014).

6.3.2 Clinical Trial Results

A clinical feasibility trial, for which the unimpaired results again formed part of the successful ethical approval, has been completed. The following results report data from three patients who have completed the trial, with remaining data and further in depth discussion appearing in Meadmore et al. (2014).

For the three patients, FES successfully facilitated movement in the upper limb at all three joints. Also using ILC to adjust the FES applied, performance error for each joint was shown to reduce over a set of six trials. For example, Figs. 6.13 and 6.14 show performance for button pressing at 80 % of reach, where there was an improvement of 63 % for the wrist, 41 % for the elbow and 22 % for the shoulder from trial 1–6. Some FES was always applied during the first trial of a set of tasks and improvements were generally larger when compared to unassisted performance.

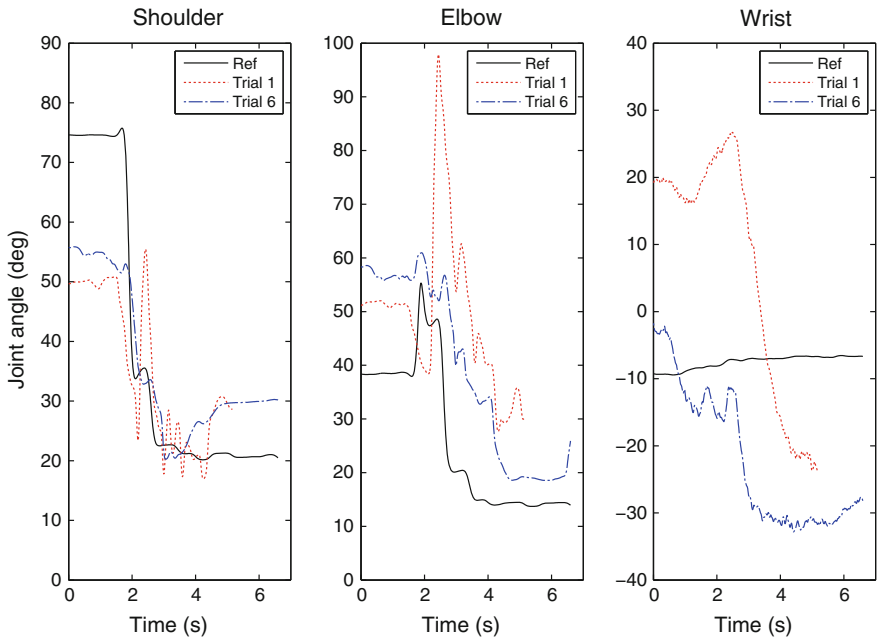

Fig. 6.13 Example of changes in performance for pressing a button located in line with the shoulder at 80 % of reach over 6 trials at the shoulder, elbow and wrist. Joint angles are shown for the ideal reference (*solid line*), trial 1 (*dotted line*) and trial 6 (*dashed line*)

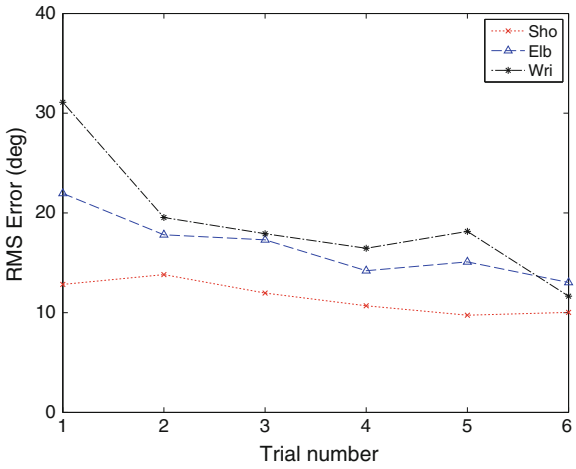

Fig. 6.14 Example of normalized RMS changes in performance for pressing a button located in line with the shoulder at 80 % of reach. Note that the participant received FES on all 6 trials. Error is shown for the shoulder (*cross*), elbow (*triangle*) and wrist (*star*)

For example, the improvements for the button pressing at 80 % of reach increased to 70 % for the wrist, 68 % for the elbow and 56 % for the shoulder when compared to unassisted performance.

Improvements also were detected for all three patients in unassisted performance when comparing performance over the 18 sessions, see Table 6.2. The Button Press at 80 % reach, Contralateral Button (75 % of reach, 45° to the hemiplegic side) and High Light Switch tasks (75 % of reach, 110° of elevation) were the three most challenging of the unassisted tasks.

The improvements found in unassisted performance were also reflected in the clinical outcome measures. As illustrated in Table 6.3, both the FMA and ARAT scores significantly increased from baseline to post-intervention. One tailed, paired t-tests confirmed that the overall 10 % increase in FMA scores ($t(2) = 3.93$, $p = 0.01$) and 9 % increase in ARAT scores ($t(2) = 6.43$, $p = 0.03$) were significant improvements. This data demonstrates a reduction in motor impairment and an increase in motor activities.

Table 6.2 Changes in unassisted performance for pressing a button at 80 % of reach, second column, pressing a button on the contralateral side, third column, and high light switch tasks, fourth column

P1 (%)	50	54	35
P2 (%)	45	63	51
P3 (%)	13	20	38
Average (%)	36	46	41

Table 6.3 Baseline and post-intervention outcome measures

P1	15	24	0	7
P2	19	24	3	7
P3	17	21	4	10
Average	17	23	2.3	8

Second and third columns are FM, maximum score = 66, baseline and post-intervention respectively. Fourth and fifth columns are ARAT, maximum score = 57, baseline and post-intervention respectively

References

Clark RA, Pua YH, Fortin K, Ritchie C, Webster KE, Denehy L, Bryant AL (2012) Validity of the Microsoft Kinect for assessment of postural control. Gait Posture 36(3):372–377

de Kroon JR, Ijzerman MJ, Lankhorst GJ, Zilvold G (2005) Relation between stimulation characteristics and clinical outcome in studies using electrical stimulation to improve motor control of upper extremity in stroke. J Rehabil Med 35:65–74

Dutta T (2012) Evaluation of the Kinect sensor for 3-D kinematic measurement in the workplace. Appl Ergon 43(4):645–649

Exell TA, Freeman CT, Meadmore KL, Kutlu M, Hallewell E, Hughes A-M, Burridge JH, Rogers E (2013) Goal orientated stroke rehabilitation utilising electrical stimulation, iterative learning and Microsoft Kinect. In: Proceedings of the international conference on rehabilitation robotics. doi:10.1109/ICORR.2013.6650493

Freeman CT (2014) Electrode array-based electrical stimulation using ILC with restricted input subspace. Control Eng Pract 23(2):32–43

Freeman CT, Tan Y (2012) Iterative learning control with mixed constraints for point-to-point tracking. IEEE Trans Control Syst Technol 21(3):604–616

Freeman CT, Exell T, Meadmore KL, Hallewell E, Hughes A-M, Burridge JH (2013) Computational models of upper limb movement during functional reaching tasks for application in electrical stimulation based stroke rehabilitation. In: Proceedings of the 4th European conference on technically assisted rehabilitation

Ingram JN, Kording KP, Howard IS, Wolpert DM (2008) The statistics of natural hand movements. Exp Brain Res 188(2):223–236

Landsmeer J (1955) Anatomical and functional investigations on the articulation of the human fingers. Acta Autom 24(2):1–69

Levin M (1996) Interjoint coordination during pointing movements. Brain 119(1):281–293

Meadmore KL, Exell TA, Hughes A-M, Hallewell E, Freeman CT, Kutlu M, Burridge JH, Rogers, E (2013) Electrical stimulation and iterative learning control for functional recovery in the upper limb post-stroke. In: Proceedings of international conference on rehabilitation robotics. doi:10.1109/ICORR.2013.6650359

Meadmore KL, Exell TA, Hallewell E, Hughes A-M, Freeman CT, Kutlu M, Benson V, Rogers E, Burridge JH (2014) The application of precisely controlled functional electrical stimulation to the shoulder, elbow and wrist for upper limb stroke rehabilitation: a feasibility study. Journal of NeuroEngineering and Rehabilitation 11:105

Soska AI, Freeman CT, Rogers E (2013) Optimal actuation site selection for surface electrode array based control of the wrist and hand. In: Proceedings of the IFAC international workshop on adaptation and learning in control and signal processing, pp 1267–1272

Theodorou E, Todorov E, Valero-Cuevas FJ (2011) Neuromuscular stochastic optimal control of a tendon driven index finger model. In: Proceedings of the American control conference, pp 348–355

Valero-Cuevas FJ (2009) A mathematical apporach to the mechanical capabilities of limbs and fingers. In: Sternad D (ed) Progress in motor control, pp 619–633

Chapter 7
Conclusions and Further Research

Stroke is the largest cause of disability in developed countries, where a relatively small percentage of patients with upper-limb impairment following stroke regain full function. In particular, many of these patients experience difficulty performing everyday reaching and grasping tasks. Functional electrical stimulation (FES) can assist stroke patients in moving their impaired limbs and has been shown to increase upper-limb function. In addition, the benefits of FES are greatest when combined with maximal voluntary effort from the patient to perform the movement. This poses the problem of how to provide the correct level of FES to assist the movement with the requirement that maximal voluntary effort is also encouraged. In control systems terms an algorithm that directly regulates the input is required as opposed to one that adapts the controller.

The underlying premise of the research reported in this monograph is the use of ILC to regulate the FES applied during rehabilitation where the patient makes repeated attempts to relearn a task by repetition. In particular, the patient is presented with a reference, such as a lighted path to follow in reaching out over a table top to a cup, and attempts to follow it guided by a robot and with FES applied to the relevant muscle. During an attempt, the error between the reference and the trajectory generated by the patient is measured and once the attempt is complete the arm is returned to the starting position and this information is used by the ILC law to compute the FES to be applied on the next attempt. Use of ILC in this application is a technology transfer from industrial robotics to next generation healthcare.

In this monograph, the results of three programs of research are reported, including clinical trial evaluation which is essential to enable the eventual take up of this work by healthcare professionals. The first program (Chap. 4) focused on initial proof of concept by considering movement in one plane and stimulated one muscle group (triceps) to control movement around the elbow joint. Patients tracked a moving trajectory with their hand whilst FES was applied to assist with the movement. Following each trial, ILC updated the FES signal for the subsequent trial. Results showed improvements in tracking accuracy during the sessions. This initial research

C.T. Freeman et al., *Iterative Learning Control for Electrical Stimulation and Stroke Rehabilitation*, SpringerBriefs in Control, Automation and Robotics, DOI 10.1007/978-1-4471-6726-6_7

did not allow the patient to attempt to lift the affected arm and also movement in the plane was tightly constrained by the support.

The second program (Chap. 5), considered a 3D task where the ability to lift the affected arm was also trained and hence, in contrast to the previous chapter, stimulation of more than one muscle is required. Given that stroke patients have difficulty lifting their affected arm, a gravity unweighing robot was employed and the final design was again used in a clinical trial with very encouraging results. For 3D tasks, the need for model based design is much stronger than in the planar case.

Given the progress with a fully prescribed reference trajectory, i.e., following a specified path from the start to the end position on each trial, an obvious next stage is to relax this assumption and consider activities directly related to daily living tasks. Moreover, stroke patients also have difficulty opening their affected hand to grasp an object. Hence there is also a need to rehabilitate the hand and this will involve stimulation of the wrist and hand extensors. These requirements are the subject of the third program (Chap. 6) again with supporting clinical trials based on the Kinect motion capture device and wrist electrogoniometers. One other advantage of the use of the Kinect is reduced cost and hence a step towards eventual home use.

Using the progress reported in this monograph as a basis, there are a large number of areas where further research should be directed. These relate to onward development of the existing results and also the possibilities of extending the use of ILC and repetitive control to regulate FES in other areas of rehabilitation. A number of these are given next with supporting references where appropriate.

- **Nonlinear and Constrained ILC Design** With the exception of the simulation based study given in Chap. 6, the vast majority of ILC designs are unconstrained. In all cases where patients are involved there will be a specified limit on the level of FES that can be applied. Further research effort should be directed to this area, building, in the case of constrained designs, on the results in Freeman and Tan (2012) and, as one option, aiming to deploy model predictive control algorithms. For muscle fatigue there is the possibility, based on initial results in Brend et al. (2013, 2015), of using multiple model adaptive control. Moreover, control of complex dynamics associated with using electrode arrays on the wrist and hand is an emerging area in which it may not be possible to identify an adequate nonlinear global model. One possible approach is to identify locally valid reduced-order linear models, as described in Freeman (2014).
- **Muscle Representations** The results in this monograph have used the Hammerstein model of the response of muscles to FES. As the control challenges increase there could be a need to switch to more general structures including Hammerstein-Wiener representations of the active component of the Hill model (Hill 1938). This latter model is used in the regulation of assistive stimulation in other areas of rehabilitation and could be more applicable to online identification in an adaptive control setting, where some initial results on this last area can be found in Le (2011).

- **Reference Trajectory Selection** The results in Chap. 6 have moved on towards reference trajectories that mimic how a human undertakes daily living tasks and need further development. For example, in Freeman et al. (2015) customised computational reference trajectories have been developed that pose human movement as a constrained optimisation problem involving each patient's biomechanical model, with results showing a close match to their unimpaired movement. This hence has potential to replace current approaches that rely on a physiotherapist assessing each patient and determining the reference trajectory manually. However, further research is needed to adapt the reference trajectory in order to ensure it continually poses a suitably difficult level of challenge. If, for example, the trajectory is too far outside the patient's current ability then this is a demotivating factor for at least some patients and likewise if the trajectory chosen is within the current capabilities of a patient then little or no benefit results. The development of methods that monitor the performance of a patient during the trials and allow a trajectory switch is an obvious area for further research.
- **Towards Home Use** The results in Chap. 6 are much closer to a system that could be taken to a patient's home but much further development is also required, aside from the need to conduct larger scale patient trials for approval by the regulatory authorities. In this respect, there is an obvious role for wearable technology and some initial results in this direction can be found in Yang et al. (2014).
- **Tremor Suppression** The combination of learning and FES has potential for exploitation to address wider neurological conditions. One of these is suppression of tremor which is widely present in neurological conditions such as multiple sclerosis, with results from a study with 10 participants confirming feasibility of the approach (Freeman et al. 2015).
- **Lower Limb** The research in this monograph has focused on upper limb rehabilitation and there has also been research on the use of ILC for lower limb rehabilitation, such as Seel et al. (2013), Ambrosini et al. (2014) and Klauer et al. (2013).
- **Multiple Sclerosis** The system of Chap. 5 has also been employed with clinical trials with multiple sclerosis patients (Sampson et al. 2015) with promising initial results.

References

Ambrosini E, Ferrante S, Schauer T, Ferrigno G, Molteni F, Pedrocchi A (2014) An automatic identification procedure to promote the use of FES-cycling training for hemiparetic patients. J Healthc Eng 5(3):275–291

Brend O, Freeman CT, French MC (2013) Norm optimal iterative learning control based on a multiple model switched adaptive framework. In: Proceedings of the 52nd IEEE conference on decision and control, pp 7297–7302

Brend O, Freeman CT, French MC (2015) Multiple model adaptive control of functional electrical stimulation. IEEE Trans Control Syst Technol, In press, doi:10.1109/TCST.2015.2394508. preprint available from http://eprints.soton.ac.uk/36162

Freeman CT (2014) Electrode array-based electrical stimulation using ILC with restricted input subspace. Control Eng Pract 23(2):32–43

Freeman CT, Tan Y (2012) Iterative learning control with mixed constraints for point-to-point tracking. IEEE Trans Control Syst Technol 21(3):604–616

Freeman CT, Exell T, Meadmore KL, Hallewell E, Hughes A-M (2015) Computational models of upper limb motion during functional reaching tasks for application in FES based stroke rehabilitation. Biomed Eng J 60(3):179–191. doi:10.1515/bmt-2014-0011

Freeman CT, Sampson PA, Burridge JH, Hughes AM (2015) Can functional electrical stimulation mediated by repetitive control suppress induced tremor. Mechatronics (in press)

Hill AV (1938) The heat of shortening and dynamics constants of muscles. Proc R Soc Lond B 126(843):136–195

Klauer C, Raisch J, Schauer T (2013) Nonlinear joint-angle feedback control of electrically stimulated and lambda-controlled antagonistic muscle pairs. In: Proceedings of the European control conference, pp 3101–3107

Le F (2011) Identification of electrically stimulated muscle after stroke. Ph.D thesis, University of Southampton, UK

Sampson PA, Freeman CT, Coote S, Demain S, Feys P, Meadmore KL, Hughes A-M (2015) Using functional electrical stimulation mediated by iterative learning control and robotics to improve arm movement for people with multiple sclerosis. IEEE Trans Neural Syst Rehabil Eng (in press). doi:10.1109/TNSRE.2015.2413906

Seel T, Schauer T, Raisch J (2013) Iterative learning control with variable pass length applied to FES-based drop foot treatment (in German). Automatisierungstechnik 61(9):630–637

Yang K, Freeman CT, Torah R, Beeby S, Tudor J (2014) Screen printed fabric electrode array for wearable functional electrical stimulation. Sens Actuators A: Phys 213:108–115

Series Editor's Biographies

Tamer Başar is with the University of Illinois at Urbana-Champaign, where he holds the academic positions of Swanlund Endowed Chair, Center for Advanced Study Professor of Electrical and Computer Engineering, Research Professor at the Coordinated Science Laboratory, and Research Professor at the Information Trust Institute. He received the B.S.E.E. degree from Robert College, Istanbul, and the M.S., M.Phil, and Ph.D. degrees from Yale University. He has published extensively in systems, control, communications, and dynamic games, and has current research interests that address fundamental issues in these areas along with applications such as formation in adversarial environments, network security, resilience in cyber-physical systems, and pricing in networks.

In addition to his editorial involvement with these Briefs, Basar is also the Editor-in-Chief of Automatica, Editor of two Birkhäuser Series on Systems & Control and Static & Dynamic Game Theory, the Managing Editor of the Annals of the International Society of Dynamic Games (ISDG), and member of editorial and advisory boards of several international journals in control, wireless networks, and applied mathematics. He has received several awards and recognitions over the years, among which are the Medal of Science of Turkey (1993); Bode Lecture Prize (2004) of IEEE CSS; Quazza Medal (2005) of IFAC; Bellman Control Heritage Award (2006) of AACC; and Isaacs Award (2010) of ISDG. He is a member of the US National Academy of Engineering, Fellow of IEEE and IFAC, Council Member of IFAC (2011–2014), a past president of CSS, the founding president of ISDG, and president of AACC (2010–2011).

Antonio Bicchi is Professor of Automatic Control and Robotics at the University of Pisa. He graduated from the University of Bologna in 1988 and was a postdoc scholar at M.I.T. A.I. Lab between 1988 and 1990. His main research interests are in:

- dynamics, kinematics and control of complex mechanichal systems, including robots, autonomous vehicles, and automotive systems;
- haptics and dextrous manipulation; and

C.T. Freeman et al., *Iterative Learning Control for Electrical Stimulation and Stroke Rehabilitation*, SpringerBriefs in Control, Automation and Robotics, DOI 10.1007/978-1-4471-6726-6

- theory and control of nonlinear systems, in particular hybrid (logic/dynamic, symbol/signal) systems.

He has published more than 300 papers in international journals, books, and refereed conferences.

Professor Bicchi currently serves as the Director of the Interdepartmental Research Center "E. Piaggio" of the University of Pisa, and President of the Italian Association or Researchers in Automatic Control. He has served as Editor in Chief of the Conference Editorial Board for the IEEE Robotics and Automation Society (RAS), and as Vice President of IEEE RAS, Distinguished Lecturer, and Editor for several scientific journals including the *International Journal of Robotics Research, the IEEE Transactions on Robotics and Automation, and IEEE RAS Magazine.* He has organized and co-chaired the first WorldHaptics Conference (2005), and Hybrid Systems: Computation and Control (2007). He is the recipient of several best paper awards at various conferences, and of an Advanced Grant from the European Research Council. Antonio Bicchi has been an IEEE Fellow since 2005.

Miroslav Krstic holds the Daniel L. Alspach chair and is the founding director of the Cymer Center for Control Systems and Dynamics at University of California, San Diego. He is a recipient of the PECASE, NSF Career, and ONR Young Investigator Awards, as well as the Axelby and Schuck Paper Prizes. Professor Krstic was the first recipient of the UCSD Research Award in the area of engineering and has held the Russell Severance Springer Distinguished Visiting Professorship at UC Berkeley and the Harold W. Sorenson Distinguished Professorship at UCSD. He is a Fellow of IEEE and IFAC. Professor Krstic serves as Senior Editor for *Automatica and IEEE Transactions on Automatic Control* and as Editor for the Springer series *Communications and Control Engineering.* He has served as Vice President for Technical Activities of the IEEE Control Systems Society. Krstic has co-authored eight books on adaptive, nonlinear, and stochastic control, extremum seeking, control of PDE systems including turbulent flows and control of delay systems.

Index

C.T. Freeman et al., *Iterative Learning Control for Electrical Stimulation and Stroke Rehabilitation*, SpringerBriefs in Control, Automation and Robotics, DOI 10.1007/978-1-4471-6726-6